

Dissertation Report

on

# **Control of Switched Reluctance Generator in Wind Energy System**

Submitted in partial fulfillment of the requirements of the degree of  
**ME Electrical Engineering**  
**(Power Electronics and Drives)**

By

**Nereus Fernandes**

Roll Number: 441406

Reg Number: FR.C-162

Guide / Supervisor :

**Mrs. Bindu R.**



Department of Electrical Engineering  
Fr. C. Rodrigues Institute of Technology  
Navi Mumbai 400 703

University of Mumbai

2015-2016

# CERTIFICATE

This is to certify that the dissertation entitled "**Control of Switched Reluctance Generator in Wind Energy System**" is a bonafide work of "**Nereus Fernandes (Roll No 441406, Reg No FR.C-162)**" submitted to the University of Mumbai in partial fulfillment of the requirement for the award of the degree of "**Postgraduate in Electrical Engineering (Power Electronics and Drives)**".

---

Mrs. Bindu R.

(Guide / Supervisor)

---

Dr. Sincy George  
(Head of Department)

---

Dr.S.M. Khot  
(Principal)

# **Dissertation Approval for M. E.**

This dissertation report, entitled “Control of Switched Reluctance Generator in Wind Energy System”, submitted by Nereus Fernandes (**Roll No 441406, Reg No FR.C-162**), is approved for the Degree of “**ME Electrical Engineering (Power Electronics and Drives)**”.

## **Examiners**

1. \_\_\_\_\_

2. \_\_\_\_\_

Date :

Place :

## **Declaration of the Student**

I declare that this written submission represents my ideas in my own words and where others' ideas or words have been included, I have adequately cited and referenced the original sources.

I also declare that I have adhered to all principles of academic honesty and integrity and have not misrepresented or fabricated or falsified any idea / data / fact / source in my submission.

I understand that any violation of the above will be cause for disciplinary action by the Institute and can also evoke penal action from the sources which have thus not been properly cited or from whom proper permission has not been taken when needed.

Signature of the student

Nereus Fernandes

Roll Number: 441406

Reg No: FR.C-162

Date:

## **Abstract**

Switched reluctance (SR) machines have several advantages like simple and rugged construction, lighter rotor, lower rotor losses and lower cost. A wind energy conversion system (WECS) with maximum power tracking (MPPT) using a SR machine operating as a generator is presented. MPPT of the wind turbine is achieved by sensing the wind speed and adjusting the wind turbine shaft speed for optimal tip speed ratio. MPPT using Hill Climbing Technique by perturbing the wind turbine shaft speed in the direction of increasing power is also implemented in the hardware setup. Outer speed loop using PI control generates the current reference used by the inner current loop. Hysteresis current control using soft-chopping is used to control the switched reluctance generator (SRG) phase currents. Initial excitation is provided by a low voltage battery and rated voltage is built-up by self-excitation. A chopper controlled dump resistor is used to maintain the output dc voltage at rated value. Power electronic circuit for the SRG is implemented in hardware using IGBT switches and DSP controller. Wind turbine is emulated using an induction motor and a vector controlled AC drive operating in torque control mode.

# Table of Contents

Chapter 1	Introduction .....	1
1.1	Current data on Wind Energy Installations .....	1
1.2	Introduction to Wind Turbine Operation.....	3
1.3	Market Trends in Wind Energy Generator technology .....	3
1.4	Introduction to Switched Reluctance Machines .....	5
1.5	Market Trends in Reluctance Machines .....	6
1.6	Summary of the Problem.....	7
1.7	Aim of this Dissertation.....	7
1.8	Scope of Work Done .....	7
Chapter 2	Literature Survey .....	9
Chapter 3	Theory and Equations.....	11
3.1	Switched Reluctance Generator Theory.....	11
3.2	Wind Turbine Theory .....	17
Chapter 4	Simulation Results.....	19
4.1	Switched Reluctance Generator (SRG) – Generic Model .....	21
4.2	Wind Turbine Simulation .....	23
4.3	MPPT Controller .....	24
4.4	Speed Controller.....	24
4.5	Position Sensing .....	25
4.6	Phase Commutation Controller .....	25
4.7	Hysteresis Current Controller.....	26
4.8	Switched Reluctance Generator (SRG) –Specific Model.....	32
Chapter 5	Hardware Implementation .....	35
5.1	Test Bench Constraints.....	35
5.2	Overview of Hardware Set-up.....	38
5.3	Wind Turbine Emulator.....	39
5.4	External Excitation Source (24V PS) .....	43
5.5	Switched Reluctance Generator (SRG) .....	43
5.6	SRG Converter and Chopper Load.....	43
5.6.1	Power Supply and Digital Input Card (PS-DI).....	43
5.6.2	Capacitor Bank Card ( EXT CAP / GEN CAP ) .....	46
5.6.3	IGBT Driver Card (IGBT SRV Ph A-Ph D) .....	48
5.6.4	Asymmetric Half Bridge Converter Card (AHBC PhA-PhB).....	49
5.6.5	Chopper Card for Dump Load (Load Chopper) .....	52
5.6.6	Analog Input Processing Card (AI IA, IB / AI IC, ID / AI VGEN ) .....	52

5.6.7	DSP Control Card.....	55
5.7	Structure of the DSP program .....	56
5.7.1	Analog Input Signal Processing .....	56
5.7.2	Speed Calculation and Rotor Position Logic.....	57
5.7.3	Commutation Logic.....	58
5.7.4	MPPT Control Logic .....	59
5.7.5	Speed Loop Logic.....	59
5.7.6	Current Loop Logic .....	60
5.7.7	DC Voltage Control Logic .....	60
Chapter 6	Results and Discussions.....	61
6.1	Motor Mode Results .....	61
6.2	Generator Mode Results .....	62
6.3	Wind Energy System Results .....	64
6.3.1	MPPT Results.....	67
6.3.2	Reason for Low Efficiency.....	67
6.3.3	Reason for Low Power Handling Capacity .....	68
6.3.4	Comparison with simulation using the specific model.....	68
Chapter 7	Summary and Conclusions .....	71
7.1	Future Scope .....	72
Appendix I	.....	73
I.1	Software used in the project .....	73
I.2	Test Equipment used in the project .....	73
I.3	Datasheet excerpts for key components .....	74
I.3.1	DC Bus Filter Capacitor Vishay 198PHR-SI .....	74
I.3.2	Isolation Amplifier TI ISO124 .....	75
I.3.3	Current Sensor LEM HX 05-P/SP2.....	77
I.3.4	Precision Op-amp TLC274.....	78
I.3.5	Precision Voltage Reference TL431.....	80
I.3.6	Power Diode VS-APH3006-F3 .....	81
I.3.7	IGBT Switch IGW40H65H5 .....	82
I.3.8	IGBT Gate Drive Optocoupler HCPL-3120.....	85
I.3.9	Digital Input Buffer SN74AHC541.....	86
I.3.10	Digital Output Buffer 74HCT541.....	87
I.3.11	DSP TMS320F28069 .....	88
References	.....	90
Publication	.....	91
Acknowledgements	.....	92

# List of Figures

Fig 1.1 Major Components of Power Generation in India and major Components of Renewable Power in India. [1] .....	1
Fig 1.2 Top 10 countries for Installed Capacity of Wind Energy Systems in the year 2015 and for Cumulative Capacity of Wind Energy Systems as of Dec 2015. [2] .....	2
Fig 1.3 Wind turbine types according to generator-drive train configuration [3] .....	3
Fig 1.4 Share of installed capacity for wind turbines by Drive-Generator Technology from 2005 to 2014 [3] .....	5
Fig 1.5 JoyGlobal-LeTourneau Wheeled Loader with SR Generator and independent electric wheel drive using SR Motors [6].....	6
Fig 1.6 ABB SynRM and SynRM <sup>2</sup> Synchronous Reluctance Motors [9][10] .....	7
Fig 3.1 Cross sectional view of 8/6 switched reluctance machine .....	11
Fig 3.2 Variation of phase inductance with rotor position and phase current. ....	12
Fig 3.3 Variation of magnetic flux paths with rotor position. ....	12
Fig 3.4 AHBC for one phase with equivalent circuits.....	13
Fig 3.5 Generation mode waveforms for one phase below base speed with soft chopping...	15
Fig 3.6 Asymmetric half bridge converter circuit with separate excitation and generation buses .....	16
Fig 3.7 Cp vs $\lambda$ for various $\beta$ . Graph for Mod2- Two Blade wind turbine [22] .....	18
Fig 3.8 Variation of wind turbine mechanical output power ( $P_m$ ) with wind turbine shaft speed ( $\omega$ ) for various wind speeds ( $v_n$ ) .....	18
Fig 4.1 Block diagram of wind energy conversion system .....	19
Fig 4.2 Simulink Simulation of Wind Energy Conversion System using Switched Reluctance Generator .....	20
Fig 4.3 Magnetization characteristics of SR machine “generic” model.....	21
Fig 4.4 Circuit for machine phase in Simulink SRM model [22].....	22
Fig 4.5 Phase connector for Simulink SRM model [11] .....	22
Fig 4.6 Wind turbine characteristic [22].....	23
Fig 4.7 MPPT Controller using sensed wind speed and Tip Speed Ratio.....	24
Fig 4.8 SRG Speed Controller.....	24
Fig 4.9 SRG Position sensing .....	25
Fig 4.10 SRG Phase Commutation Controller Logic .....	26
Fig 4.11 SRG Phase Commutation Controller with Turn-On and Turn-Off angle advance tables.....	26
Fig 4.12 Hysteresis Current Controller.....	26
Fig 4.13 Upper Switch Disable Logic .....	27
Fig 4.14 Waveforms for MPPT Controller, Speed Controller and Phase A wavefroms for Position Sensing Logic, Commutation Controller and Phase Hysteresis Controller .....	28
Fig 4.15 Waveforms for SR Generator.....	29
Fig 4.16 Maximum power point tracking with changes in wind speed.....	31
Fig 4.17 Flux Density Plot at Phase A aligned position with 6A excitation current.....	32
Fig 4.18 Surface Plot of Flux linkages Vs stator current and rotor position using FEMM data.....	33

Fig 4.19 Surface Plot of Phase Torque Vs stator current and rotor position using FEMM data.....	33
Fig 4.20 Magnetization characteristics of SR machine “specific” model .....	34
Fig 5.1 Block Diagram of hardware set-up .....	35
Fig 5.2 SRG Hardware Setup .....	36
Fig 5.3 SRG Power Electronics and Controller.....	36
Fig 5.4 System Level Connection Diagram.....	37
Fig 5.5 Siemens G120 AC Drive Configuration for Wind Turbine Speed-Power Characteristics [25].....	40
Fig 5.6 Vector Controlled AC Drive Configured for Wind Turbine Emulation– Output Power vs Speed.....	42
Fig 5.7 Vector Controlled AC Drive Configured for Wind Turbine Emulation – Output Torque vs Speed .....	42
Fig 5.8 Power Supply and Digital Input Card Circuit Diagram .....	44
Fig 5.9 SRG Position Sensors.....	45
Fig 5.10 Motor Mode: Position Sensor Waveforms, Phase A Voltage and Current .....	46
Fig 5.11 Generator Mode: Position Sensor Waveforms, Phase A Voltage and Current.....	46
Fig 5.12 Capacitor Bank Card – For Excitation Bus and Generation Bus Circuit Diagram ...	47
Fig 5.13 IGBT Driver Card Circuit Diagram .....	48
Fig 5.14 IGBT Driver Card Waveforms.....	49
Fig 5.15 Asymmetric Half Bridge Converter Card – One Phase Circuit Diagram .....	50
Fig 5.16 Chopper For Dump Load Circuit Diagram .....	51
Fig 5.17 Analog Input Processing Card Circuit Diagram .....	53
Fig 5.18 Current Processing Circuit Waveforms.....	54
Fig 5.19 Voltage Processing Circuit Waveforms .....	54
Fig 5.20 Hill Climbing Algorithm for Maximum Power Point Tracking (MPPT) .....	59
Fig 6.1 Motor Mode Waveforms – Gate Drive, Phase Voltage and Current .....	62
Fig 6.2 Generator Mode Phase Voltage Waveforms.....	62
Fig 6.3 Generator Mode Waveforms – Gate Drive, Phase Voltage and Current .....	63
Fig 6.4 Generation Mode Waveforms – Excitation and Generation Phase Current.....	64
Fig 6.5 Dump Load Waveforms (Wind Speed = 9.99 m/s, SRG Shaft Speed = 905 rpm, Load Power=53.3 W).....	64
Fig 6.6 Dump Load Power (W) Vs SRG Shaft Speed Setpoint (RPM) .....	66
Fig 6.7 Effect of non-linear magnetic characteristics on energy conversion .....	68
Fig 6.8 Simulation using FEMM results with Simulink SRM specific model for comparison with Hardware Test Results. Test for 950 rpm, 120W input power.....	70

## List of Tables

Table 4.1 Wind Turbine maximum output power and shaft speed for the selected wind speeds .....	23
Table 4.2 System performance with variation in wind speed.using SR Machine “generic” model .....	31
Table 4.3 System performance with variation in wind speed suing SR Machine “specific” model. ....	34
Table 5.1 Torque – Speed Characteristic Configuration of the Vector Controlled AC Drive	41
Table 5.2 SRG Position Sensors Output and Phase Inductance measurements for 15 degree rotor position increments .....	45
Table 5.3 EPWM Outputs .....	55
Table 5.4 ADC Inputs.....	55
Table 5.5 GPIO Inputs.....	56
Table 5.6 GPIO Outputs .....	56
Table 5.7 Current Signal Processing .....	56
Table 5.8 Voltage Signal Processing.....	57
Table 5.9 Speed Calculations .....	58
Table 5.10 Phase Excitation for clock-wise rotation at speeds below 100 rpm .....	58
Table 5.11 Phase Excitation for clock-wise rotation at speeds above 100 rpm .....	58
Table 5.12 Dump Load Resistance.....	60
Table 6.1 Speed Control in Motor Mode (Supply Voltage = 100V).....	61
Table 6.2 SRG Readings for Lower Wind Speed.....	65
Table 6.3 SRG Readings for Higher Wind Speed .....	65
Table 6.4 Simulation Results using the specific model with system parameters similar to the hardware setup .....	69

## List of Symbols

$P_{\text{opt}}$	:	Optimal power output of wind turbine
$K_{\text{opt}}$	:	Constant for wind turbine optimal power curve
$\omega_r$	:	Generator shaft speed
$\theta$	:	Rotor angular position with respect to stator pole
$\theta_a$	:	Rotor at aligned position
$\theta_{ua}$	:	Rotor at un-aligned position
$\theta_{\text{on}}$	:	Rotor position where phase excitation is started
$\theta_{\text{off}}$	:	Rotor position where phase excitation is stopped
$\lambda$	:	Phase flux linkage
$u_{\text{ph}}$	:	DC bus voltage
$e_{\text{ph}}$	:	Induced emf
$i_{\text{ph}}$	:	Phase current
$R_{\text{ph}}$	:	Phase resistance
$l$	:	Incremental phase inductance
$p_{ph}$	:	Instantaneous input power for a phase
$p_a$	:	Instantaneous air gap power for a phase
$T_e$	:	Electrical torque
$T_L$	:	Load torque
$E_k$	:	Kinetic energy of wind
$m$	:	Mass of wind incident on swept area of the wind turbine per second
$\rho$	:	Density of air
$C_p$	:	Power coefficient of wind turbine
$R$	:	Radius of the rotor blades
$\beta$	:	Rotor blade pitch angle
$\omega$	:	Wind turbine shaft speed
$v$	:	Wind velocity
$\lambda$	:	Tip Speed Ratio
$c_1$ to $c_6$	:	Wind turbine coefficients
$W_f$	:	Field energy of the switched reluctance machine
$W_m$	:	Converted energy of the switched reluctance machine
$V_{\text{gen}}$	:	Generation bus voltage

## List of Abbreviations

SCIG	:	Squirrel Cage Induction Generator
WRIG	:	Wound Rotor Induction Generator
DFIG	:	Doubly Fed Induction Generator
D-EE/D-EESG	:	Direct Drive Electrically Excited Synchronous Generators
D-PM/D-PMSG	:	Direct Drive Permanent Magnet Synchronous Generator
E-EE/E-EESG	:	Gear Driven Electrically Excited Synchronous Generators
E-PM/E-PMSG	:	Gear Driven Permanent Magnet Synchronous Generator
SR	:	Switched Reluctance
SRM	:	Switched Reluctance Machine
SRG	:	Switched Reluctance Generator
IE4	:	Super Premium Efficiency Standard of the International Electrotechnical Commission
IE5	:	Ultra Premium Efficiency Standard of the International Electrotechnical Commission
SynRM	:	Synchronous Reluctance Motor
DOL SynRM	:	Line Start Synchronous Reluctance Motor
SynRM <sup>2</sup>	:	Synchronous Reluctance Motor with rotor ferrite magnets
MPPT	:	Maximum Power Point Tracking
PWM	:	Pulse Width Modulation
DC	:	Direct Current
AC	:	Alternating Current
AHBC	:	Asymmetric Half Bridge Converter
PI	:	Proportional Integral
SODAR	:	Sound Detection and Ranging
LIDAR	:	Light Detection and Ranging
FEMM	:	Finite Element Method Magnetics
ITBL	:	Current Table for MATLAB SR machine model
TTBL	:	Torque Table for MATLAB SR machine model
HCC	:	Hysteresis Current Controller
DSP	:	Digital Signal Processor
DSO	:	Digital Storage Oscilloscope
VOC	:	Voltage Oriented Control

DPC : Direct Power Control

# Chapter 1

## Introduction

Fossil fuels that are currently supplying the world's increasing energy requirements cause pollution, climate change and their reserves are rapidly declining. So renewable energy sources are gaining importance and wind is a major source of clean, non-polluting and inexhaustible energy.

### 1.1 Current data on Wind Energy Installations

Fig 1.1 shows the composition of India's "Power Installed Capacity" and "Renewable Power Installed Capacity" [1].

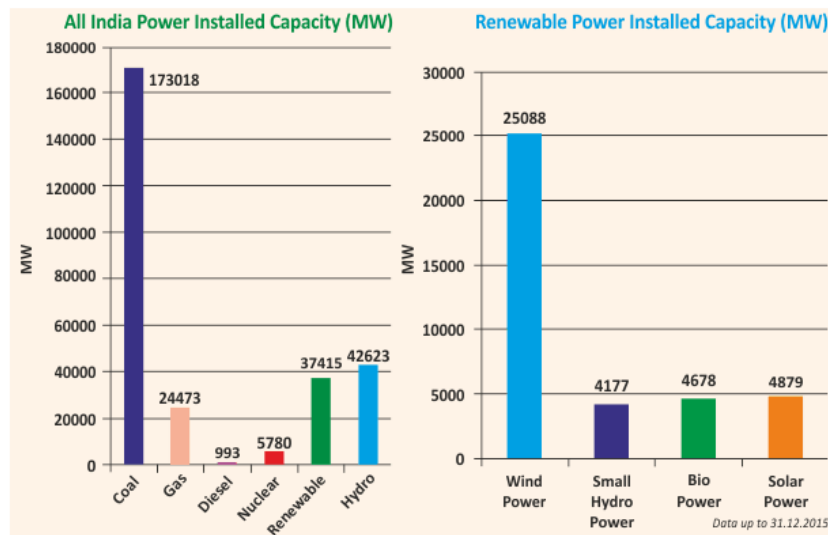


Fig 1.1 Major Components of Power Generation in India and major Components of Renewable Power in India. [1]

Fig 1.2 shows the total new installed capacity world-wide for wind energy in the year 2015 and also the cumulative installed capacity for wind energy world-wide as of December 2015 [2]. India has the fourth largest installed capacity of wind energy systems in the world after China, USA and Germany. India's total wind energy generation capacity in December 2015 was 25,088 MW.

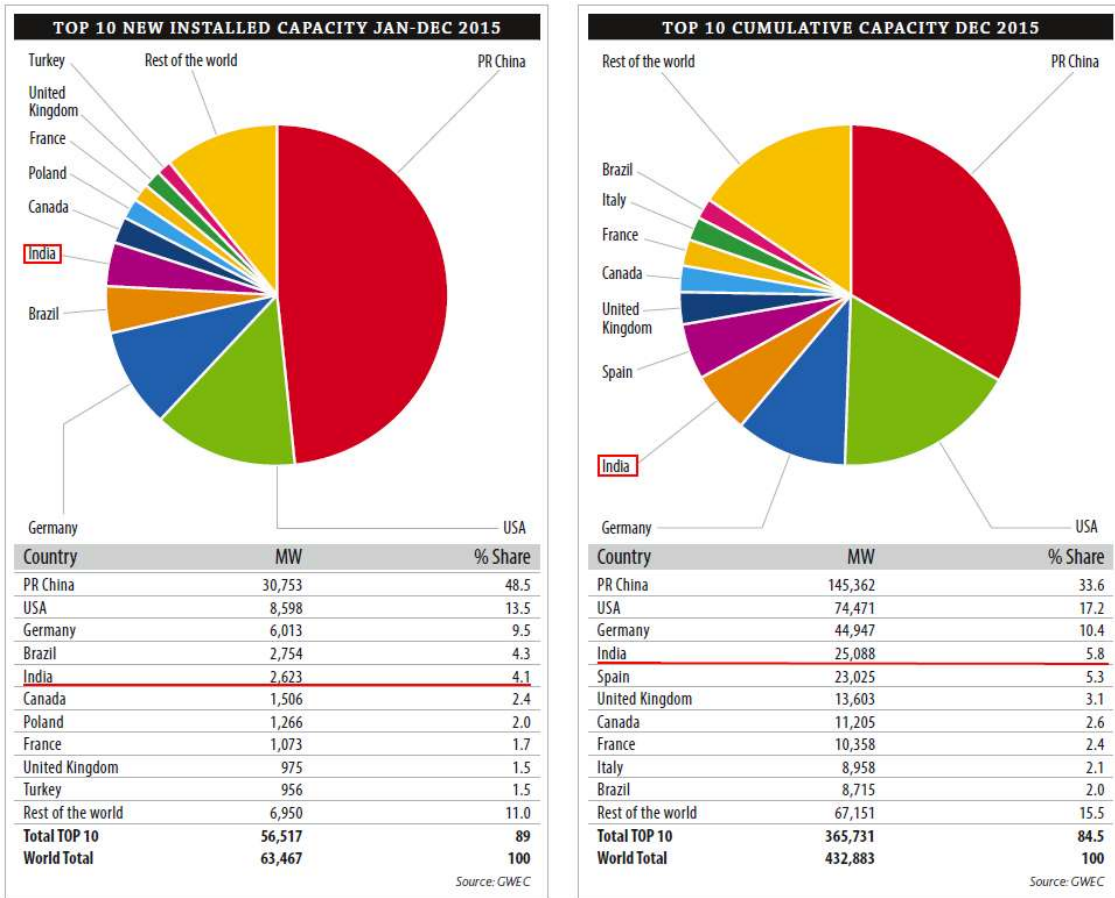


Fig 1.2 Top 10 countries for Installed Capacity of Wind Energy Systems in the year 2015 and for Cumulative Capacity of Wind Energy Systems as of Dec 2015. [2]

## 1.2 Introduction to Wind Turbine Operation

Power extracted by a wind turbine depends on the mass and velocity of air flowing through it. As the wind turbine rotational speed increases, the flow of air through it is reduced due to turbulence and the power extracted from the wind reduces. The wind-turbine extracts maximum power from the wind when the optimal tip speed ratio is maintained.

## 1.3 Market Trends in Wind Energy Generator technology

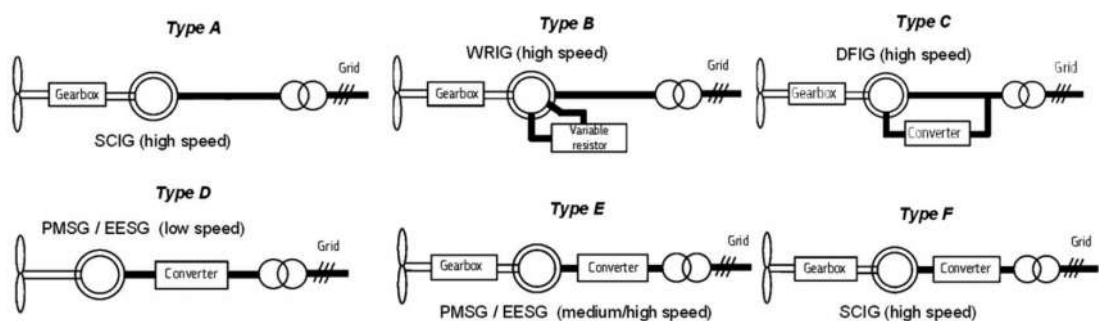


Fig 1.3 Wind turbine types according to generator-drive train configuration [3]

The generators and drive trains used in wind energy systems are shown in Fig 1.3 and described below [3]:

### Type A - Squirrel Cage Induction Generators (SCIG)

**Advantages:** simple, low cost, no power converter, robust low-maintenance generator

**Disadvantages:** No speed control – fixed speed operation, low aero-dynamic efficiency, gear box required, low grid integration : no fault ride through capability, no reactive power control

### Type B - Wound Rotor Induction Generators (WRIG)

**Advantages:** -10% Speed control around synchronous speed by varying rotor resistance, no power converter

**Disadvantages:** High electrical losses, slip rings and gear box required, low grid integration : no fault ride through capability, no reactive power control

### Type C - Doubly Fed Induction Generators (DFIG)

**Advantages:**  $\pm 30\%$  Speed control around synchronous speed, rotor converter rating is 30% of rated power so less expensive, reactive power control possible

**Disadvantages:** complex control needed for fault ride through capability, rotor loss, slip rings and gear box required

**Type D - Full Power Converter and Direct Drive.** The generators used are Electrically Excited Synchronous Generators (D-EE/D-EESG) and Permanent Magnet Synchronous Generators (D-PM/D-PMSG)

**Advantages:** Control over full speed range, full power converter enables decoupling of the generator from the grid frequency, complete control over reactive power, gear box not required

**Disadvantages:** Expensive full scale converter, heavier electric generator, price and supply fluctuations of rare earth permanent magnets in case of D-PM, complex and heavier rotor in case of D-EE

**Type E - Full Power Converter and Gear-box.** The generators used are Electrically Excited Synchronous Generators (E-EE/E-EESG) and Permanent Magnet Synchronous Generators (E-PM/E-PMSG)

**Advantages:** Control over full speed range, Full power converter enables decoupling of the generator from the grid frequency, size of gear box and generator can be optimized, complete control over reactive power, reduced size and weight of the electric generator as compared to Type-D, reduces gear box ratio and weight as compared to A, B, C and F

**Disadvantages:** Expensive full scale converter, gear box required, ,price and supply fluctuations of rare earth permanent magnets in case of E-PM, complex and heavier rotor in case of E-EE

**Type F - Squirrel Cage Induction Generators with full converter and gear-box**

**Advantages:** Control over full speed range, complete control over reactive power, robust low-maintenance generator

**Disadvantages:** Expensive full scale converter, gear box required

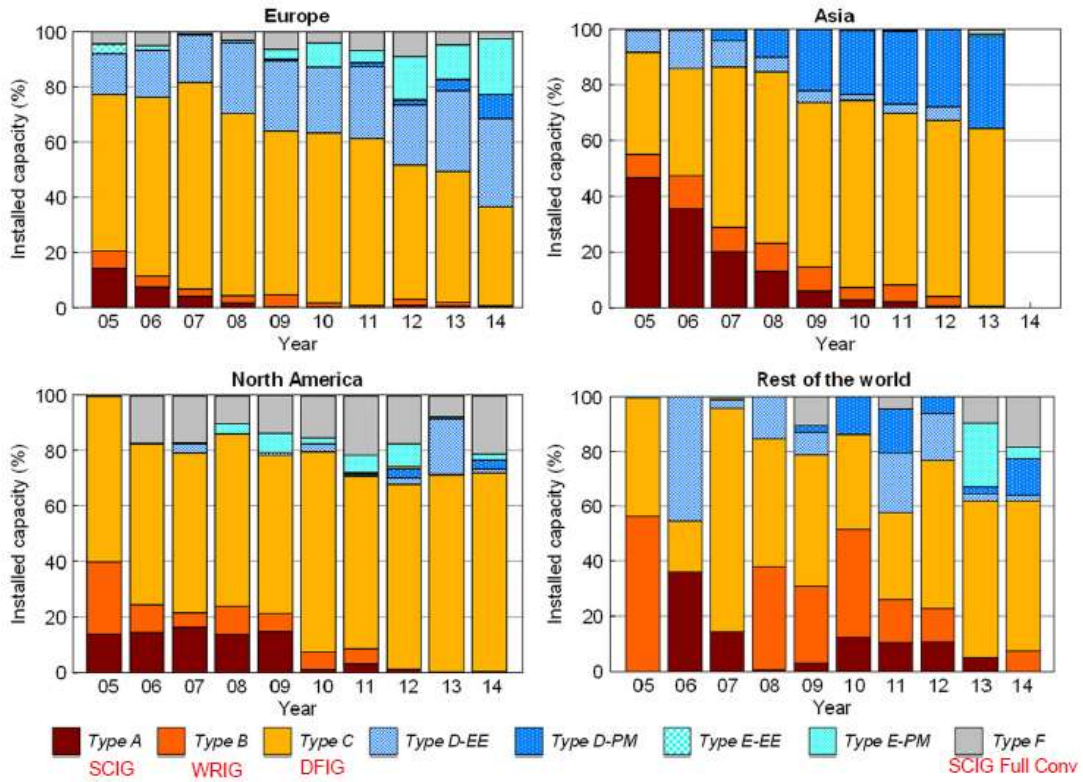


Fig 1.4 Share of installed capacity for wind turbines by Drive-Generator Technology from 2005 to 2014 [3]

From Fig 1.4 it is observed that currently the dominant generator technology in the wind energy industry is the Type-C (High-Speed DFIG). Type D, E and F are showing growing trends.

## 1.4 Introduction to Switched Reluctance Machines

The switched reluctance (SR) machine has a simple and rugged construction. The rotor consists of stacked steel laminations and does not have windings, brushes or magnets. The rotor temperature rise is low due to absence of conductors and copper loss. The stator windings are physically, magnetically and electrically independent of each other, with reduced risk of phase-to-phase failure. The power electronic controller topology makes the supply short-circuit proof and thus increases reliability. SR machines can operate at rated torque over a wide speed range. The main drawbacks of the SR machine are torque pulsation and acoustic noise, but these can be greatly reduced by proper design of the machine and controller. Salient poles on both the stator and the rotor are required to

produce the reluctance torque but give rise to non-linear magnetic characteristics. As a result, the inductance and induced emf change with angular position and the modeling and controller design needs to be computer assisted. Switched reluctance generator (SRG) needs position sensing for control, typically employing optical or Hall-effect sensors. The position can also be estimated using inductance calculated from the phase current and voltage measurements, thereby eliminating the need of position sensors [5].

## 1.5 Market Trends in Reluctance Machines

Reluctance Machines need power electronics control and they could be effectively used only after the 1970s. Large installed base of mains line operated machines like induction motors with established supply chains, production lines and economies of scale have inhibited the acceptance of reluctance machines in industry. Only a few specialized applications can be found.

Switched Reluctance Machines are used in all-electric and hybrid-electric vehicles. Fig 1.5 shows the JoyGlobal-LeTourneau Wheeled Loader series which weighs upto 180 tons and with rock bucket capacity of upto 38 tons. The loader has independent electric wheel drive and uses Nidec-SR motors and SR generators with 1000 hp-3000 hp power ranges.

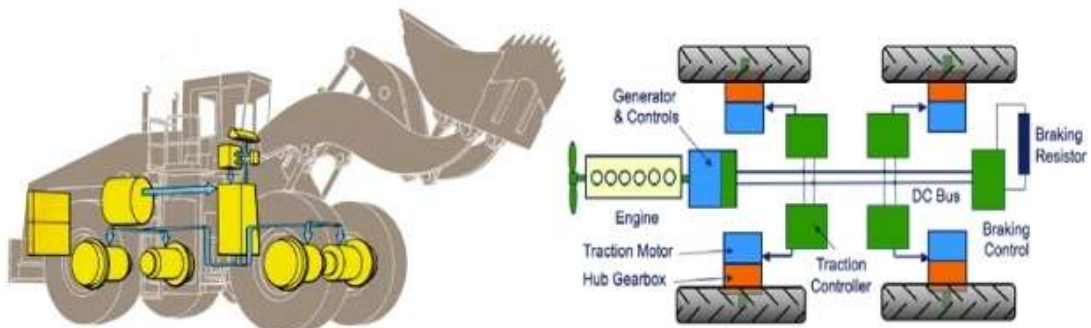


Fig 1.5 JoyGlobal-LeTourneau Wheeled Loader with SR Generator and independent electric wheel drive using SR Motors [6]

Synchronous reluctance motors are used for IE4 Super Premium Efficiency applications as these motors exhibit improved efficiency even with partial load. Some examples are

- Siemens SIMOTICS reluctance motors with power rating upto 30 kW [7]

- ABB Synchronous Reluctance Motor (SynRM) with power rating upto 300 kW[8] as shown in Fig 1.6
- ABB Line Start Synchronous Motors (DOLSynRM) (prototype) [9]
- ABB SynRM<sup>2</sup> with rotor ferrite magnets for future IE5 Ultra Premium efficiency standards. (prototype) [10] as shown in Fig 1.6



Fig 1.6 ABB SynRM and SynRM<sup>2</sup> Synchronous Reluctance Motors [9][10]

## 1.6 Summary of the Problem

- Need to harness wind energy
- All current generator systems have drawbacks :
  - DFIG : rotor loss, brush maintenance and grid support
  - PMSG : fluctuation in rare-earth PM prices
  - EESG : complex rotor
  - SCIG : rotor loss
- Switched Reluctance Generator is free from these drawbacks but needs power electronics control for stable operation.

## 1.7 Aim of this Dissertation

To control the Switched Reluctance Generator for maximum power point tracking of a wind turbine

## 1.8 Scope of Work Done

Simulation is done in MATLAB and the SRG is controlled to obtain maximum power point tracking (MPPT) of the wind turbine by maintaining the optimum tip speed ratio. Hardware implementation is done using power electronic devices, sensors and DSP

controller. A vector controlled induction motor drive in torque control mode with pre-programmed speed torque characteristics is used for wind turbine emulation.

MPPT Controller is implemented using two schemes:

- Assuming that wind speed is sensed, the SRG shaft speed is controlled to the optimal speed that is calculated using Tip Speed Ratio. ( Simulation and Hardware )
- Using Hill Climbing Technique, the SRG shaft speed is perturbed in the direction of increasing power. ( Hardware )

Speed control loop compares the actual SRG shaft speed with the reference speed provided by the MPPT Controller and uses PI controller to generate the current reference. The four current control loops use hysteresis to control the phase currents. A voltage control loop uses PWM control of the dump load chopper to maintain the generation bus DC voltage. The power dissipated in the dump load is the output power of the system.

## **Chapter 2**

### **Literature Survey**

An accurate SR machine model can be generated using finite element method computation if the dimensions and materials used for different parts of the machine are known or by actual measurements of inductance and torque for incremental angular positions and incremental currents. Alternatively, an approximate model can be analytically generated using a few easily measurable parameters [11][12].

Some power electronic converter circuit topologies for SR machines share components between the machine phases or use a single switch per machine phase [5]. While these converter topologies have the advantages of reduced component count and reduced switching loss they also have disadvantages like reduced control flexibility and redundancy. The asymmetric half bridge converter (AHBC) provides the most flexibility for control and redundancy [5] and is the most widely used in literature.

The generated torque and power of the SRG is controlled by controlling the excitation current. Below base speed, the induced emf is less than the rated DC bus voltage and the excitation must be turned on repeatedly to maintain the phase current level. Due to non-linearity of the machine, a proportional integral (PI) controller with gain scheduling based on position and current is needed [13]. Alternatively, simple hysteresis current control is also effective [14][15][16]. Above base speed the induced emf is larger than the

rated DC bus voltage and the phase current is controlled by adjusting the excitation turn-on and turn-off angles [17].

There are several techniques for maximum power point tracking (MPPT) of a wind turbine. The most accurate techniques make use of wind speed sensors like cup anemometers, and the wind turbine characteristic curves [15]. SODAR (Sound Detection and Ranging) or LIDAR (Light Detection and Ranging) sensors can detect changes in wind speed and direction ahead of the wind-turbine and take advance action [18]. Sensor based MPPT is more accurate and fast. The disadvantages are the need for the additional wind sensor with proper positioning and the requirement for wind turbine parameter data. A sensor-less MPPT scheme uses wind turbine parameters for estimation of the optimal power curve  $P_{\text{opt}} = K_{\text{opt}}\omega_r^3$ , where  $\omega_r$  is the generator side rotational speed and  $K_{\text{opt}}$  is a constant that depends on blade aerodynamics, gear box ratio and wind turbine parameters [19]. The disadvantage of this scheme is that wind turbine parameter data is needed for calculations. Other sensor-less MPPT schemes use hill climbing techniques that perturb the shaft speed in the direction of increased generated power [20]. The advantage of hill climbing schemes is that knowledge of wind turbine data is not needed. The disadvantages are the hunting of shaft speed around the optimum speed due to constant perturbing. Both the sensor-less schemes have the disadvantage of delayed response as the controller reacts after a change in wind speed.

# Chapter 3

## Theory and Equations

### 3.1 Switched Reluctance Generator Theory

A cross-sectional view of a four phase, 8/6 SR machine is shown in Fig 3.1. It has eight stator poles ( $A, A', B, B', C, C', D, D'$ ) and six rotor poles.

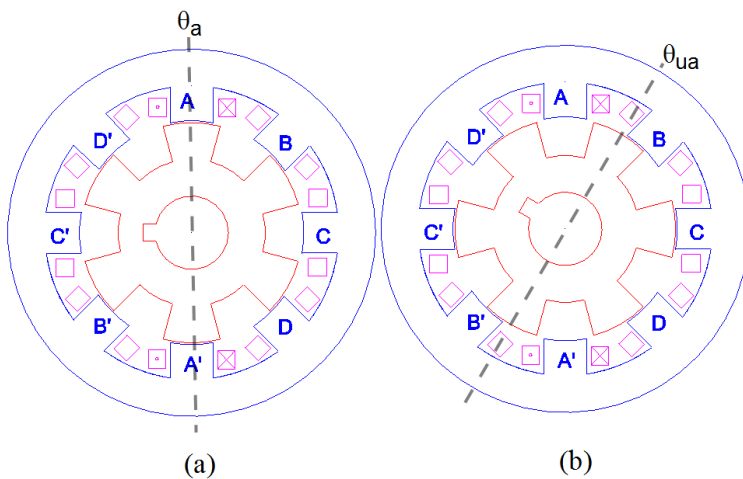


Fig 3.1 Cross sectional view of 8/6 switched reluctance machine

When the rotor tooth is at  $\theta_a$ , it is in the aligned position for phase A as in Fig 3.1(a). When the rotor is rotated clockwise by  $30^\circ$ , and the rotor tooth is centered at  $\theta_{ua}$  it is in the unaligned position for phase A as in Fig 3.1(b). The phase inductance varies from

minimum at the unaligned position to maximum at the aligned position as shown in Fig 3.2. The phase inductance also varies with changes in phase current. As the phase current increases from  $I_1$  to  $I_3$ , the inductance decreases due to saturation.

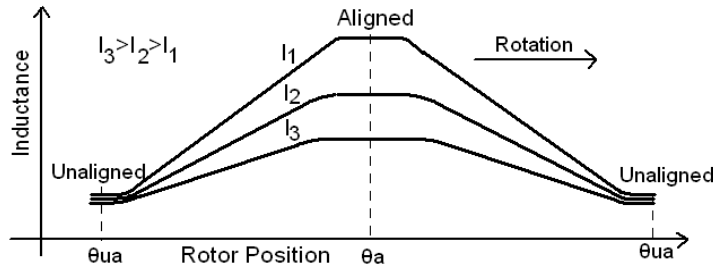


Fig 3.2 Variation of phase inductance with rotor position and phase current.

The torque production in a SR machine is based on the principle that a magnetic field tends to align a magnetic material to its minimum reluctance position. In generation mode, the stator pole is excited when a rotor pole is aligned with it and the magnetic flux lines have minimum length as seen in Fig 3.3(a). When the rotor pole is moved away by the prime-mover, negative reluctance torque is generated as the magnetic flux lines are stretched as seen in Fig 3.3(b) and work is done against the magnetic field. This results in the conversion of mechanical energy into magnetic field energy. When the winding is de-energized and the magnetic field collapses this magnetic field energy is converted to electrical energy. In generation mode, the movement of a rotor pole from aligned to unaligned position is known as one stroke.

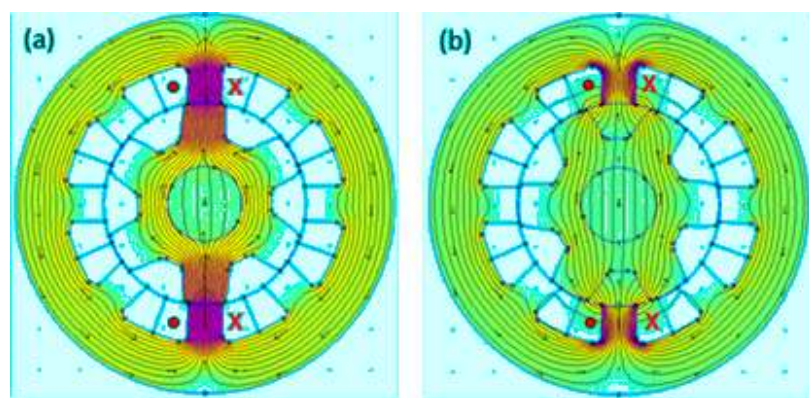


Fig 3.3 Variation of magnetic flux paths with rotor position.

Converter configuration for AHBC for one phase of the SRG is shown in Fig 3.4(a). The AHBC consists of two high frequency switches,  $S_1$  and  $S_2$ , and diodes,  $D_1$  and  $D_2$ ,

connected to a stator winding of the SRG.  $R_{ph}$  is the phase resistance,  $\lambda(i_{ph}, \theta)$  is the phase flux linkage,  $l(i_{ph}, \theta)$  is the incremental phase inductance,  $u_{ph}$  is the dc bus voltage and  $i_{ph}$  is the phase current.

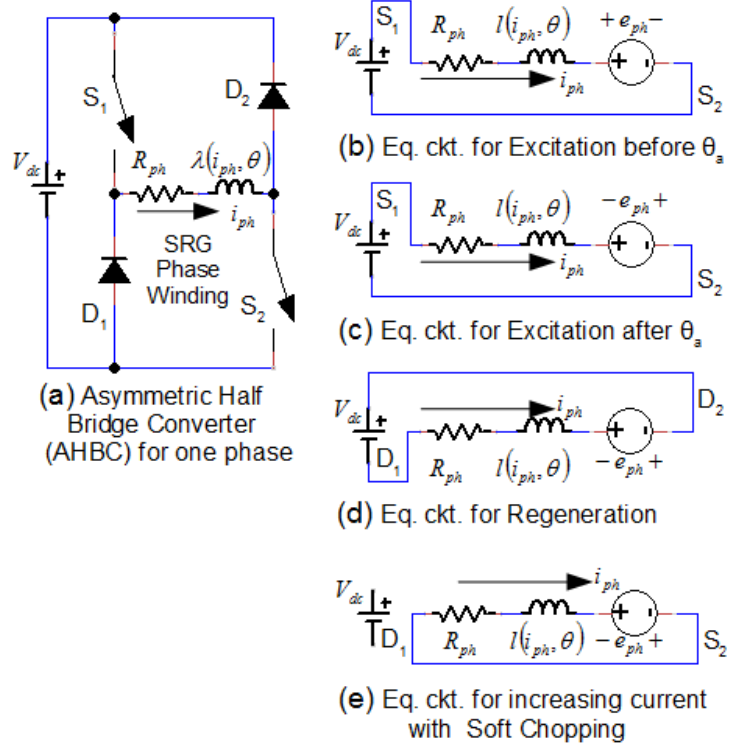


Fig 3.4 AHBC for one phase with equivalent circuits

The phase voltage equation of the SRG is given by

$$u_{ph} = R_{ph}i_{ph} + \frac{d\lambda(i_{ph}, \theta)}{dt} \quad (3.1)$$

$$u_{ph} = R_{ph}i_{ph} + \frac{\partial\lambda(i_{ph}, \theta)}{\partial i_{ph}} \frac{di_{ph}}{dt} + \frac{\partial\lambda(i_{ph}, \theta)}{\partial \theta} \frac{d\theta}{dt} \quad (3.2)$$

$$u_{ph} = R_{ph}i_{ph} + l(i_{ph}, \theta) \frac{di_{ph}}{dt} + e_{ph} \quad (3.3)$$

For speed,  $\omega_r = \frac{d\theta}{dt}$ ,

the induced emf is  $e_{ph} = \omega_r \frac{\partial\lambda(i_{ph}, \theta)}{\partial \theta}$

and incremental inductance is  $l(i_{ph}, \theta) = \frac{\partial\lambda(i_{ph}, \theta)}{\partial i_{ph}}$

$l(i_{ph}, \theta)$  is the slope of the magnetization curve at position  $\theta$  for current  $i_{ph}$ .

Thus Eq 3.3 is similar to a separately excited DC motor voltage equation with the right hand side terms corresponding to the resistive voltage drop, inductive voltage drop and induced emf.

Substituting the incremental inductance in Eq 3.2 and multiplying by current gives the instantaneous input power  $p_{ph}$  as

$$p_{ph} = u_{ph} i_{ph} = R_{ph} i_{ph}^2 + l(i_{ph}, \theta) i_{ph} \frac{di_{ph}}{dt} + i_{ph}^2 \frac{dl(i_{ph}, \theta)}{dt} \quad (3.4)$$

Noticing that

$$\frac{d}{dt} \left[ \frac{1}{2} l(i_{ph}, \theta) i_{ph}^2 \right] = l(i_{ph}, \theta) i_{ph} \frac{di_{ph}}{dt} + \frac{1}{2} i_{ph}^2 \frac{dl(i_{ph}, \theta)}{dt} \quad (3.5)$$

Substituting Eq 3.5 in Eq 3.4 gives

$$p_{ph} = u_{ph} i_{ph} = R_{ph} i_{ph}^2 + \frac{d}{dt} \left[ \frac{1}{2} l(i_{ph}, \theta) i_{ph}^2 \right] + \frac{1}{2} i_{ph}^2 \frac{dl(i_{ph}, \theta)}{dt} \quad (3.6)$$

The Eq 3.6 is in the familiar form implying that the electrical power in the phase is the sum of the resistive loss, rate of change of field energy and the air gap power  $p_a$  given by the last term.

$$p_a = T_e \omega_m = T_e \frac{d\theta}{dt} = \frac{1}{2} i_{ph}^2 \frac{l(i_{ph}, \theta)}{dt} \quad (3.7)$$

$$T_e = \frac{1}{2} i_{ph}^2 \frac{l(i_{ph}, \theta)}{d\theta} \quad (3.8)$$

SR machine torque depends on the square of the phase current and the rate of change of phase inductance with position. During generation, the SR machine operates in the region from aligned to unaligned position where  $dl/d\theta$  is negative so torque  $T_e$  is negative. The direction of the torque is to oppose the movement of the rotor tooth away from the aligned position. Continuous unidirectional torque can be produced by synchronizing each phase's excitation with the rotor position.

Fig 3.4(b) shows the phase equivalent circuit for excitation before the aligned position with switches  $S_1$  and  $S_2$  conducting. Since the machine is operating in the region of

increasing flux linkages, the induced emf,  $e_{ph}$  opposes the increase in phase current. Fig 3.4(c) shows the phase equivalent circuit for excitation after the aligned position with switches  $S_1$  and  $S_2$  conducting. Since the machine is operating in the region of decreasing flux linkages, the induced emf,  $e_{ph}$ , assists the increase in phase current. Fig 3.4(d) shows the phase equivalent circuit during regeneration when switches  $S_1$  and  $S_2$  are turned off and diodes  $D_1$  and  $D_2$  are conducting and current is fed back to the dc bus. During regeneration if the phase current falls below the reference value the switches  $S_1$  and  $S_2$  can be turned on again as in Fig 3.4(c) and the dc bus voltage can be used to build up phase current. This is known as hard chopping. Fig 3.4(e) shows the phase equivalent circuit when only switch  $S_2$  is turned on after the aligned position. The winding is shorted through switch  $S_2$  and diode  $D_1$  and the induced emf,  $e_{ph}$ , is used to build up current in the phase winding to the rated value. This is known as soft chopping. Soft-chopping has advantages like lower dv/dt, lower switching loss, lower current ripple, lower torque ripple and lower acoustic noise [5].

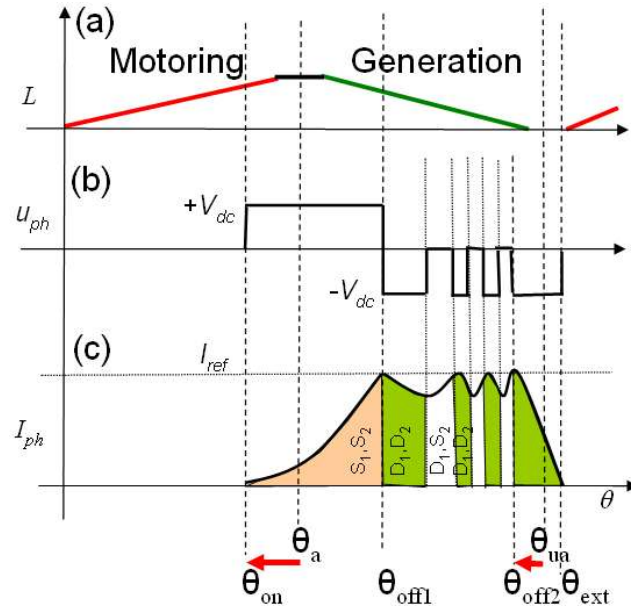


Fig 3.5 Generation mode waveforms for one phase below base speed with soft chopping

Fig 3.5 shows the waveforms for one phase in generation mode with soft chopping. Fig 3.5(a) shows the variation of phase inductance ( $L$ ) with rotor position ( $\theta$ ). Fig 3.5(b) shows the variation of phase voltage ( $u_{ph}$ ) which depends on the state of switches  $S_1$  and  $S_2$ . At the aligned position  $\theta_a$ , the phase inductance is large, so the phase is excited by turning on switches  $S_1$  and  $S_2$  at  $\theta_{on}$  before the aligned position, so that the current has

time to build-up as shown in Fig 3.5(c). Below base speed, the induced emf,  $e_{ph}$  is typically less than the supply voltage  $u_{ph}$  and the phase current  $i_{ph}$  falls when the switches are turned off at  $\theta_{off1}$ . Switch  $S_2$  is turned on again repeatedly to increase the current back to the reference value. At  $\theta_{off2}$ , near the unaligned position, the switches are finally turned off to enable the current to fall to zero before the rising inductance slope. Hysteresis current control (HCC) is used to maintain the current at the reference level.

AHBC with separate excitation and generation dc buses, as shown in Fig 3.6, is used for the four phase machine. A chopper controlled dump load consisting of switch  $S_L$  and resistor  $R_L$  is used to maintain the generation bus voltage at rated value. In an actual wind energy conversion system, a battery charging system or a grid interface converter would be used in place of the dump load. Part of the generated current, as required to maintain excitation bus voltage, is fed back to the excitation bus capacitor  $C_E$  over diode  $D_E$ .

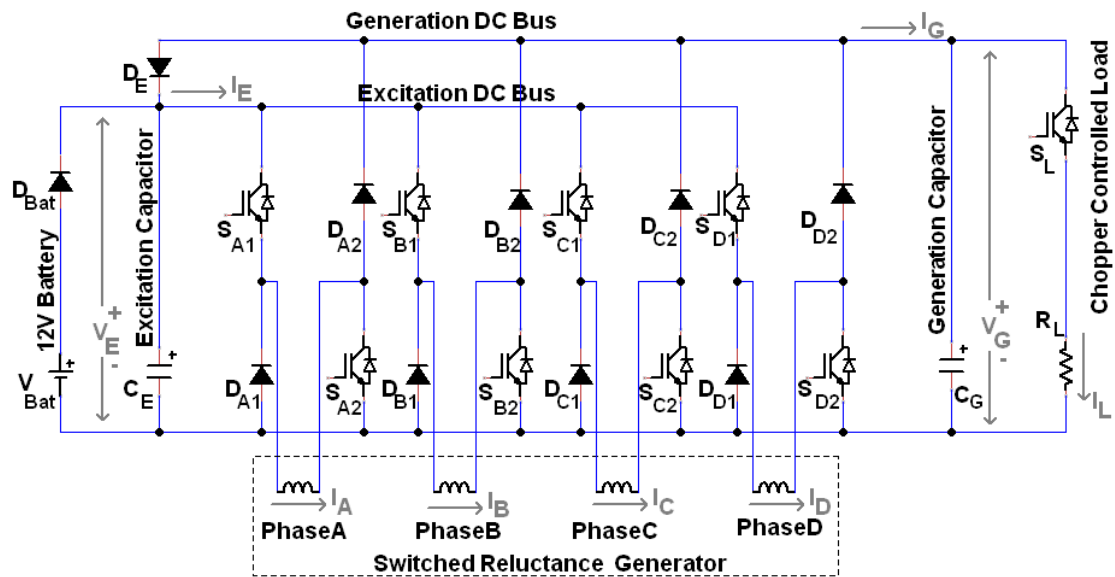


Fig 3.6 Asymmetric half bridge converter circuit with separate excitation and generation buses

## 3.2 Wind Turbine Theory

The kinetic energy in wind is given by the equation

$$E_k = \frac{1}{2}mv^2 \quad (3.9)$$

The mass of wind incident on the swept area of the wind turbine per second is

$$m = \rho Av \quad (3.10)$$

where  $\rho=1.225 \text{ kg/m}^3$  is the density of air,  $A = \pi R^2$  is the rotor-swept area of the wind-turbine and  $v$  is the velocity of the wind.

From Eq 3.9 and Eq 3.10 the power in wind incident on the wind turbine is given by

$$P_{WindInput} = \frac{1}{2} \rho A v^3 \quad (3.11)$$

The mechanical output of the wind-turbine is given by

$$P_m = C_p(\lambda, \beta) \frac{1}{2} \rho A v^3 \quad (3.12)$$

The efficiency of the wind-turbine depends on the power coefficient  $C_p$  [21].  $C_p$  is the ratio of the fraction of energy extracted by the wind-turbine to the energy of the moving air mass that would pass through the rotor-swept area if the wind turbine was absent. For an open flow system without flow concentrators like ducts or diffusers, the maximum value of  $C_p$  is given by the Betz limit as 0.5925.

$$C_p(\lambda, \beta) = c_1(c_2/\lambda_i - c_3\beta - c_4)e^{-c_5/\lambda_i} + c_6\lambda \quad (3.13)$$

where

$$\frac{1}{\lambda_i} = \frac{1}{\lambda + 0.08\beta} - \frac{0.035}{\beta^3 + 1}$$

$$\text{The Tip Speed Ratio is } \lambda = \frac{\omega R}{v} \quad (3.14)$$

$R$  is the radius of the rotor blades,  $\beta$  is the rotor blade pitch angle,  $\omega$  is the wind turbine shaft speed and  $v$  is the wind velocity.

For Mod2 wind-turbine used in Simulink the coefficients  $c_1$  to  $c_6$  are  $c_1=0.5176$ ,  $c_2=116$ ,  $c_3=0.4$ ,  $c_4=5$ ,  $c_6=0.0068$ . The  $C_p$ - $\lambda$  characteristics for different values of the pitch angle  $\beta$

are shown in Fig 3.7. The maximum value of  $C_p$  ( $C_{p\max} = 0.48$ ) is achieved for  $\beta=0^\circ$  and  $\lambda=8.1$ . This value of  $\lambda$  is defined as the nominal value  $\lambda_{nom}$ .  $C_p$  and  $P_m$  are maximum for an optimal value of  $\lambda_{nom}$  [22].

Thus from Eq 3.12 and Eq 3.14 for a given wind speed ( $v$ ), power output of the wind turbine increases ( $P_m \uparrow$ ) as the rotor size increases ( $A \uparrow, R \uparrow$ ). As the rotor size increases, to maintain optimal value of  $\lambda_{nom}$ , the rotor speed decreases ( $\omega \downarrow$ ).

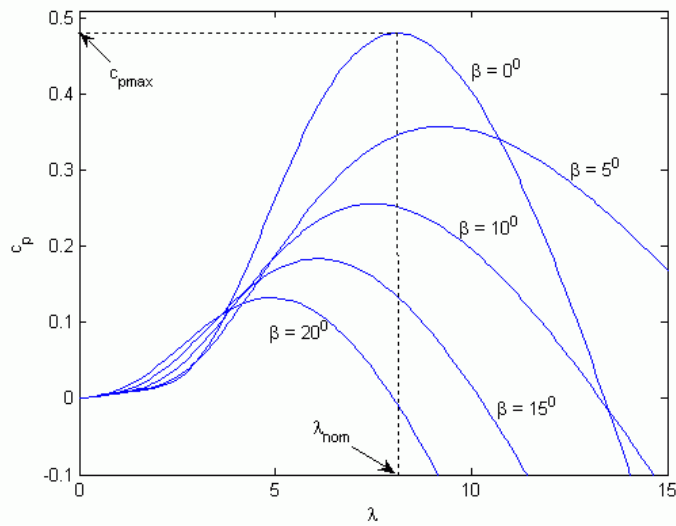


Fig 3.7  $C_p$  vs  $\lambda$  for various  $\beta$ . Graph for Mod2- Two Blade wind turbine [22]

Wind turbine characteristics for various wind speeds are shown in Fig 3.8. MPPT controller should sense the actual wind speed  $v$ , and adjust the turbine shaft speed  $\omega$ , so that optimal tip speed ratio  $\lambda_{opt}$  is maintained. As wind speed changes from  $v_1$  to  $v_2$ , the shaft speed should change from  $\omega_{opt1}$  to  $\omega_{opt2}$  so that maximum power is obtained as shown by the  $P_{opt}$  curve.

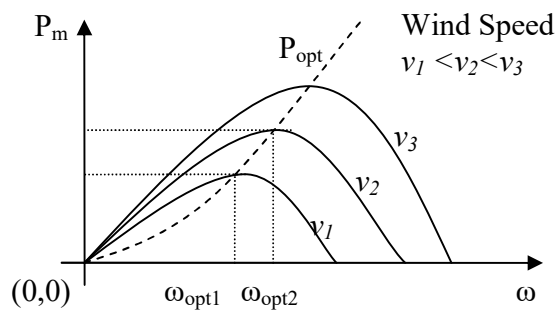


Fig 3.8 Variation of wind turbine mechanical output power ( $P_m$ ) with wind turbine shaft speed ( $\omega$ ) for various wind speeds ( $v_n$ )

## Chapter 4

### Simulation Results

A MATLAB simulation is done to analyze the working of an SRG for implementation of MPPT in a wind energy system. The block diagram of the wind energy conversion system is shown in Fig 4.1. The Simulink model is shown in Fig 4.2 and the major blocks are explained in the following sections.

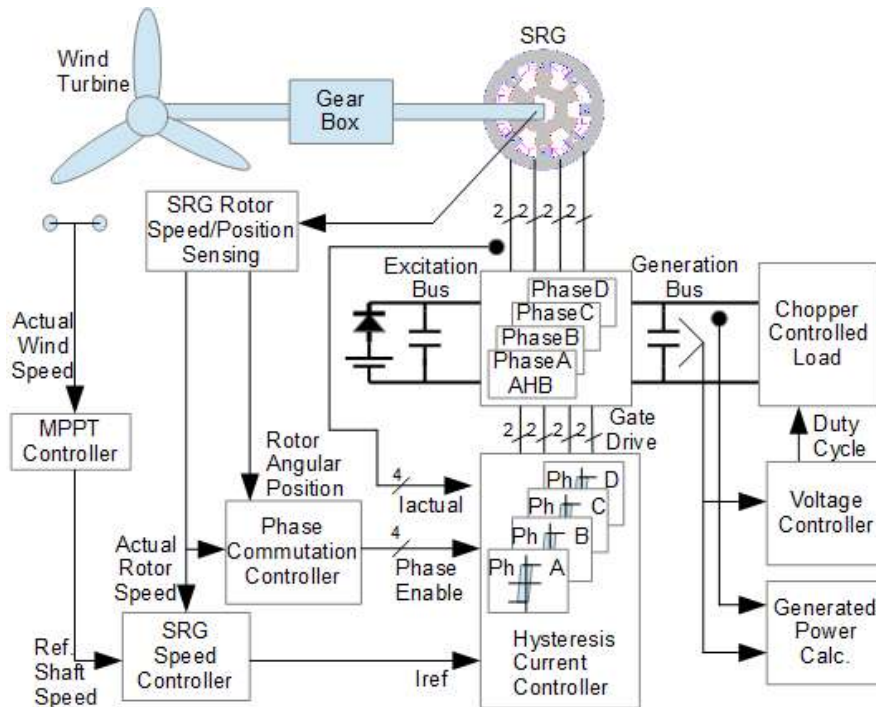


Fig 4.1 Block diagram of wind energy conversion system

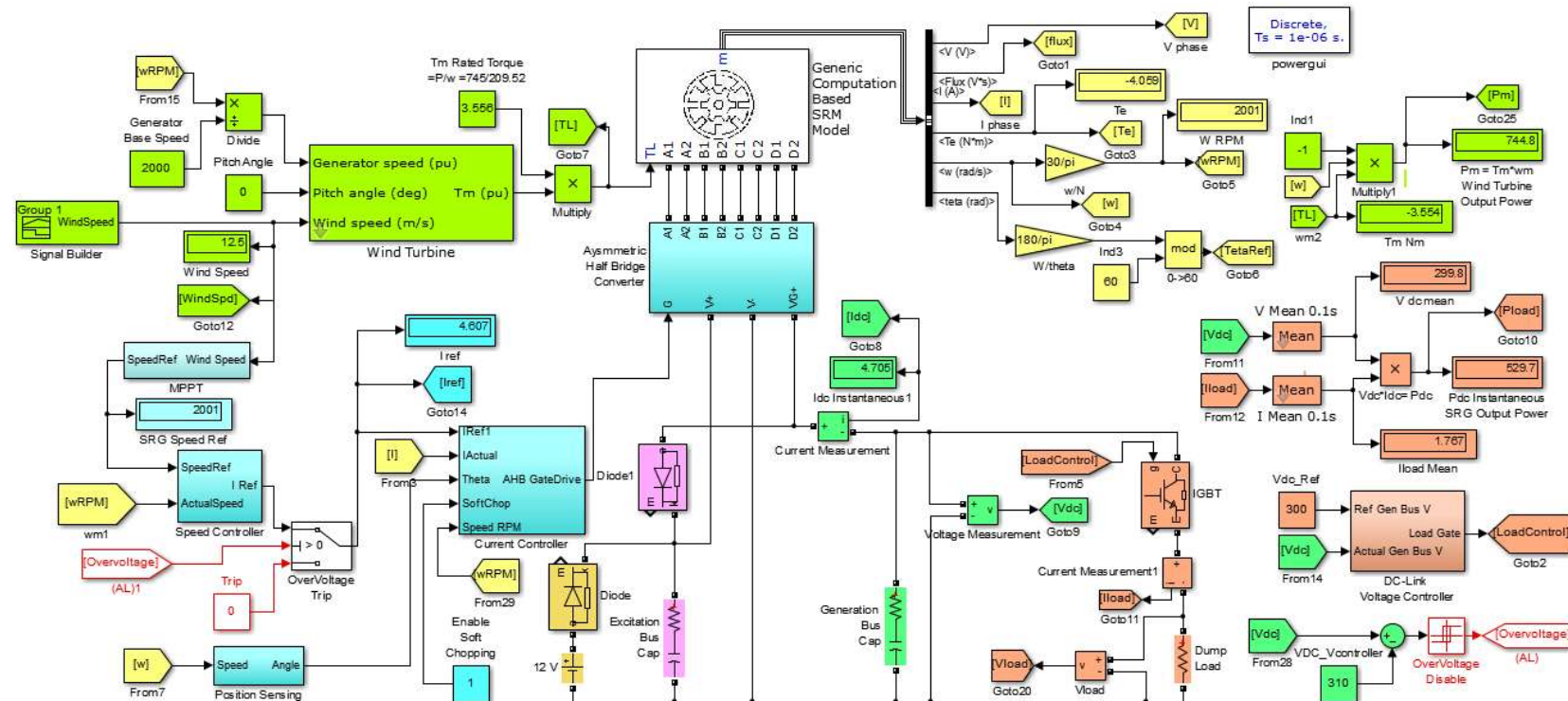


Fig 4.2 Simulink Simulation of Wind Energy Conversion System using Switched Reluctance Generator

## 4.1 Switched Reluctance Generator (SRG) – Generic Model

The Simulink SR machine model is used with the generic option. A 745W, 8/6 SRG is used in the simulation as a similar machine is planned for the hardware implementation. Since the physical machine was not available during the early stages of the project, machine data from similar machines found in literature was used [23] with some modifications in the aligned inductance values to enhance the characteristics and hence machine performance. As the project progressed more information on the motor construction was available from the manufacturer so FEMM analysis was performed and the simulation was rerun using the FEMM results as described in section 4.8

The SR machine model is configured using the following parameters:

Machine Type: 8/6, Machine Model : Generic, Stator Resistance :  $2.15 \Omega$ , Inertia :  $0.004 \text{ Kgm}^2$ , Unaligned Inductance :  $8.7 \text{ mH}$ , Unsaturated Aligned Inductance :  $250 \text{ mH}$ , Saturated Aligned Inductance :  $0.5 \text{ mH}$ , Maximum Current :  $5 \text{ A}$ , Maximum Flux Linkage :  $0.3 \text{ Vs}$ , Initial position : zero rad

The Simulink “generic” model assumes standard symmetric SRM construction and internally uses a non-linear function to represent the variation of magnetic flux linkage as a function of rotor position [11]. The Simulink “generic” model calculates flux as a function of current and position. The magnetization characteristic of the SRG showing variation in flux linkages with current for various rotor positions from aligned to unaligned position is plotted using MATLAB as shown in Fig. 4.3.

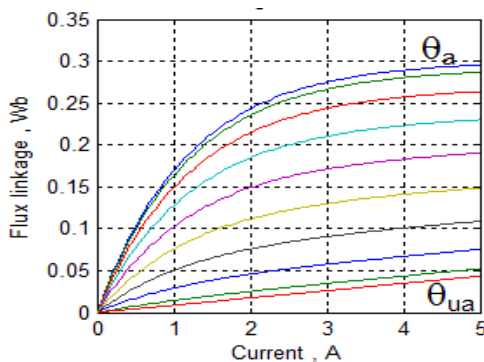


Fig 4.3 Magnetization characteristics of SR machine “generic” model

The Simulink SR Machine model internally generates 2D look-up tables - ITBL for Current (Flux, Angular Position) and TTBL for Torque (Current, Angular Position). Fig 4.4 shows the SR machine model for stator phases. Voltage, flux, torque and position signals are multiplexed for the four phases. The voltage across the machine model phase terminals is obtained from the power converter switching pattern and is used by the model for calculating flux. The current is calculated by the model from flux and the angular position using ITBL and is injected at the machine model's terminals as shown in Fig 4.5. Electrical torque is calculated from current and angular position using TTBL.  $T_e$  is the total electrical torque of the machine and is the sum of the electrical torques of the individual phases. Speed  $w$  is calculated from  $T_e$ , load torque  $T_L$ , inertia and friction.

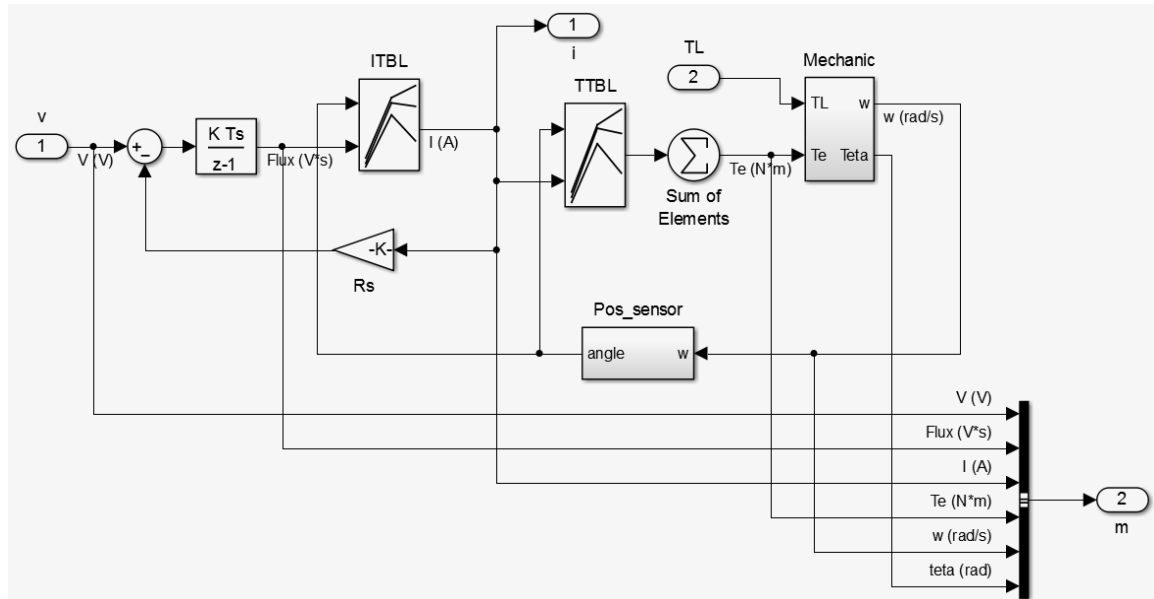


Fig 4.4 Circuit for machine phase in Simulink SRM model [22]

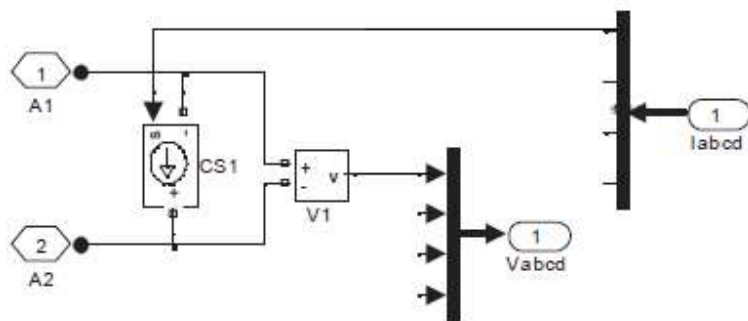


Fig 4.5 Phase connector for Simulink SRM model [11]

## 4.2 Wind Turbine Simulation

As per theory in section 3.2 the Simulink per-unit model for Mod2 wind turbine is configured for 745 W as 1 pu of output mechanical power of the wind turbine at rated

wind speed of 12.5 m/s. For  $C_p=0.48$ , and from Eq 3.12,  $A = \frac{2P_m}{C_p \rho v^3}$ ,  $R = \sqrt{\frac{A}{\pi}}$ , the

turbine radius is calculated as 0.908 m. For  $\lambda=8.1$  and from Eq 3.14  $\lambda = \frac{\omega R}{v}$  the rated

turbine speed calculated as 1064 rpm and corresponds to 1 pu. SRG rated speed of 2000 rpm is selected, so that the phase current needed to generate the required torque is within the ratings of the machine. Gear ratio of 1.88 is assumed to match the wind turbine rated speed with the SRG rated speed. Simulink internally uses Eq 3.12-Eq 3.14 for generation of the wind turbine characteristics as shown in Fig 4.6. Wind turbine maximum output power and shaft speed for the selected wind speeds is shown in Table 4.1

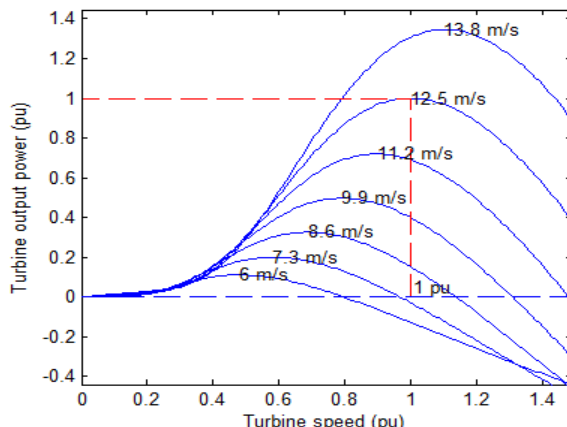


Fig 4.6 Wind turbine characteristic [22]

Table 4.1 Wind Turbine maximum output power and shaft speed for the selected wind speeds

Wind Speed (m/s)	Turbine speed for $P_{max}$ (pu)	Turbine $P_{out}$ (pu)	SRG speed for $P_{max}$ (rpm)	Turbine $P_{out}$ (W)
8.6	0.7	0.32	1400	238
12.5	1	1	2000	745
13.8	1.1	1.35	2200	1005

### 4.3 MPPT Controller

The MPPT controller uses the tip speed ratio from Eq. 3.14. The wind speed is sensed and the optimal SRG speed is calculated as shown in Fig 4.7. Fig 4.14(a) and Fig 4.14(b) give the input and output waveforms for the MPPT controller.

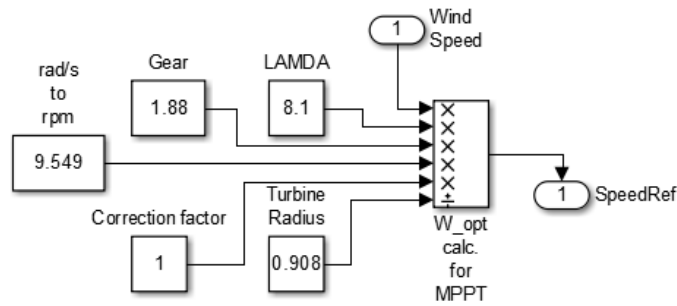


Fig 4.7 MPPT Controller using sensed wind speed and Tip Speed Ratio

MPPT using Hill-Climbing was attempted for the simulation but the current control needed a very small simulation step-size while the hill climbing algorithm required a run time in tens of seconds. As a result the simulations took a very long time to execute thereby causing MATLAB to hang. Hill climbing has been successfully implemented in hardware, as described in Section 5.7.4.2 and Section 6.3.1.2.

### 4.4 Speed Controller

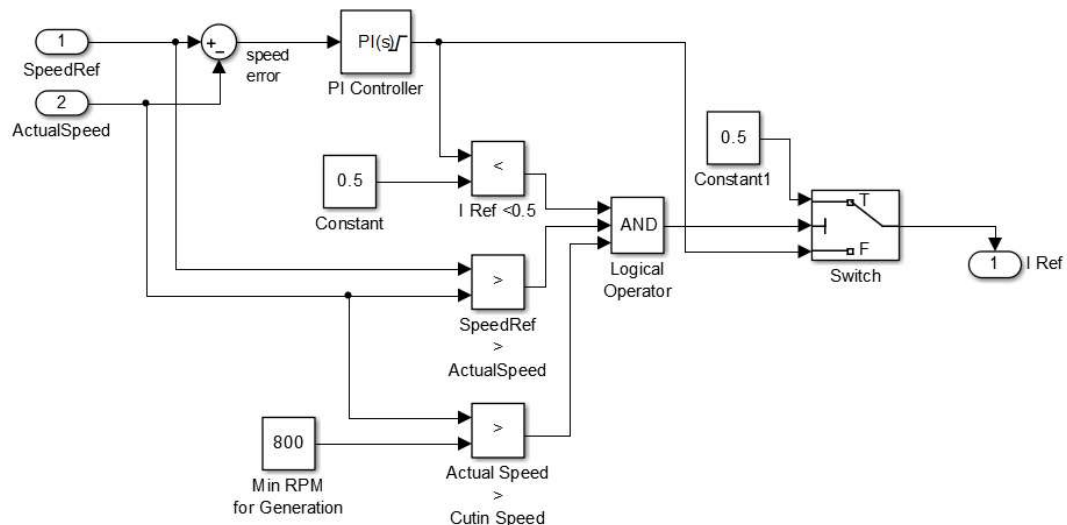


Fig 4.8 SRG Speed Controller

The SRG speed controller, shown in Fig 4.8, compares the actual SRG shaft speed with the speed reference from the MPPT controller and uses PI control to generate the current reference from the speed error. Some additional logic is added to enable minimum generation once the cut-in speed is reached. Fig 4.14(b)-(d) gives the waveforms for the speed controller.

## 4.5 Position Sensing

As mentioned in section 4.1, the SRM model is configured for initial angular position as  $0^\circ$ , corresponding to Phase A aligned position. The position sensing logic, as shown in Fig 4.9, integrates the speed to get the mechanical angular position. Initial values for the integrator are  $[0^\circ -15^\circ -30^\circ -45^\circ]$  corresponding to [PhaseA PhaseB PhaseC PhaseD] with Phase A at aligned position. The integrator output is divided by  $60^\circ$  to give the electrical angle of each of the four phases multiplexed on the “Angle” output. The “Angle” output of  $0^\circ$  corresponds to the phase aligned position,  $30^\circ$  corresponds to the phase unaligned position. The sequence repeats every  $60^\circ$  for an 8/6 machine. The output of the position sensing logic for Phase A is shown in Fig 4.14 (f).

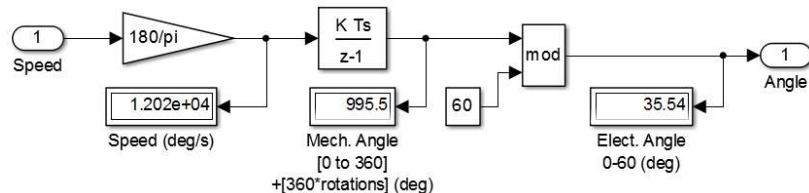


Fig 4.9 SRG Position sensing

## 4.6 Phase Commutation Controller

The phase commutation controller, shown in Fig 4.10, enables the phase at the correct angular position.  $\theta_{on}$  and  $\theta_{off}$  are manually adjusted for minimum torque ripple at fixed speeds and then interpolated over the entire speed range using Look-Up Tables as shown in Fig 4.11. Fig 4.14 (g) shows the Phase A enable signal.

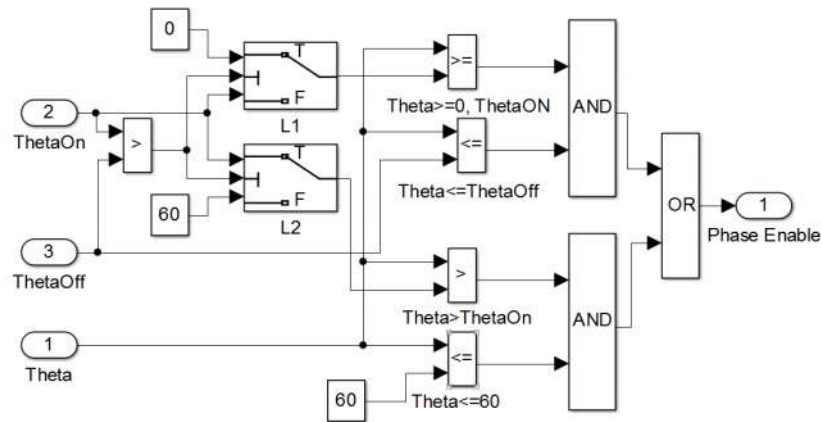


Fig 4.10 SRG Phase Commutation Controller Logic

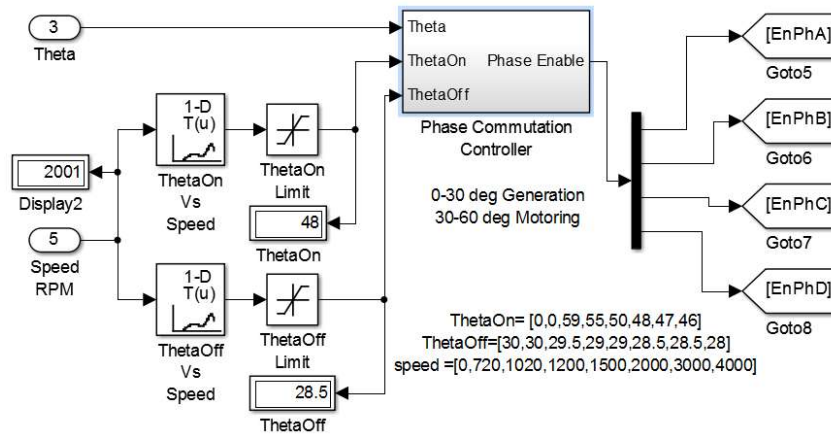


Fig 4.11 SRG Phase Commutation Controller with Turn-On and Turn-Off angle advance tables

## 4.7 Hysteresis Current Controller

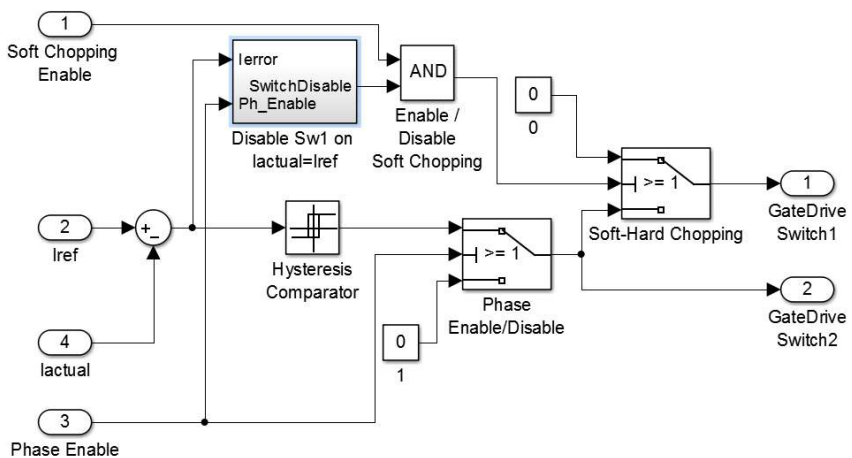


Fig 4.12 Hysteresis Current Controller

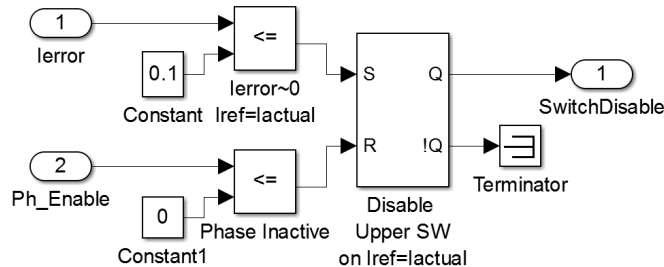


Fig 4.13 Upper Switch Disable Logic

The current reference from the speed controller and the phase enable signal from the phase controller are inputs to the phase hysteresis current controller (HCC) as shown in Fig 4.12. The HCC output is used to drive the switches of the AHBC when the phase is enabled. In soft-chopping mode, once the current reaches the reference value the upper switch in the phase AHBC is disabled for the rest of the stroke using the logic circuit shown in Fig 4.13.

The signals shown in Fig 4.14(d)-(g) are the inputs to the Phase HCC and its outputs are shown in Fig 4.14(h)-(i). The resulting Phase A voltage waveform is shown in Fig 4.14(j). For Phase A, on phase enable at  $\theta_{on}$ , switches  $S_{A1}$  and  $S_{A2}$  are turned on. The excitation dc bus voltage,  $V_E$  is applied across the phase winding till the actual phase current equals the reference phase current, then both switches are turned off and switch  $S_{A1}$  is disabled for the rest of the stroke. Once both switches are turned off, regeneration current flows through the diodes  $D_{A1}$  and  $D_{A2}$  and negative regeneration bus voltage,  $-V_G$ , appears across the phase winding. When the phase current falls below the reference current, only switch  $S_{A2}$  is turned on again, effectively shorting the phase winding. This allows the phase current to build-up again using the induced emf. Once the actual phase current reaches the reference value, switch  $S_{A2}$  is turned off and again the regeneration current flows through diodes  $D_{A1}$  and  $D_{A2}$  to the generation dc bus. This process is repeated until  $\theta_{off}$ .

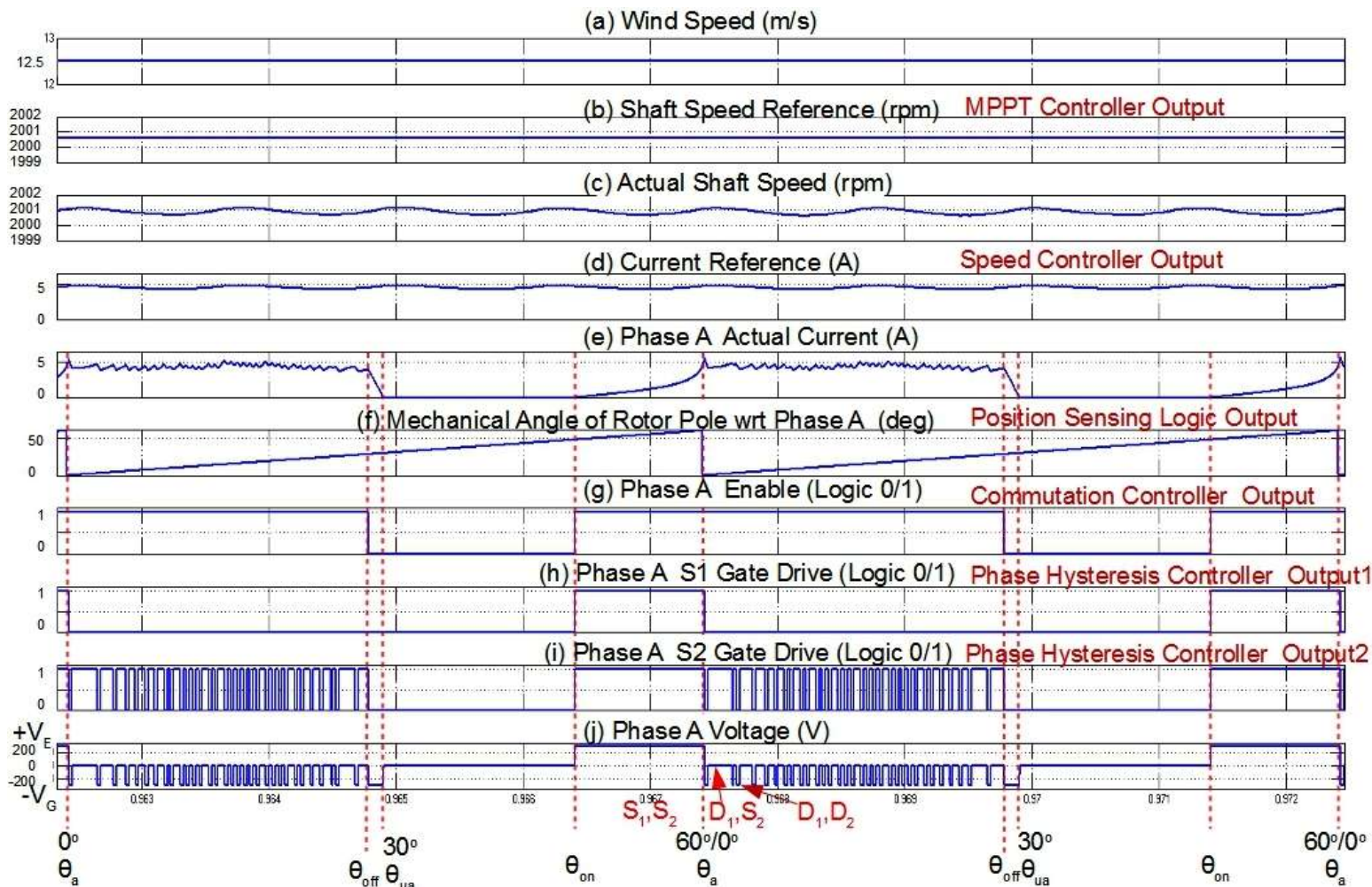


Fig 4.14 Waveforms for MPPT Controller, Speed Controller and Phase A waveforms for Position Sensing Logic, Commutation Controller and Phase Hysteresis Controller

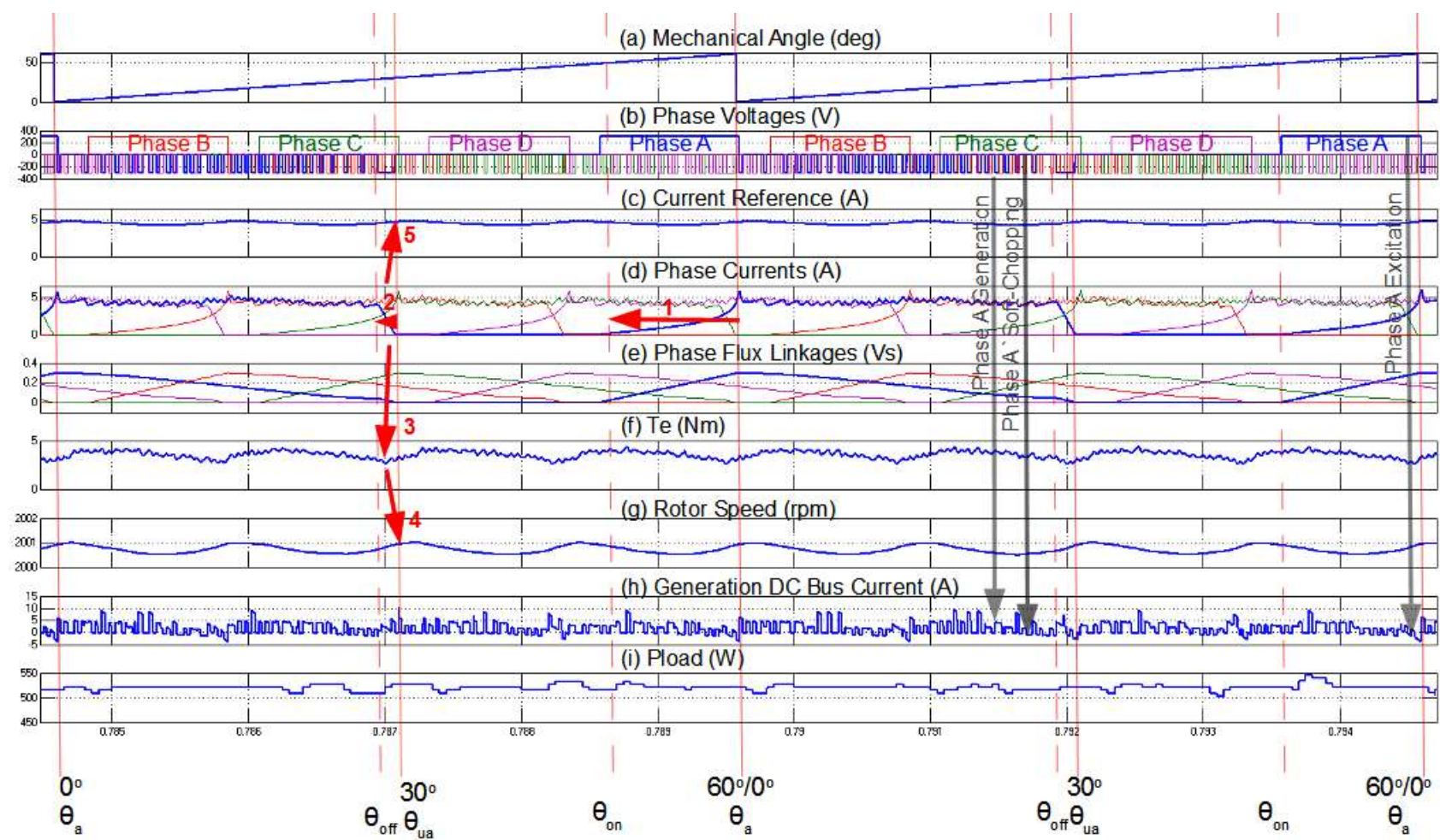


Fig 4.15 Waveforms for SR Generator

Fig 4.15 shows the waveforms of key system variables for all four phases with wind speed of 12.5 m/s. Fig 4.15(a) shows the angular position of the rotor with respect to Phase A, varying from zero to 60 degrees.

Motor rotation direction is counter-clockwise with motor phase positions as shown in Fig 3.1. The colors blue, red, green and violet are used for phase A, B, C and D to indicate the phase voltages, currents and flux linkages in Fig 4.15(b), (d) and (e) respectively. The current reference waveform is shown in Fig 4.15(c). Fig 4.15(e) shows the flux linkages of the phase windings that increase from zero at  $\theta_{on}$ , to the rated value of 0.3 Vs near the aligned position and decrease back to zero when the phase current falls to zero. The total electrical torque,  $T_e$  developed by the SRG is shown in Fig 4.15(f). SRG rotor speed is shown in fig 4.15(g).

The advance angles for  $\theta_{on}$  and  $\theta_{off}$  for Phase A is shown by the red arrows 1 and 2. During phase change-over there is a decrease in the net current in the phases generating braking torque, this results in a decrease in the braking torque as indicated by red arrow 3. Decrease in braking torque results in increase in the rotor speed as indicated by the red arrow 4. The speed controller attempts to correct this increase in rotor speed by increasing the current reference as indicated by the red arrow 5. By adjusting the  $\theta_{on}$  and  $\theta_{off}$  times and shaping the individual phase reference currents it is possible to reduce or even eliminate the torque ripple during phase changeover.

The actual phase current follows the current reference but high frequency ripple is observed due to the hysteresis current control. Small amplitude high frequency torque ripple is observed due to the effect of hysteresis current control and larger amplitude lower frequency torque ripple is observed due to phase change over. Ripple in rotor speed corresponds to the torque ripple with some smoothing effect due to rotor inertia.

Generation dc bus current corresponding to the total of all the phase currents during regeneration is shown in Fig 4.15(h). With one phase generating, the typical peak value of the generated current pulse is equal to the current reference of approximately 5A at wind speed of 12.5m/s. The pulse peaks of approximately 10A are due to the simultaneous generation of two phases. The regions between the current pulses correspond to the flux build up periods when the phase windings are shorted and phase current is built up to the reference value. The lower positive peaks and negative current

pulses correspond to the current drawn by the excitation bus over diode  $D_E$ . Fig 4.15(i) shows the average dc power available at the load for the given wind speed of 12.5 m/s.

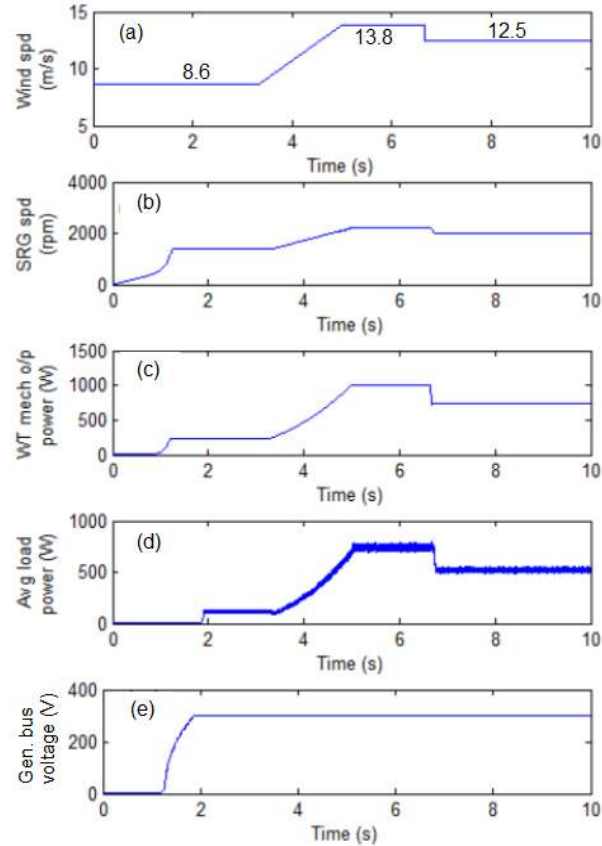


Fig 4.16 Maximum power point tracking with changes in wind speed

For changes in wind speed as shown in Fig 4.16(a), the MPPT controller adjusts the SRG shaft speed as shown in Fig 4.16(b). Maximum wind turbine output power is tracked as shown in Fig 4.16(c) and average power available with the load is shown in Fig 4.16(d). Initial excitation is provided by a 12 V dc battery and the dc bus voltage is built up to rated voltage of 300 V DC in 2 s as shown in Fig 4.16(e). Voltage is maintained at 300 V dc by the chopper controlled dump load.

Table 4.2 System performance with variation in wind speed.using SR Machine “generic” model

Wind Speed (m/s)	SRG speed (rpm)	Turbine Output (W)	$P_{load}$ (W)	$I_{ph}$ (A)
8.6	1377	242	120	2.6
12.5	2001	745	520	4.5
13.8	2210	1002	740	5.25

Table 4.2 summarizes the MPPT results and they compare well with the ideal values obtained from the wind turbine characteristics shown in Table 4.1. As the wind speed increases, the SRG speed is increased to track maximum power. The phase current reference is adjusted by the speed loop to generate the optimum torque needed to maintain the optimum speed for maximum power. As phase current increases, the machine operates in the non-linear saturated region of its magnetic characteristics resulting in increased energy conversion and efficiency. In order to limit wind turbine speed and mechanical power to safe limits, it is assumed that necessary mechanical control systems for pitch, stall or furl are available.

## 4.8 Switched Reluctance Generator (SRG) –Specific Model

Using the motor design data given by the SR machine manufacturer a FEMM model was developed and solved. Fig 4.17 shows the FEMM results for Phase A aligned position with phase current of 6A.

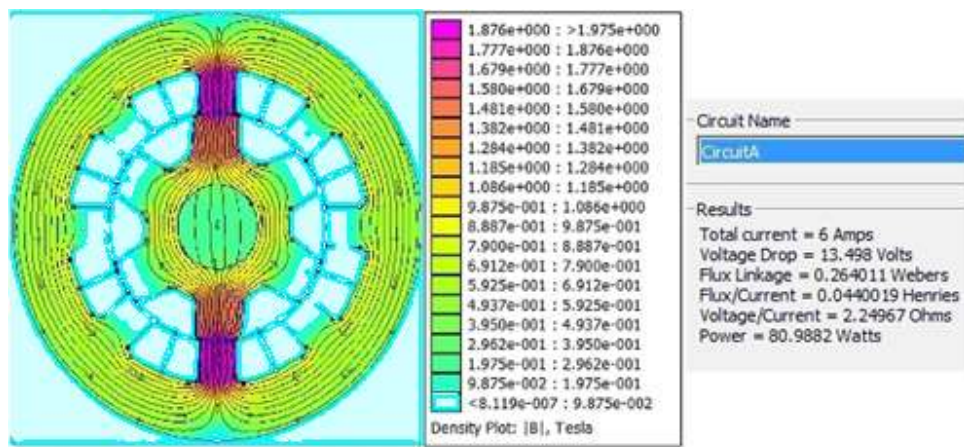


Fig 4.17 Flux Density Plot at Phase A aligned position with 6A excitation current

Using the Lua script functionality of FEMM the model was solved for various current and position increments. The FEMM solution results were plotted in MATLAB as shown in Fig 4.18 for Flux vs Position and Current, ie. Flux(Position, Current) and in Fig 4.19 for Torque vs Position and Current, ie. Torque(Position, Current). The highly non-linear nature of the SR machine is clearly visible from these plots. From the FEMM simulation, the maximum torque that can be generated by a phase is found to be 3.39 Nm.

Using the FEMM data in MATLAB-Simulink, the SRM “specific” model is found to generate more than 4Nm of torque. This is due to the simultaneous excitation of two phases effectively generating higher net torque in the machine.

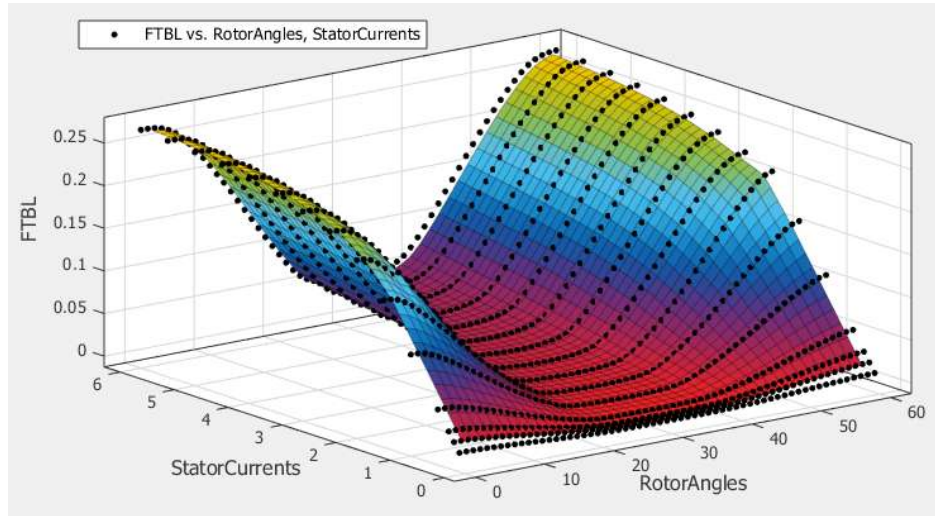


Fig 4.18 Surface Plot of Flux linkages Vs stator current and rotor position using FEMM data

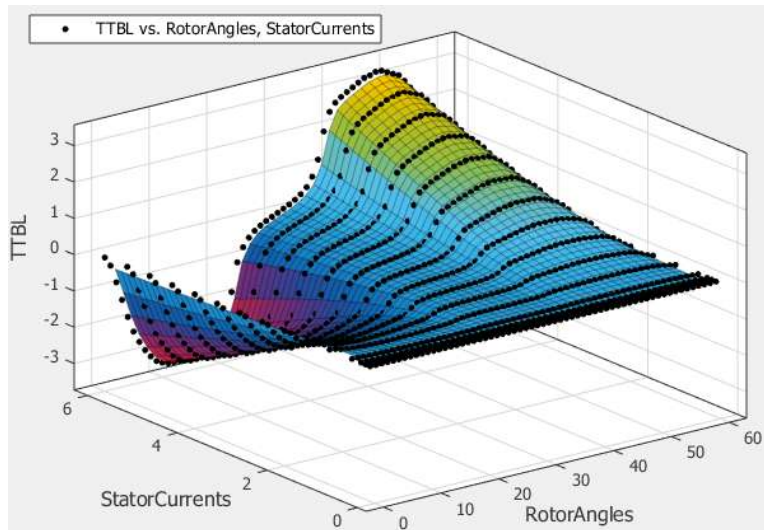


Fig 4.19 Surface Plot of Phase Torque Vs stator current and rotor position using FEMM data

The magnetization characteristics of the Simulink SR machine “specific” model using the FEMM generated data is shown in Fig 4.20.

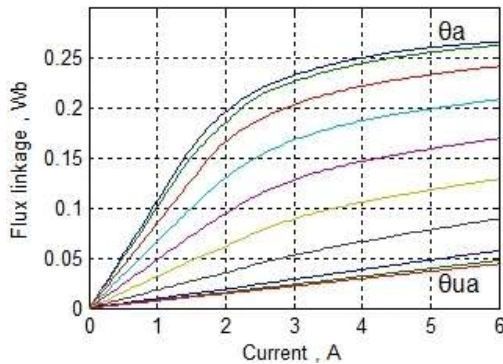


Fig 4.20 Magnetization characteristics of SR machine “specific” model

Table 4.3 System performance with variation in wind speed suing SR Machine “specific” model.

Wind Speed (m/s)	SRG speed (rpm)	Turbine Output (W)	$P_{load}$ (W)	$I_{ph}$ (A)
8.6	1377	242	110	3
12.5	2001	745	510	5
13.8	2210	1002	710	5.7

The simulation was re-run using the Simulink “specific” model for SRG and the readings at maximum power points for the test wind speeds are as in Table 4.3.

Comparing Fig 4.3 with Fig 4.20 and Table 4.3 with Table 4.2, it is observed that for a given phase current the “specific” model has lower flux linkages as compared to the “generic” model that was configured earlier using assumed data, hence the “specific” model draws more current to generate the same torque as compared to the “generic” model.

# Chapter 5

## Hardware Implementation

Block Diagram of the hardware set-up is shown in Fig 5.1.

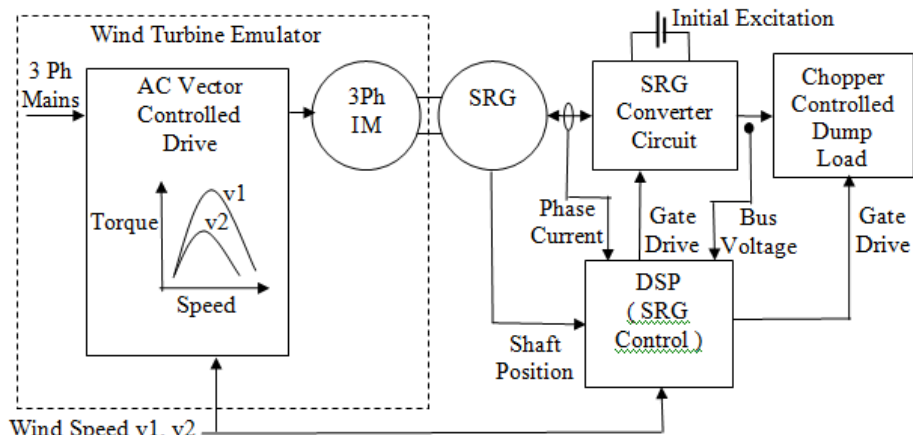


Fig 5.1 Block Diagram of hardware set-up

### 5.1 Test Bench Constraints

To ensure safe operation in the college lab environment and also to avoid delays and additional expenses due to hardware failure the following constraints were placed on the operation of the system:

1. DC Bus Voltages not to exceed 150V DC
2. Machine shaft speed not to exceed 1200 rpm
3. Switching frequency not to exceed 10 kHz

The complete hardware setup is shown in Fig 5.2. Hardware implementation for the SRG drive consists of the power electronics, sensors and DSP controller as shown in Fig 5.3.

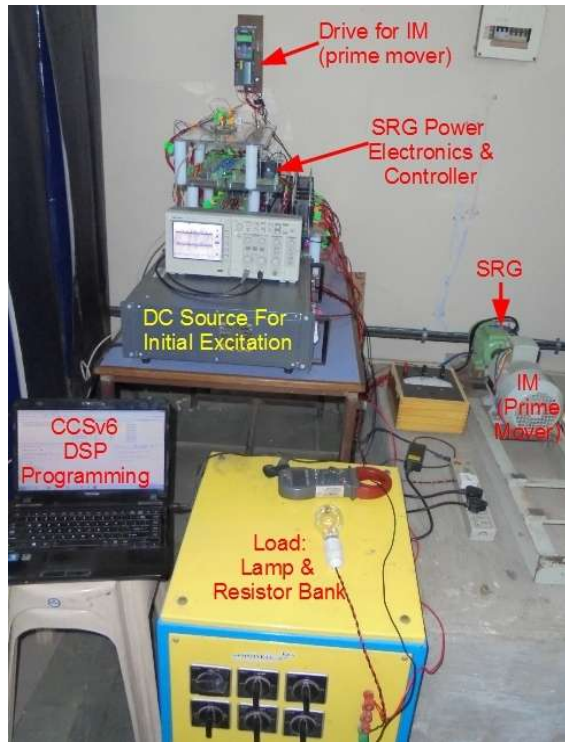


Fig 5.2 SRG Hardware Setup



Fig 5.3 SRG Power Electronics and Controller

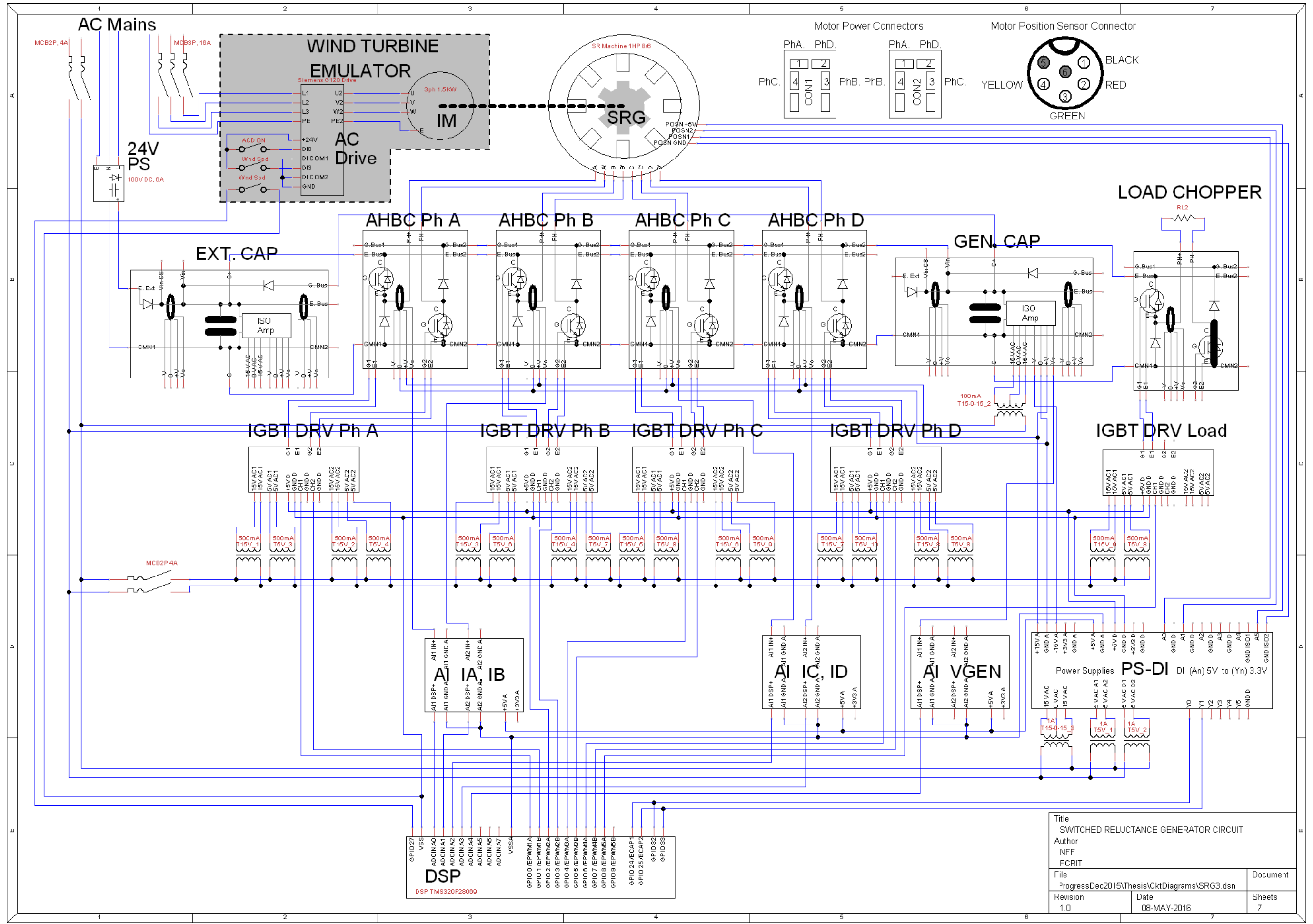


Fig 5.4 System Level Connection Diagram

## 5.2 Overview of Hardware Set-up

The system hardware consists of the following components as shown in the system level connection diagram in Fig 5.4.

- Wind Turbine Emulator
  - Vector Controlled AC Drive (AC Drive)
  - 3 phase AC Induction Motor (IM)
- Switched Reluctance Generator ( SRG )
- External Initial Excitation (24V PS )
- SRG Converter and Chopper Load - Power Electronic Circuits
  - Power Supply and Digital Input Card (PS-DI) – 1 no
  - Capacitor Bank Card – 2 nos
    - (EXT CAP) for the excitation bus
    - (GEN CAP) for the generation bus
  - IGBT Driver Card – 5 nos
    - (IGBT DRV Ph A)
    - (IGBT DRV Ph B)
    - (IGBT DRV Ph C)
    - (IGBT DRV Ph D)
    - (IGBT DRV Load)
  - Asymmetric Half Bridge Converter Card – 4 nos
    - (AHBC Ph A)
    - (AHBC Ph B)
    - (AHBC Ph C)
    - (AHBC Ph D)
  - Chopper Card for Dump Load (LOAD CHOPPER) – 1 no
  - Analog Input Processing Card – 3 nos
    - (A1 IA, IB) for currents of Phase A and Phase B
    - (A1 IC, ID) for currents of Phase C and Phase D
    - (A1 VGEN) for generation bus voltage
  - DSP Control Card – 1 no

The following sections explain each of the components in detail.

### 5.3 Wind Turbine Emulator

Wind Turbine is emulated by an induction motor driven by a vector controlled drive.

#### **Induction Motor (IM) :**

Make: Siemens, Phases: 3, Power: 1.5 kW, Voltage: 415 V AC, Rated Current: 3.45A, Stator Poles: 4, Rated Speed: 1450 rpm

#### **Drive (AC Drive) :**

Make: Siemens G120 Power: 1.5 kW. Support for Vector Control with both speed control and torque control modes. Power Module: PM240-2 Control Unit: CU240 E-2 , Operator Panel: BOP-2.

As shown in Fig 5.5, the vector controlled AC drive is configured with two Torque-Speed profiles (PLI0 and PLI1) that correspond to two wind speeds. The wind speeds can be selected using a switch connected to a digital input (DI3) of the AC drive that connects the appropriate Torque-Speed profile to the Torque Set-point (p1503[0]) of the AC drive [25].

Corresponding to the two wind speeds  $v_1$  and  $v_2$ , Table 5.1 gives the two Tables, for the Power and corresponding Torque for various shaft speeds of the AC Drive.

For wind speed  $v_1$ , the AC Drive is configured so that maximum power occurs at 750 rpm and for wind speed  $v_2$  the maximum power occurs at 950 rpm.

The curves are arbitrarily created to give increase in power with increase in speed upto the maximum power point and then decrease in power with increase in speed. This is found to be sufficient to demonstrate MPPT techniques. If desired, the curves could be generated using the wind turbine equations Eq 3.12-3.14. It is assumed that the shaft of the induction motor that is coupled to the SRG is the output of a wind turbine after gear.

The Power-Speed and Torque-Speed data for wind speeds  $v_1$  and  $v_2$  from Table 5.1 is used to plot the Output Power vs Shaft Speed and the Torque vs Shaft Speed curves for the wind turbine emulator as shown in Fig 5.6 and Fig 5.7.

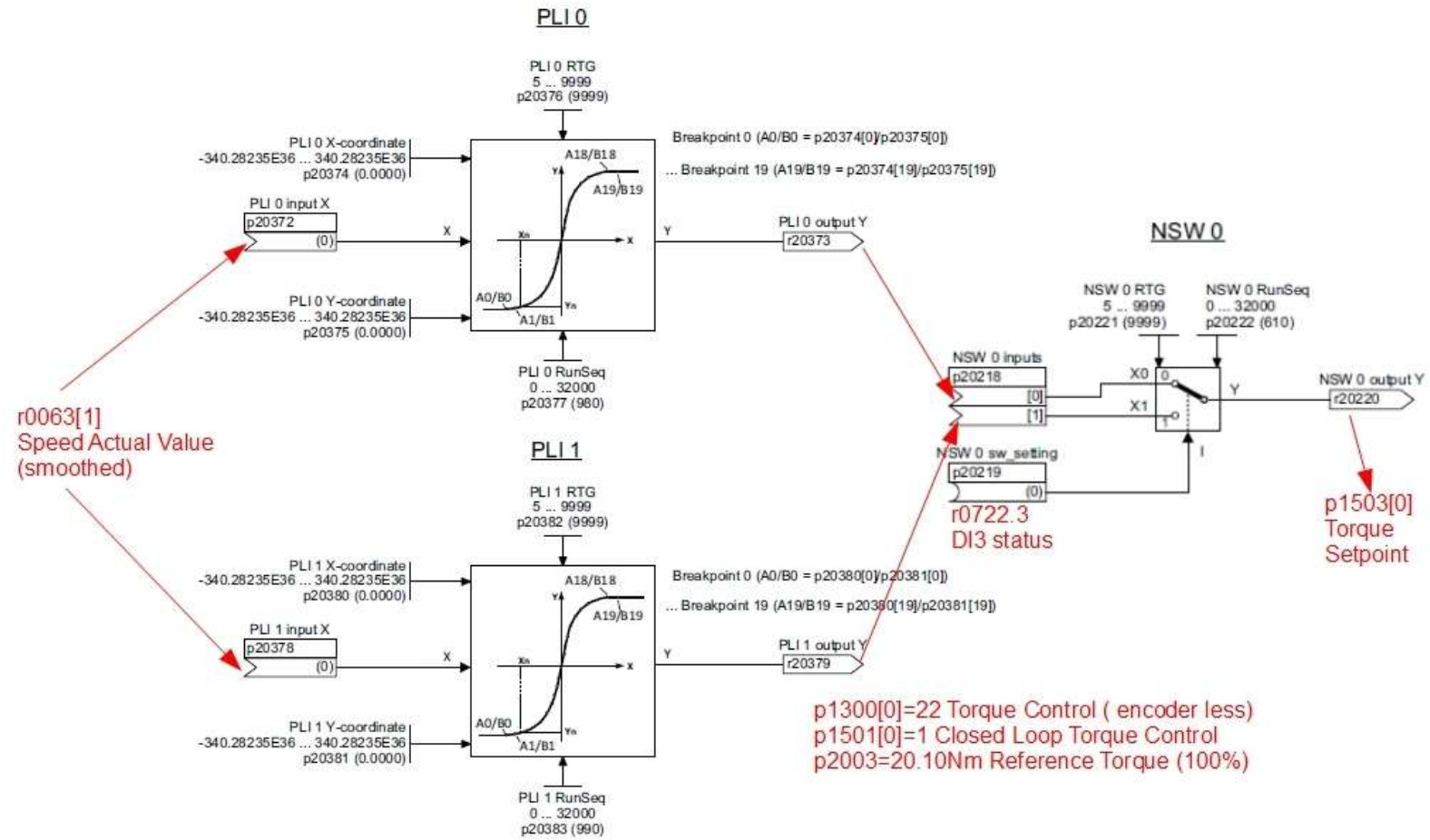


Fig 5.5 Siemens G120 AC Drive Configuration for Wind Turbine Speed-Power Characteristics

Table 5.1 Torque – Speed Characteristic Configuration of the Vector Controlled AC Drive

Sr No	Wind Speed 1 ( $v_1$ ) = 7.88m/s (Siemens G120 p20219=DI3=0)					Wind Speed 2 ( $v_2$ )= 9.99m/s (Siemens G120 p20219=DI3=1)				
	Vector Drive Speed (RPM)	Vector Drive Output Power (W)	Torque (Nm)	Siemens G120 p20374 Speed (%)	Siemens G120 p20375 Torque (%)	Vector Drive Speed (RPM)	Vector Drive Output Power (W)	Torque (Nm)	Siemens G120 p20380 Speed (%)	Siemens G120 p20381 Torque (%)
0	0			0.0000	0.0471	0			0.0000	0.0472
1	100	10	0.9545	0.0667	0.0473	100	10	0.9545	0.0667	0.0473
2	200	40	1.9091	0.1333	0.0947	200	40	1.9091	0.1333	0.0947
3	300	60	1.9091	0.2000	0.0947	300	60	1.9091	0.2000	0.0947
4	500	75	1.4318	0.3333	0.0710	500	75	1.4318	0.3333	0.0710
5	600	88	1.4000	0.4000	0.0694	600	88	1.4000	0.4000	0.0694
6	700	95	1.2955	0.4667	0.0642	700	95	1.2955	0.4667	0.0642
7	750	100	1.2727	0.5000	0.0631	750	105	1.3364	0.5000	0.0663
8	800	95	1.1335	0.5333	0.0562	800	110	1.3125	0.5333	0.0651
9	850	88	0.9882	0.5667	0.0490	850	115	1.2914	0.5667	0.0640
10	900	80	0.8485	0.6000	0.0421	900	117	1.2409	0.6000	0.0615
11	950	68	0.6833	0.6333	0.0339	950	120	1.2057	0.6333	0.0598
12	1000	50	0.4773	0.6667	0.0237	1000	117	1.1168	0.6667	0.0554
13	1050	0	0.0000	0.7000	0.0000	1050	95	0.8636	0.7000	0.0428
14	1100	0	0.0000	0.7333	0.0000	1100	70	0.6074	0.7333	0.0301
15	1150	0	0.0000	0.7667	0.0000	1150	30	0.2490	0.7667	0.0123
16	1200	0	0.0000	0.8000	0.0000	1200	0	0.0000	0.8000	0.0000
17	1300	0	0.0000	0.8667	0.0000	1300	0	0.0000	0.8667	0.0000
18	1400	0	0.0000	0.9000	0.0000	1400	0	0.0000	0.9000	0.0000
19	1500	0	0.0000	1.0000	0.0000	1500	0	0.0000	1.0000	0.0000

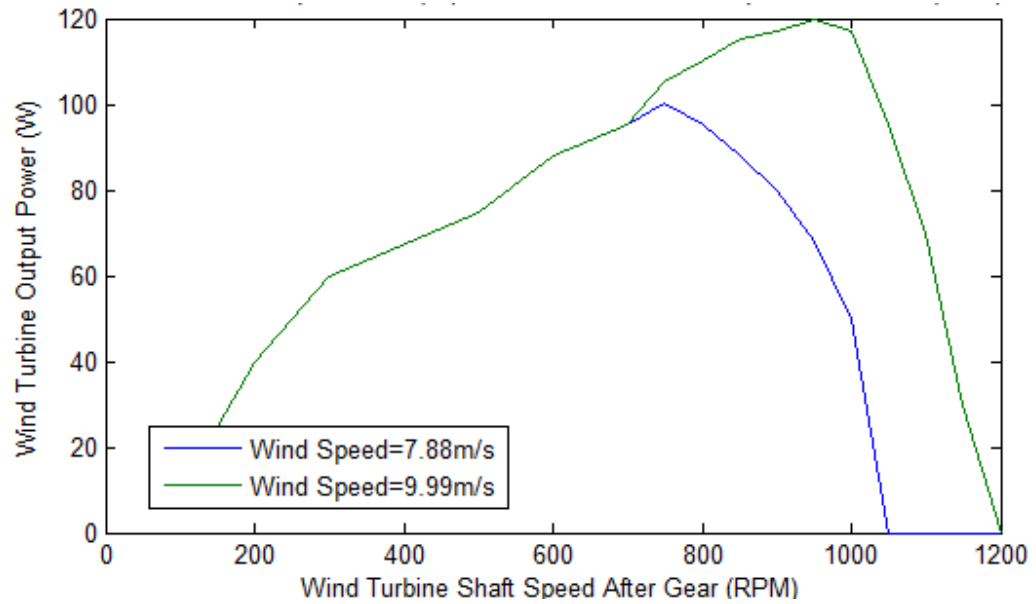


Fig 5.6 Vector Controlled AC Drive Configured for Wind Turbine Emulation– Output Power vs Speed

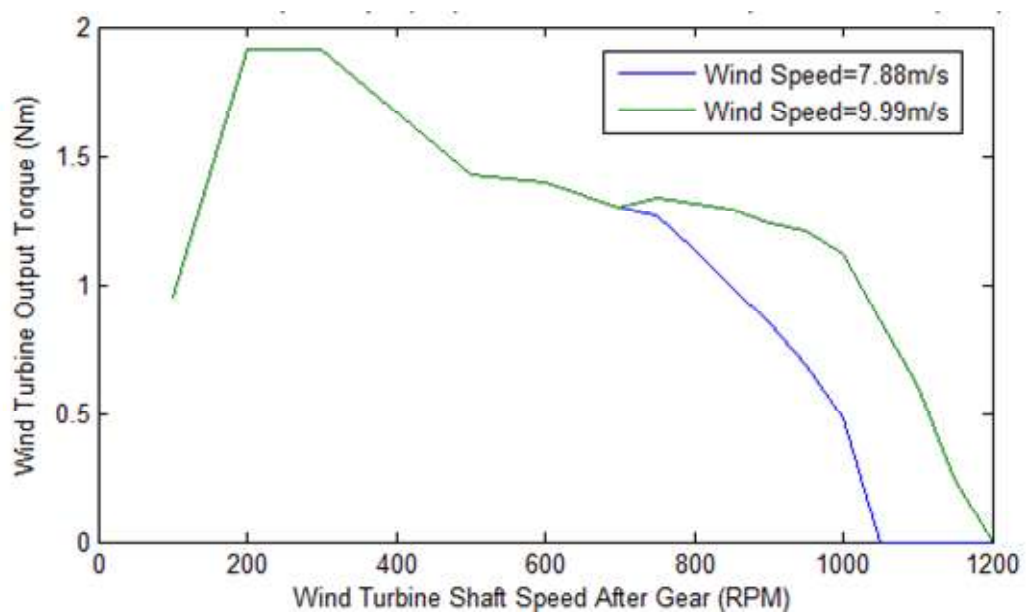


Fig 5.7 Vector Controlled AC Drive Configured for Wind Turbine Emulation – Output Torque vs Speed

## **5.4 External Excitation Source (24V PS)**

For the excitation bus, an external DC Power Supply (or battery) must be connected to the EXT IN terminal of the Excitation Bus Capacitor Bank Card. When operating in Motor mode the DC Power Supply is set at 100V DC (or the rated system operating voltage). When operating in Generator mode the DC Power Supply is set between 24V to 30V DC to provide initial excitation. Once generation has started and generation bus voltage has built-up to a level greater than the DC Power Supply, the DC Power Supply is effectively disconnected from the circuit by the diode located at the EXT IN terminal of the Excitation Bus Capacitor Bank Card. During simulation 12V DC supply was found to be sufficient to start self excitation voltage build-up. In the hardware set-up self-excitation voltage build-up occurred only for dc supply voltages greater than 24 V DC.

## **5.5 Switched Reluctance Generator (SRG)**

A Switched reluctance motor is used in generation mode.

### **Switched Reluctance Motor Specification:**

Make: Eddy Current Controls, Power: 745 W (1 HP), Voltage: 300 V DC, Current: 5 A, Phases: 4, Stator Poles: 8, Rotor Poles: 6, Winding Resistance:  $4.5 \Omega$ , Aligned Position Inductance: 57 mH, Unaligned Position Inductance: 9 mH ( measured using LCR meter )

## **5.6 SRG Converter and Chopper Load**

Hardware implementation consists of the power electronics, sensors and DSP controller.

### **5.6.1 Power Supply and Digital Input Card (PS-DI)**

As shown in Fig5.8, The PS-DI card provides  $\pm 15$  V, 5 V, 3.3 V supplies for the analog circuits on the Analog Input Processing Card and the Capacitor Bank Card. 5 V and 3.3 V supplies are also provided for the digital circuits on the low voltage side of the IGBT Driver Card and digital input processing section that is co-located on the Power Supply Card. The SR machine mounted, rotor position and speed sensing opto-coupler is supplied with 5 V by the PS-DI card. Buffer IC 74AHC541 is used to convert from 5 V to 3.3 V pulses for the DSP input GPIOs.

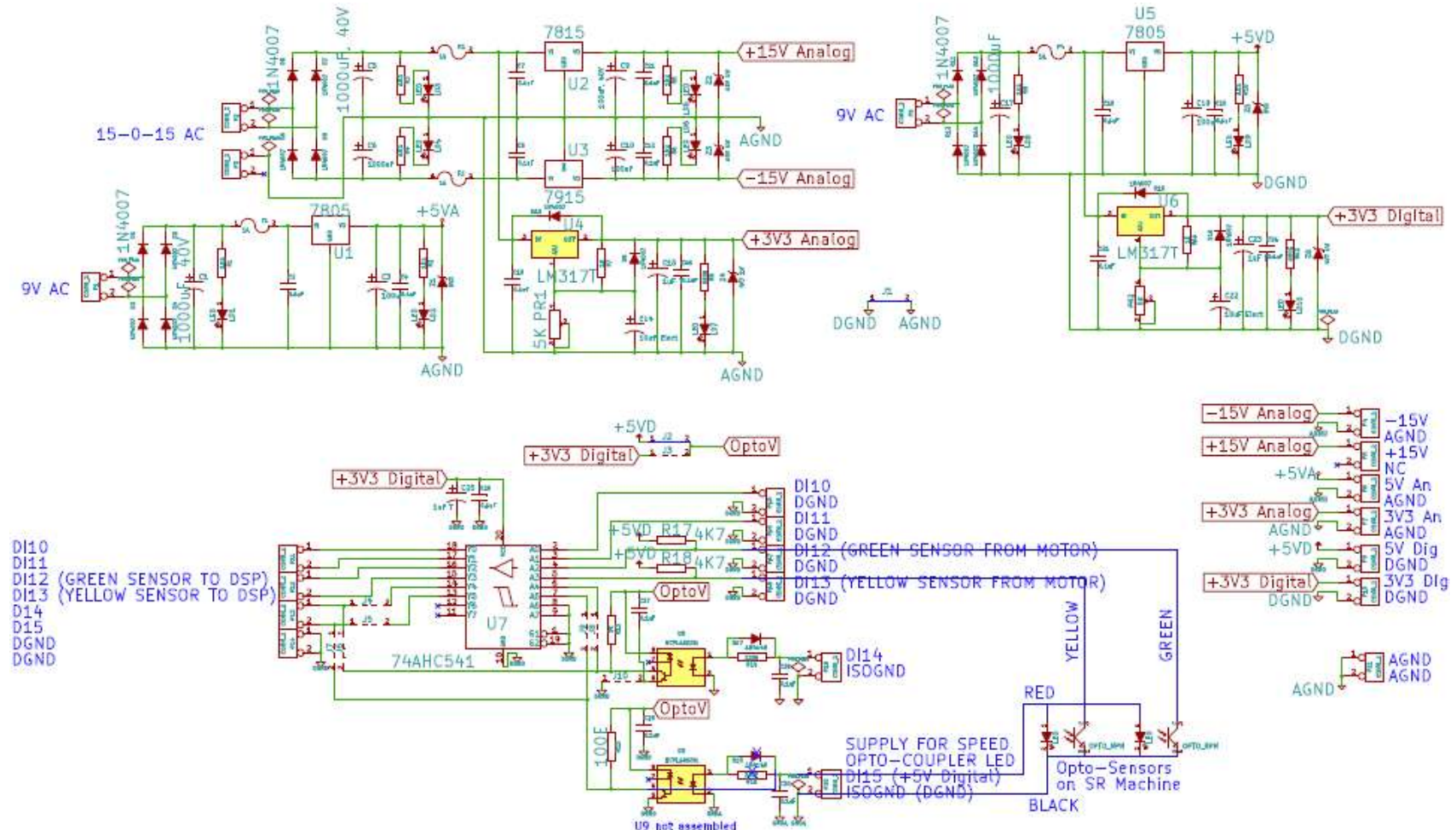


Fig 5.8 Power Supply and Digital Input Card Circuit Diagram

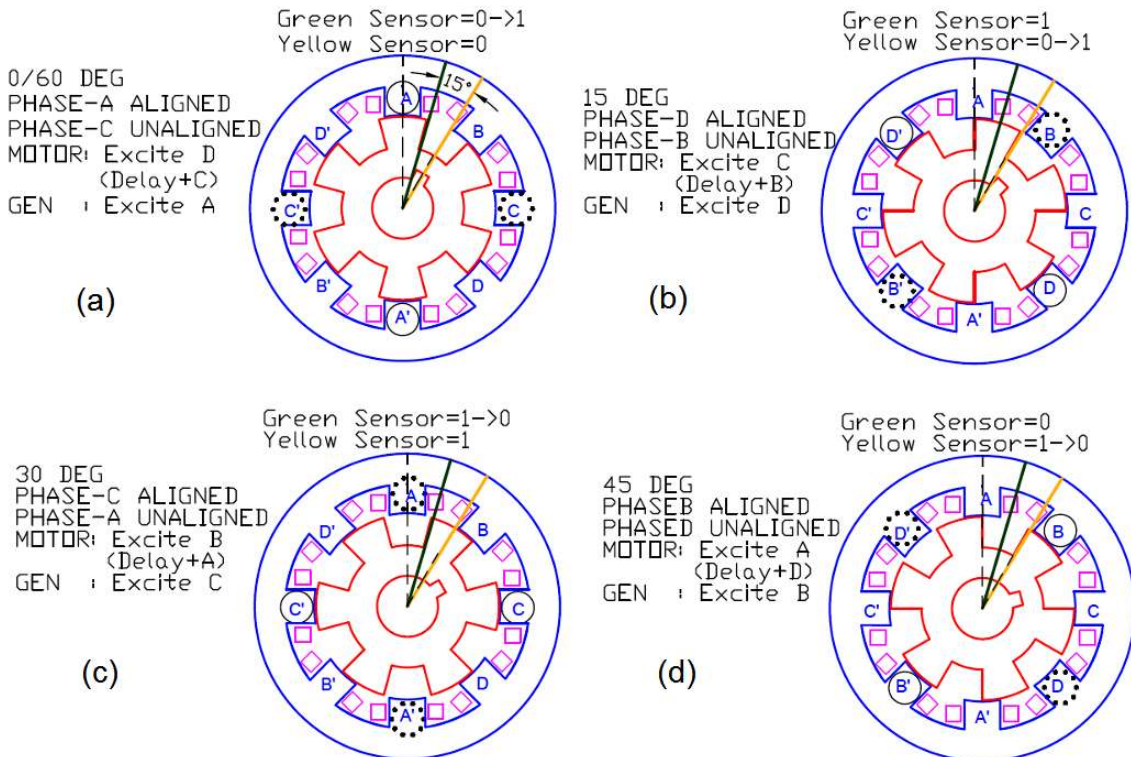


Fig 5.9 SRG Position Sensors

Table 5.2 SRG Position Sensors Output and Phase Inductance measurements for 15 degree rotor position increments

Fig	Angular Position (deg)	Green Sensor o/p	Yellow Sensor o/p	A (mH)	B (mH)	C (mH)	D (mH)	Aligned Phase	Un-aligned Phase
a	0/60	↑	0	57.3	27.12	8.8	38.73	A	C
b	15	1	0	14.42	9.1	43	57.58	D	B
c	30	0	1	10.08	41.4	55.6	14.32	C	A
d	45	0	0	37.68	57.3	19.5	9.6	B	D

SRG rotor position and speed is sensed using the opto-coupler and interrupter disc mounted on the SRG as shown in Fig 5.9 for clockwise rotation. Table 5.2 shows the readings of the opto-coupler sensor outputs and phase inductance at  $15^\circ$  angular position increments in clockwise direction. The shape of the interrupter disc is similar to that of the rotor stamping. The opto-coupler output is high when interrupted by a tooth and low when un-interrupted by a gap. Though not evident in Fig 5.9, the rotor teeth on the actual machine are narrower than the gaps. Hence the opto-coupler high (ON) time is narrower than the low (OFF) times. The opto-coupler sensors are identified by the color of their connecting wires as Sensor 1 or Green Sensor and Sensor 2 or Yellow sensor. Based on the position and speed information obtained from the opto-coupler pulses, the machine phases are excited as per the mode of operation. The rising edge of the Green sensor indicates the aligned position for Phase A. In motor

mode, the Phase A is excited at its unaligned position ( $30^\circ$ ) as shown in Fig 5.10. In generator mode the Phase A is excited at its aligned position ( $0^\circ$ ) as shown in Fig 5.11.

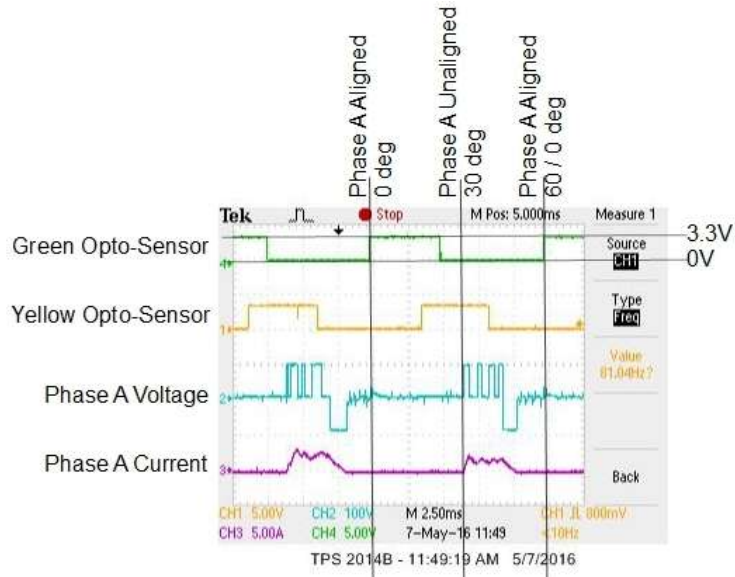


Fig 5.10 Motor Mode: Position Sensor Waveforms, Phase A Voltage and Current

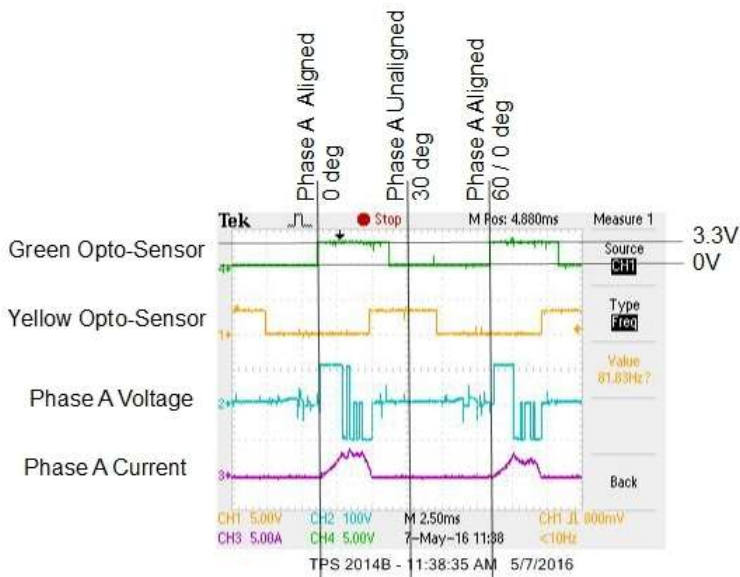


Fig 5.11 Generator Mode: Position Sensor Waveforms, Phase A Voltage and Current

### 5.6.2 Capacitor Bank Card ( EXT CAP / GEN CAP )

The circuit diagram for the capacitor bank card is shown in Fig. 5.12. Capacitance values were selected by trial and error using the MATLAB-Simulation to get minimum ripple. High current ripple power capacitors selected are Vishay Roederstein MAL219857681E3 Electrolytic capacitor, snap-in, 198 PHR-SI Series, 680  $\mu\text{F}$ ,  $\pm 20\%$ , 450 V, 35 mm, 0.14 ohm. The “Excitation Bus Capacitor” Card (EXT CAP) has a single 680  $\mu\text{F}$ , 450 V capacitor. The “Generation Bus Capacitor” Card (GEN CAP) has two 680  $\mu\text{F}$ , 450 V capacitors giving total capacitance of 1360  $\mu\text{F}$ .

DC bus voltage is sensed using voltage divider and isolation amplifier IC ISO124 so that 0-350 V corresponds to 0-3.5 V. The output of the ISO124 is provided to the Analog Input Processing Card that is configured for voltage processing.  $\pm 15V$  DC supply needed for the high voltage side of the ISO124 is placed on the Capacitor Bank Card itself. The  $\pm 15V$  DC supply needed for the low voltage side of the ISO124 is obtained from the Power Supply & DI (PS-DI) Card.

For a dc bus voltage of 350 V, capacitance of 1360  $\mu F$ , four series discharge resistors of  $5 k\Omega$ , 10W each were used. RC time constant = 27.2 s. Using the capacitor discharge equation

$V_c = V_o e^{-\frac{t}{RC}}$ , within 1 minute ( $t = 60$  s =  $2.2RC$ ) after power off the capacitor voltage discharges to 38.55 V. Power dissipated by the discharge resistors during normal system operation at 100 V is  $(100^2)/(4 \times 5000) = 0.5$  W and can be neglected.

Hall effect current sensors shown in the circuit diagram are not assembled on the physical PCB and the sensing terminals in the power circuit are shorted together.

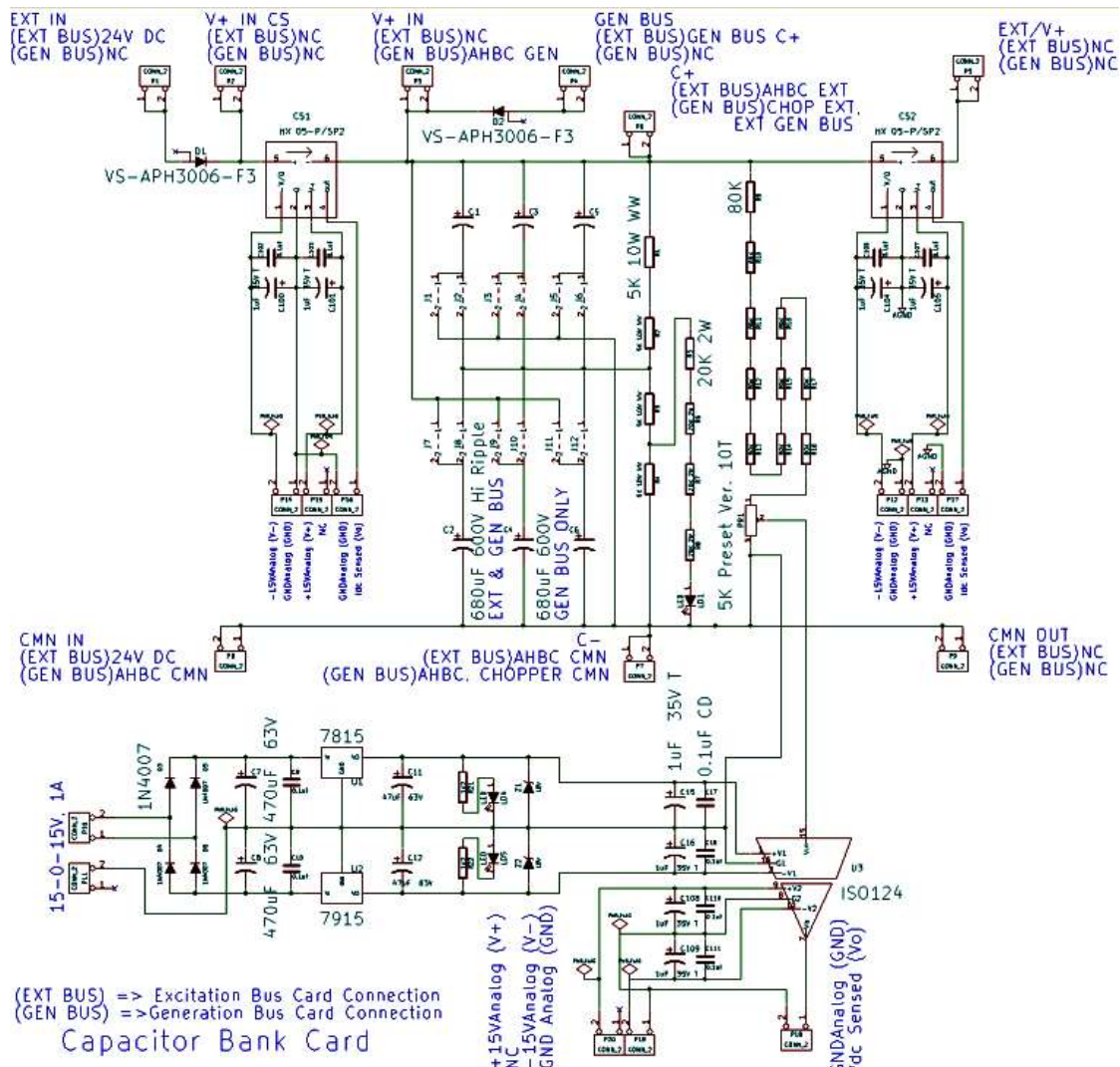


Fig 5.12 Capacitor Bank Card – For Excitation Bus and Generation Bus Circuit Diagram

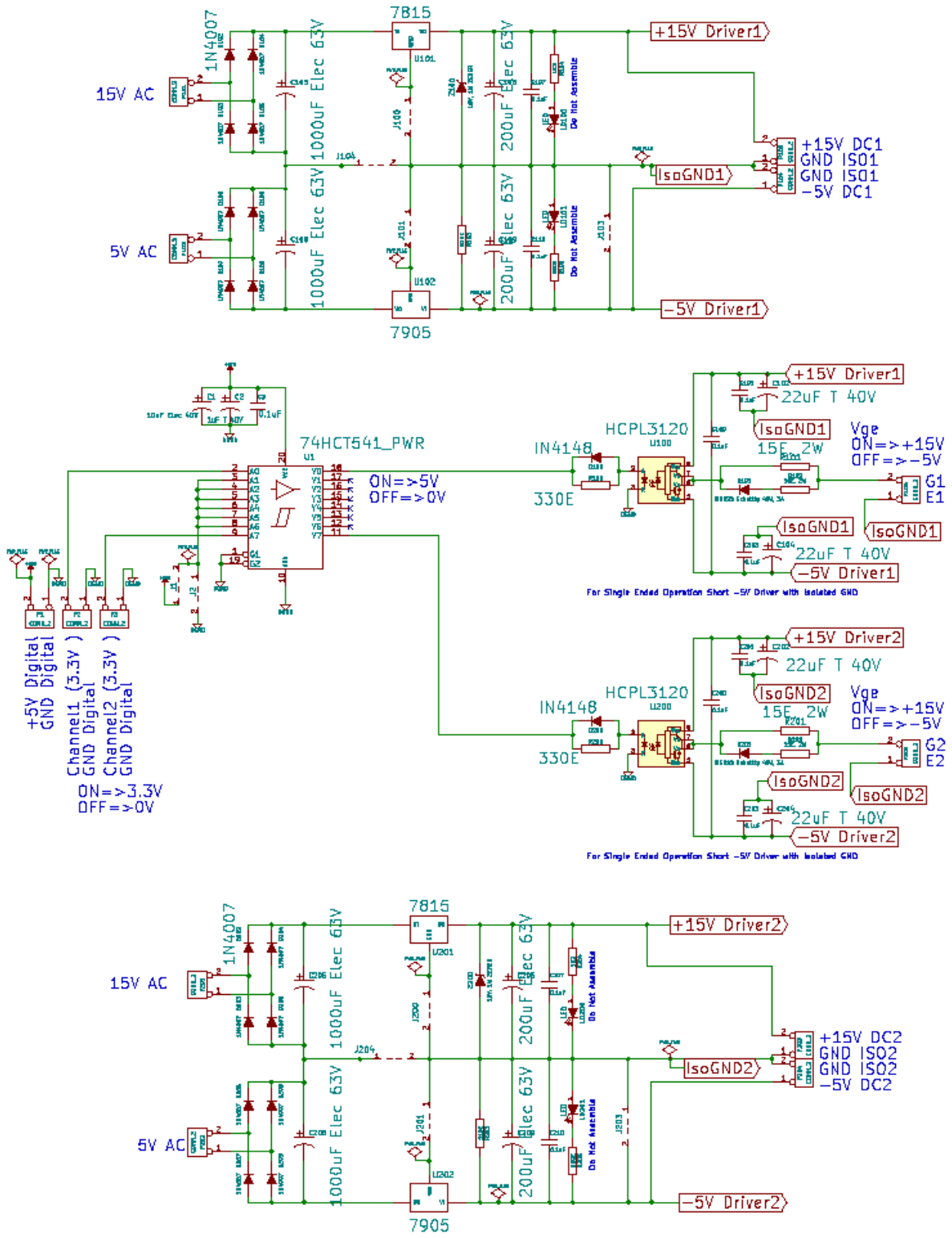


Fig 5.13 IGBT Driver Card Circuit Diagram

### 5.6.3 IGBT Driver Card (IGBT SRV Ph A-Ph D)

Driver circuit for IGBTs is shown in Fig 5.13. The gate drive opto-coupler IC HCPL3120 is used for isolation and level-shifting with on-state voltage level of 15 V and off-state voltage level of -5 V. Buffer IC 74HCT541 is used between the DSP output and the drive opto-

coupler input to convert from 3.3 V to 5 V and avoid loading of the DSP output.  $330\ \Omega$  resistor is used between the 74HCT541 and the HCPL3120 input to provide 15 mA drive current to the opto-coupler LED. The regulator ICs 7815 and 7905 provide the +15 V and -5 V supplies. 200  $\mu\text{F}$  Electrolytic Capacitors act as charge reservoirs and 22  $\mu\text{F}$  Tantalum capacitors provide the large and quick current pulses needed for turn on and turn off. Gate circuit resistor of  $15\ \Omega$  is selected to limit the turn-on current to 1A. The IGBT Driver Card input is zero to 3.3V pulses from the DSP EPWM outputs and the output is -5V to +15V signal to the IGBT gate-emitter pins as shown in Fig 5.14.

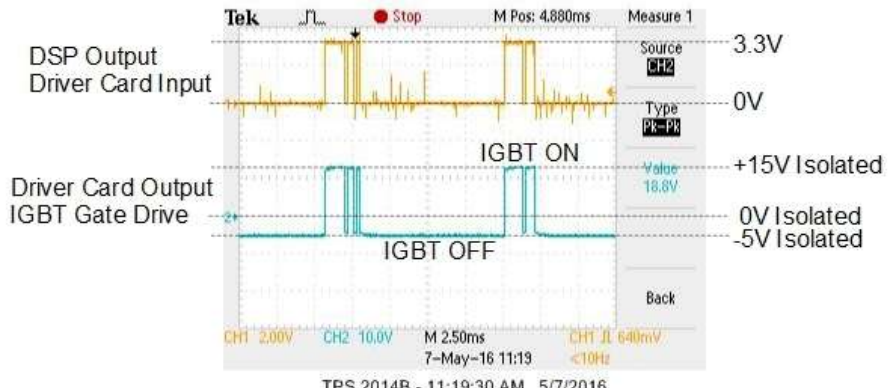


Fig 5.14 IGBT Driver Card Waveforms

#### 5.6.4 Asymmetric Half Bridge Converter Card (AHBC PhA-PhB)

Circuit diagram for the “Asymmetric Half Bridge Converter” Card for each phase is shown in Fig 5.15. It consists of 40 A, 650 V high speed hard switching IGBTs IGW40N65H5 and 30 A, 600 V Hyper-Fast Diodes VS-APH3006-F3. SRG winding current is sensed using 15 A Hall effect current sensors, HX 05-P/SP2, with unipolar output so that 0-15 A corresponds to 2.5-4.375 V.  $10\ \text{k}\Omega$  resistor is placed between the gate emitter terminals to pull down the gate terminal to emitter voltage level in case the driver circuit is disconnected and to prevent the IGBT from turning on due to noise pick-up. The back to back zener diodes in the gate circuit limit the gate emitter voltages to +18 V and -6.8 V.

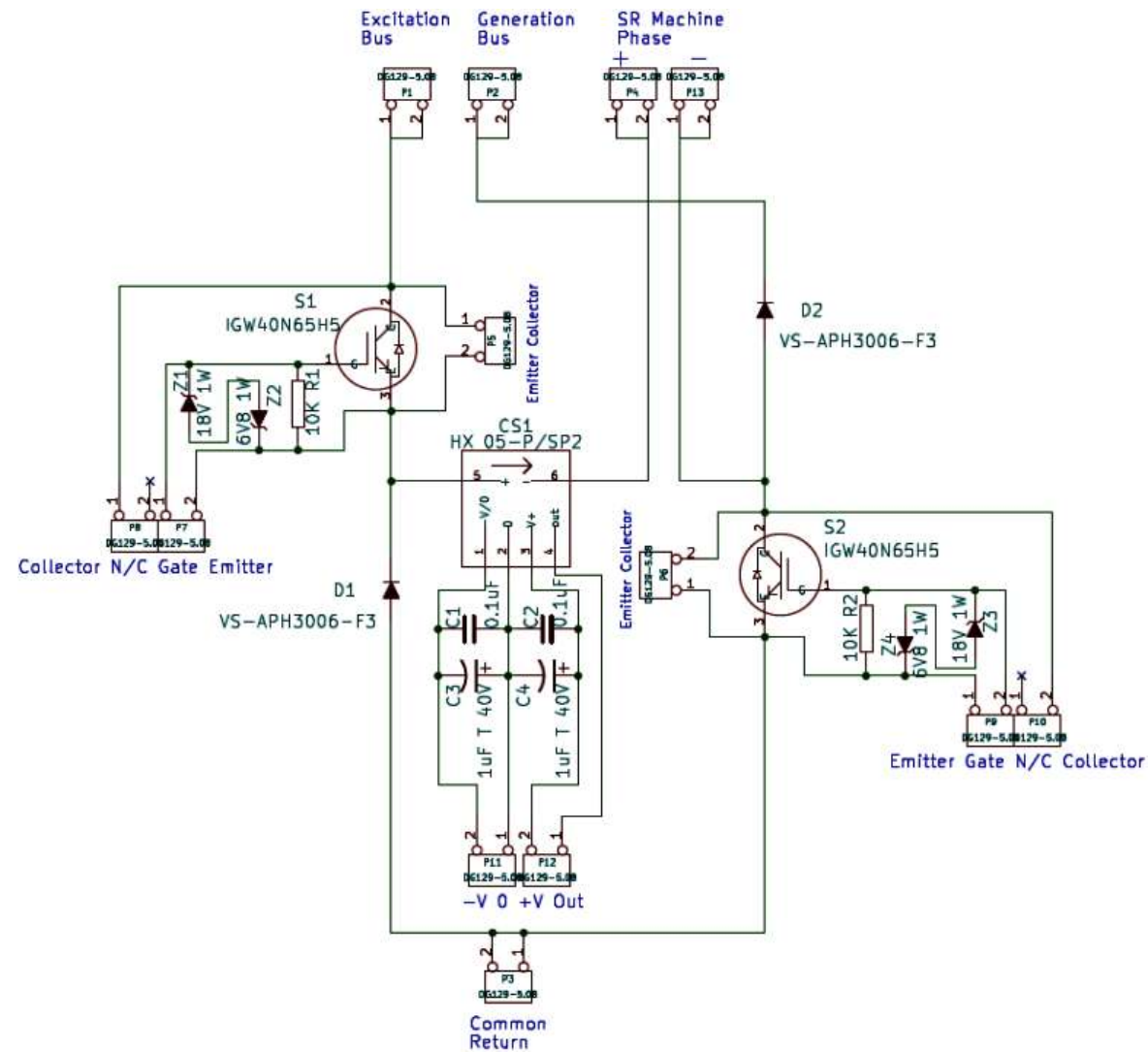


Fig 5.15 Asymmetric Half Bridge Converter Card – One Phase Circuit Diagram

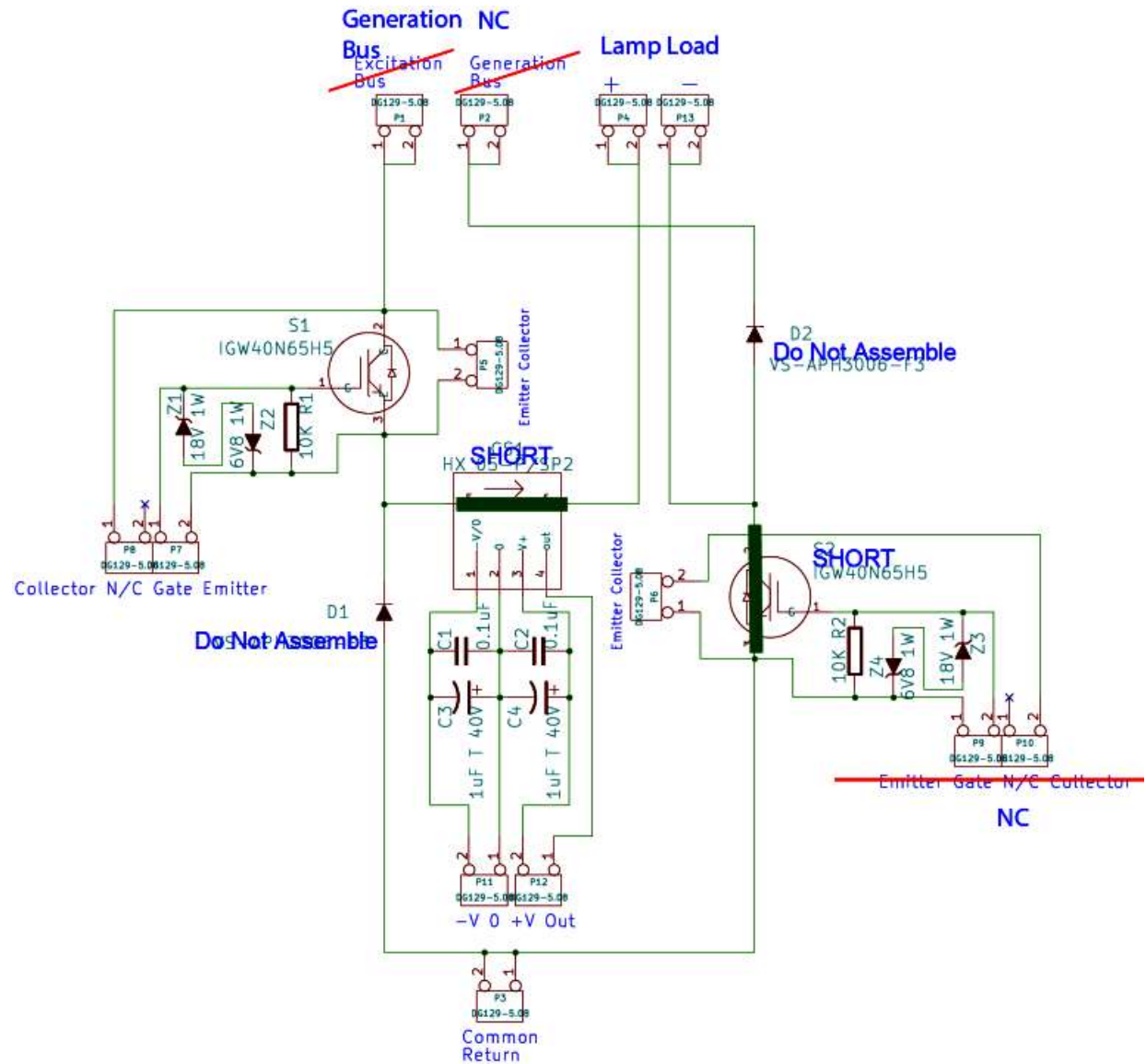


Fig 5.16 Chopper For Dump Load Circuit Diagram

### **5.6.5 Chopper Card for Dump Load (Load Chopper)**

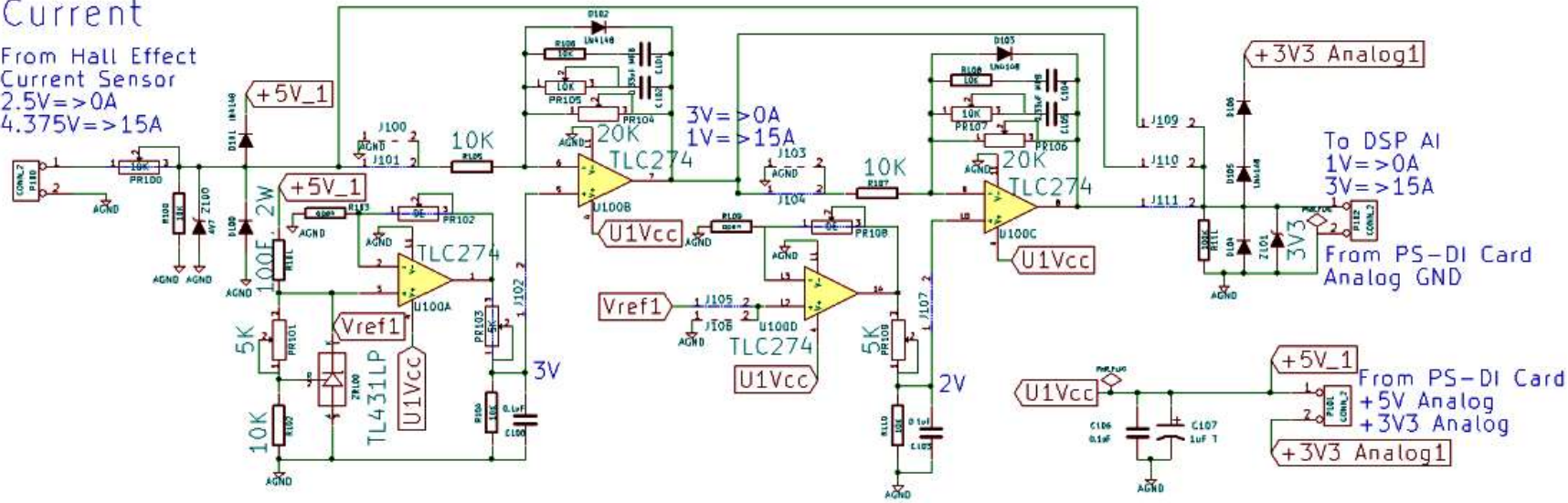
Circuit diagram for the “Chopper For Dump Load” Card shown in Fig 5.16 . It is a modified “Asymmetric Half Bridge Converter” Card with only switch S1 IGBT IGW40N65H5 assembled. The “Excitation Bus” terminal is connected to the “Generation Bus Capacitor” Card “C+” terminal and the “Common” terminal is connected to the “Generation Bus Capacitor” Card “C-“ terminal. The lamp load is connected across the SRM Phase “+” and “-“ terminals. Current sensor is not assembled and the sensing terminals are shorted. Switch S2 is not assembled and the collector emitter terminals are shorted.

### **5.6.6 Analog Input Processing Card (AI IA, IB / AI IC, ID / AI VGEN )**

Circuit diagram for the “Analog Input Processing” Card is shown in Fig 5.17. It consists of unipolar level shifting and scaling circuit using op-amp TLC274 configured as two cascaded inverting amplifiers. All analog inputs to the DSP are scaled in the 1-3 V range. TL431 Precision Voltage Reference followed by op-amp gates of TLC274 configured as voltage followers are used to provide the bias voltages. The same PCB can be configured for current or voltage processing by assembling the appropriate components.

## Current

From Hall Effect Current Sensor  
 $2.5V \Rightarrow 0A$   
 $4.375V \Rightarrow 15A$



## Voltage

From Isolation Amplifier  
 $0V \Rightarrow 0V$   
 $3.5V \Rightarrow 350V$

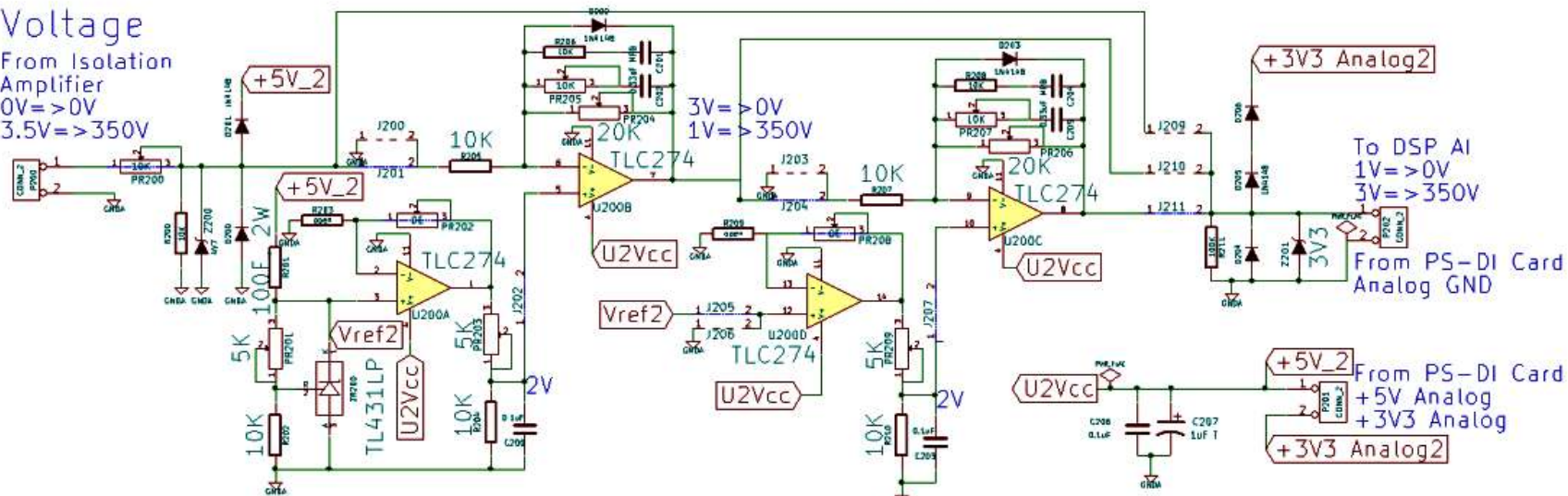


Fig 5.17 Analog Input Processing Card Circuit Diagram

The upper circuit in Fig 5.17 shows the configuration for a current processing channel.

Fig 5.18 shows the current processing circuit waveforms. The first trace is the phase current measured by CRO current probe at the “SRM PH +” terminal of the AHBC card, as shown in Fig 5.15. The second trace is the voltage after the Hall-effect Sensor of the ABHC card and is same as the input voltage to the “Analog Input Processing” Card-Current channel. The third trace is the voltage after level shifting and scaling at the output of the “Analog Input Processing” Card-Current channel. The high frequency noise is observed when the “Analog Input Processing” Card-Current channel output is connected to the DSP ADC input. An RC low pass filter consisting of a  $100 \Omega$  resistor in series with the op-amp output and  $100 \text{ pF}$  capacitor in parallel with the ADC input may reduce the noise seen at the DSP ADC input but is not currently implemented.

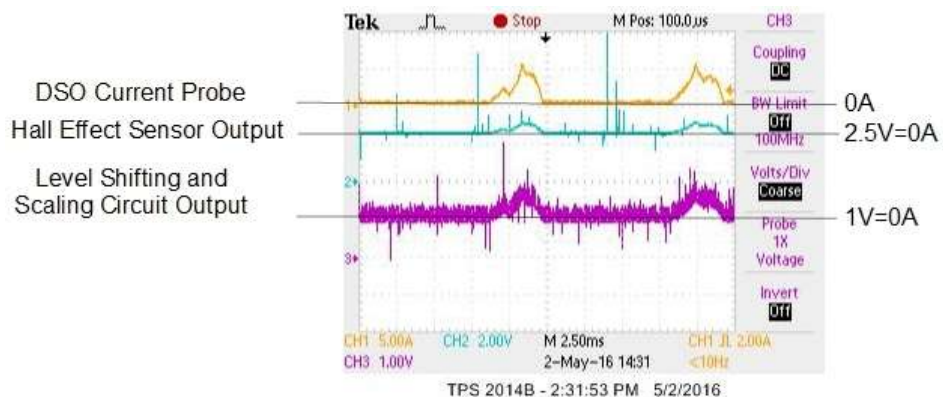


Fig 5.18 Current Processing Circuit Waveforms

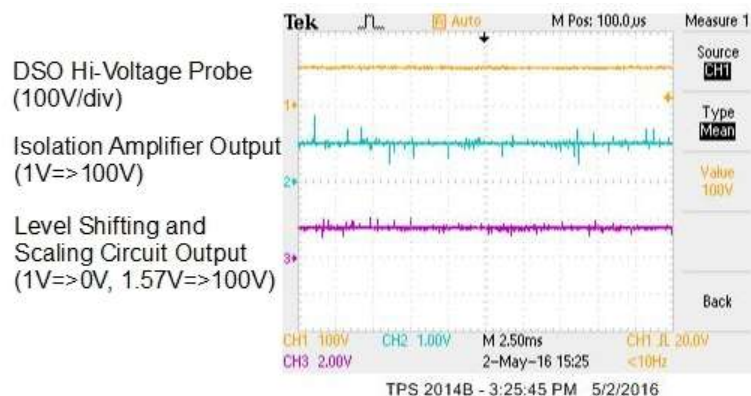


Fig 5.19 Voltage Processing Circuit Waveforms

The lower circuit in Fig 5.17 shows the configuration for a voltage processing channel.

Fig 5.19 shows the voltage processing circuit waveforms. The first trace is the phase voltage measured by CRO voltage probe across the “C+” and “C-” terminals of the “Generation Bus Capacitor Bank” card as shown in Fig 5.12. The second trace is the voltage after the Isolation Amplifier at the “Vo” output of the “Generation Bus Capacitor Bank” Card, and is same as the input voltage to the “Analog Input Processing” Card-Voltage channel. The third trace is

the voltage after level shifting and scaling at the output of the “Analog Input Processing” Card-Voltage channel and is given as input to the DSP ADC input pin.

### 5.6.7 DSP Control Card

DSP control board used is the TI 28069 Experimenter’s Kit.

Pulse width modulated outputs are shown in Table 5.3. ePWM1-4 are used to drive the AHBC IGBTs to control the phase currents. ePWM5 is used to drive the chopper controlled dump load IGBT and control the generation bus voltage. Analog inputs are shown in Table 5.4. ADCINA0-3 are used to sense the SRG phase currents. ADCINA4 is used to sense the DC link voltage. GPIO inputs are shown in Table 5.5. GPIO32-33 are used as digital inputs to sense the opto-coupler signals for estimating the position and speed. GPIO27 is used for wind speed detection. GPIO outputs are shown in Table 5.6. GPIO34 is used as digital output and blinked at 1s intervals to provide visual indication that the program is running.

System GND is connected to the DSP card GND pin. Frequent communication breaks were observed while connecting CCS to the DSP card via the USB cable. This issue was solved when the System GND was connected to the Mains Earth. Alternatively connecting a non-isolated DSO’s ground terminal to the System Digital GND also solved the PC communication issue.

Table 5.3 EPWM Outputs

Sr No	GPIO	EPWM	Switch
1	GPIO-0	EPWM-1A	A1
2	GPIO-1	EPWM-1B	A2
3	GPIO-2	EPWM-2A	B1
4	GPIO-3	EPWM-2B	B2
5	GPIO-4	EPWM-3A	C1
6	GPIO-5	EPWM-3B	C2
7	GPIO-6	EPWM-4A	D1
8	GPIO-7	EPWM-4B	D2
9	GPIO-8	EPWM-5A	Load

Table 5.4 ADC Inputs

Sr No	ADC In	Measured System Variable
1	ADCINA0	Ia
2	ADCINA1	Ib
3	ADCINA2	Ic
4	ADCINA3	Id
5	ADCINA4	Vgen

Table 5.5 GPIO Inputs

Sr No	GPIO	Sensed System Variable
1	GPIO-32	Position Sensor-Yellow
2	GPIO-33	Position Sensor-Green
3	GPIO-27	Wind Speed 0=>v <sub>1</sub> , 1=>v <sub>2</sub>

Table 5.6 GPIO Outputs

Sr No	GPIO	System Variable
1	GPIO-31	RED LED2 on DSP board (not used)
2	GPIO-34	RED LED3 on DSP board (blink @ 1s)

## 5.7 Structure of the DSP program

TI Code Composer Studio v6 (CCSv6) is used for control logic coding and debugging.

### 5.7.1 Analog Input Signal Processing

All EPWM modules are synchronized and operated at 10 kHz. The EPWM module TBPRD event is used to trigger the SOCs for all the ADCs. Thus the ADCs sample the phase currents and DC link voltage in the middle of the switch ON times, thereby avoiding switching noise. The last EOC is used to trigger the ADC ISR that also executes the current and voltage control loops. ADC ISR is thus called at the same frequency as the EPWM modules ie at 10 kHz.

#### 5.7.1.1 Current Signal Processing

Table 5.7 summarizes the current, voltage and counts at the stages of the Current Processing Circuit. Also refer section 5.6.6.

Table 5.7 Current Signal Processing

Sr No.	Current (A)	Hall Sensor o/p (V)	Analog Processing ckt o/p = DSP Analog Input(V)	DSP ADC (count)
1	NA	NA		0
2	0	2.5		1241
3	5	3.125	1.666666667	2068
4	15	4.375	3	3724
5	NA	NA	3.3	4096

Conversion from the sensed “ADC Count” (1241-3724) to “Current in Amps” for signals measured on the AI pins is given by the equation:

$$\text{Current in Amps} = \frac{[(\text{ADC Count} - 1241) \times 15]}{2482} \quad (5.1)$$

Conversion from “Current in Amps” to “ADC Count” (1241-3724) for user set-points from the CCS watch window is given by the equation:

$$\text{ADC Count} = \left[ \frac{2482 \times \text{Current in Amps}}{15} \right] + 1241 \quad (5.2)$$

### 5.7.1.2 DC Voltage Signal Processing

Table 5.8 summarizes the voltage and counts at the stages of the Current Processing Circuit.

Also refer section 5.6.6.

Table 5.8 Voltage Signal Processing

Sr No.	Voltage (V)	ISO Amp o/p (V)	Analog Processing ckt o/p = DSP Analog Input (V)	DSP ADC (count)
1	NA	NA	0	0
2	0	0	1	1241
3	350	3.5	3	3724
4	NA	NA	3.3	4096

Conversion from sensed “ADC Count” (1241-3724) to “Voltage in Volts” for signals measured on the AI pins is given by the equation

$$\text{Voltage in Volts} = \frac{[(\text{ADC Count} - 1241) \times 350]}{2482} \quad (5.3)$$

Conversion from “Voltage in Volts” to “ADC Count” (1241-3724) for user set-points from the CCS watch window is given by the equation

$$\text{ADC Count} = \left[ \frac{2482 \times \text{Voltage in Volts}}{350} \right] + 1241 \quad (5.4)$$

## 5.7.2 Speed Calculation and Rotor Position Logic

### 5.7.2.1 Speed Calculation

The time between the rising edges of the opto-sensors corresponds to  $60^\circ$  and is used for speed calculation by counting the 0.1ms timer ticks between each of the rising edges.

$$\text{Time for } 60^\circ \text{ rotation} = \text{Timer Tick Count} \times 0.1\text{e-3 s} \quad (5.5)$$

$$\text{Time for } 360^\circ \text{ rotation} = \text{Time for } 60^\circ \text{ rotation} \times 6 \quad (5.6)$$

$$\text{RPS} = 1 / (\text{Time for } 360^\circ \text{ rotation}) \quad (5.7)$$

$$\text{RPM} = \text{RPS} \times 60 \quad (5.8)$$

Using the above equations the results for some speeds are presented in Table 5.9

Table 5.9 Speed Calculations

Sr No	Speed (rpm)	Speed (rps)	time for 1 rotation (s)	time for 60 deg (s)	0.1ms ticks for 60 deg rotation (Count)
1	1500	25	0.04	0.006666667	66.66666667
2	1000	16.66667	0.06	0.01	100
3	100	1.666667	0.6	0.1	1000

### 5.7.2.2 Position Calculation

The green opto-sensor rising edge corresponds to the Phase A aligned position and is taken as reference to set the angle to  $0^\circ$ .

$$\text{Angle} = 0$$

Every 0.1ms the angular position is updated using

$$\text{Angle} = \text{Angle} + (0.1e - 3 \times RPM \times 60) \quad (5.9)$$

### 5.7.3 Commutation Logic

Refer Fig 5.9, with rotation in the clock-wise direction.

For Motor mode speed below 100 rpm phase excitation is based on the sensor outputs to ensure starting without hesitation and / or reverse rotation as shown in Table 5.10

Table 5.10 Phase Excitation for clock-wise rotation at speeds below 100 rpm

Sr No	Green Position Sensor	Yellow Position Sensor	Partially Aligned Phase with increasing inductance (excite first for 0.5s)	Unaligned Phase (excite after 0.5s delay)
1	1	0	Phase D	Phase C
2	1	1	Phase C	Phase B
3	0	1	Phase B	Phase A
4	0	0	Phase A	Phase D

For speed greater than 100 rpm in both Motor and Generator Mode phase excitation is as per Table 5.11 below.

Table 5.11 Phase Excitation for clock-wise rotation at speeds above 100 rpm

Sr No	Angular Position (Deg)	Motor Mode Unaligned Phase Excited	Generator Mode Aligned Phase Excited
1	0-15	Phase C	Phase A
2	15-30	Phase B	Phase D
3	30-45	Phase A	Phase C
4	45-60	Phase D	Phase B

## 5.7.4 MPPT Control Logic

### 5.7.4.1 MPPT based on Speed Sensing

Based on the sensed wind speed the SRG speed reference is set. In continuation with the Mod2 Wind Turbine theory developed in sections 3.2, 4.2 and 5.3, we assume  $\lambda=8.1$ ,  $R=0.908\text{m}$ . For the SRG shaft speeds of 750rpm and 950 rpm, we assume a 1.12 gear ratio to get wind turbine shaft speeds of 671rpm and 850rpm. Using the Eq  $\lambda = \frac{\omega R}{v}$  we get

$v_1=7.88\text{m/s}$  and  $v_2=9.99\text{m/s}$ . Wind Speed is assumed to be sensed and simulated by a switch connected to the GPIO-27 configured as an input with values  $0=>v_1$  and  $1=>v_2$ . Power output of this assumed wind turbine is the power output of the emulating drive.

### 5.7.4.2 MPPT based on Hill Climbing

Basic Hill Climbing algorithm is implemented as shown in pseudo-code below and is executed every 5 seconds.

```
IF (Power Increases as Speed Increases) THEN Increase Speed  
If (Power Increases as Speed Decreases) THEN Decrease Speed  
IF (Power Decreases as Speed Increases) THEN Decrease Speed  
If (Power Decreases as Speed Decreases) THEN Increase Speed
```

The increment / decrement step used is 50 RPM.

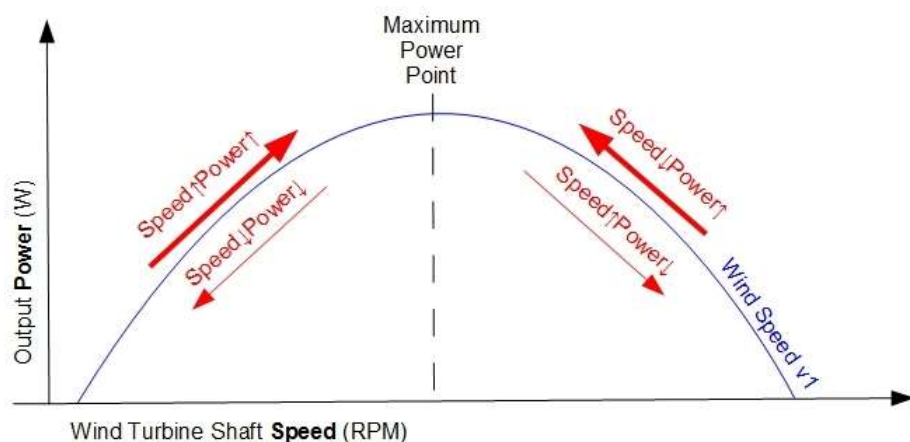


Fig 5.20 Hill Climbing Algorithm for Maximum Power Point Tracking (MPPT)

## 5.7.5 Speed Loop Logic

Speed Control Loop executes every time a new calculated speed is available and uses PI control to generate the Reference Current for the Current loop. As per the Speed Calculation Table 5.10 the Speed Loop Logic will execute every 100 ms at 100 rpm and every 10 ms at 1000 rpm.

### 5.7.6 Current Loop Logic

The existing EPWM infrastructure of the DSP is used to implement the Hysteresis Current Control (HCC) as this enables use of the in-built synchronization of the ADC sensing to avoid the switching instants thereby reducing incorrect readings. EPWM TBCLK=10 MHz, so for a carrier frequency of 10 kHz there will be 1000 TBCLK pulses. EPWM modules are configured with Up-Down count mode for center-symmetric PWM, hence TBPRD=500. So for hysteresis operation CPMA=0 (CPMB=0) gives continuous high output ie. 100% PWM duty cycle and CMPA=501 (CMPB=501) gives continuous low output ie. 0% PWM duty cycle. Hysteresis Band is set as  $\pm 0.1$  A.

### 5.7.7 DC Voltage Control Logic

Generation Bus DC link voltage is controlled by adjusting the Duty Cycle of the Chopper Dump Load using PI control with PWM.

Four 40W Lamps connected in parallel are used as the dump load. 40W Lamp hot resistance used in Load Power Calculation as shown in Table 5.12

Table 5.12 Dump Load Resistance

Voltage (V)	Current (A)	Lamp Hot Resistance ( $\Omega$ )	Hot Resistance 4 lamps in parallel ( $\Omega$ )
100	0.118	847.4576	212.5

Output Power in the Dump Load is calculated using the equation:

$$\text{Output Load Power} = \frac{(\text{Generation Bus Voltage} \times \text{Chopper Duty Cycle})^2}{\text{Lamp Load Hot Resistance}} \quad (5.10)$$

# **Chapter 6**

## **Results and Discussions**

### **6.1 Motor Mode Results**

Machine was initially tested in motor mode. Machine could start without any hesitation and no reverse rotation was observed at the time of start-up. Jerky motion was observed below 100 rpm. Stable operation and speed control was possible from 100 rpm to 1000 rpm as in Table 6.1. As shown in Fig 6.1, current control is achieved using soft chopping.

Table 6.1 Speed Control in Motor Mode (Supply Voltage = 100V)

Sr No	SR Motor Speed	
	Setpoint (RPM)	Actual (RPM)
1	<100	jerky movement
2	100	100
3	150	151
4	200	202
5	300	302
6	400	402
7	500	503
8	600	602
9	700	703
10	800	802
11	900	900
12	1000	1001

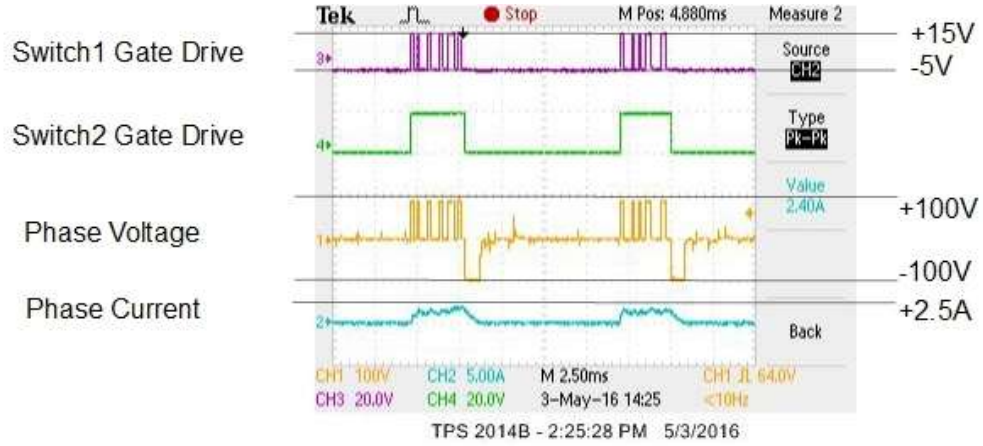


Fig 6.1 Motor Mode Waveforms – Gate Drive, Phase Voltage and Current

## 6.2 Generator Mode Results

Voltage waveforms for all the phases in generator mode are shown in Fig 6.2. Refer the “Asymmetric Half Bridge Converter” Card for a phase of the SR machine shown in Fig 5.15. The phase voltages are measured across the SR Machine Phase "+" and "-" terminals. The voltage waveforms are as per the commutation sequence described in section 5.7.3 and Table 5.12. Even though each phase is excited for  $15^\circ$ , there is some overlap between the phases as the phase current of the out-going phase takes some time to decay to zero. Note that in Fig 6.2, both switches of Phase A are turned off at  $15^\circ$  and the negative Phase A voltage after  $15^\circ$  indicates that the diodes are conducting the generation current to the generation DC bus.

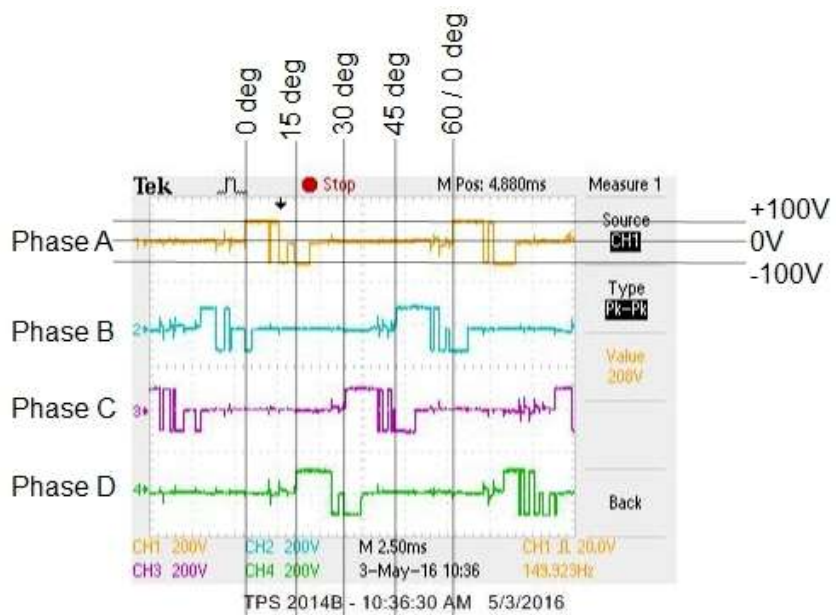


Fig 6.2 Generator Mode Phase Voltage Waveforms

Initially phase current control using soft-chopping was implemented in generator mode. However due to the noise in the current sensing circuit, the Excitation bus was disconnected before sufficient current was built up in the phase winding. Hence the magnetic flux of the

phase winding was low and as a result the induced emf was low and insufficient to build up current in the shorted winding. To solve this problem hard chopping was used exclusively in the early stages of testing. Finally a qualification count was added and when the number of times the current exceeded the upper hysteresis limit equaled the qualification count then the phase current control switched over from hard-chopping mode to soft-chopping mode. Currently the qualification count is set to 3. Improvement in the current sensing circuit to filter out noise can enable use of soft-chopping exclusively. Refer the "Asymmetric Half Bridge Converter" Card for a phase of the SR machine shown in Fig 5.15. In Fig 6.3, the Switch 1 Gate Drive is measured across the "Switch 1 Emitter" and "Switch 1 Gate" terminals. The Switch 2 Gate Drive is measured across the "Switch 2 Emitter" and "Switch 2 Gate" terminals. The Phase Voltage is measured across the SR Machine Phase "+" and "-" terminals. The Phase Current is measured at the SR Machine Phase "+" terminal.

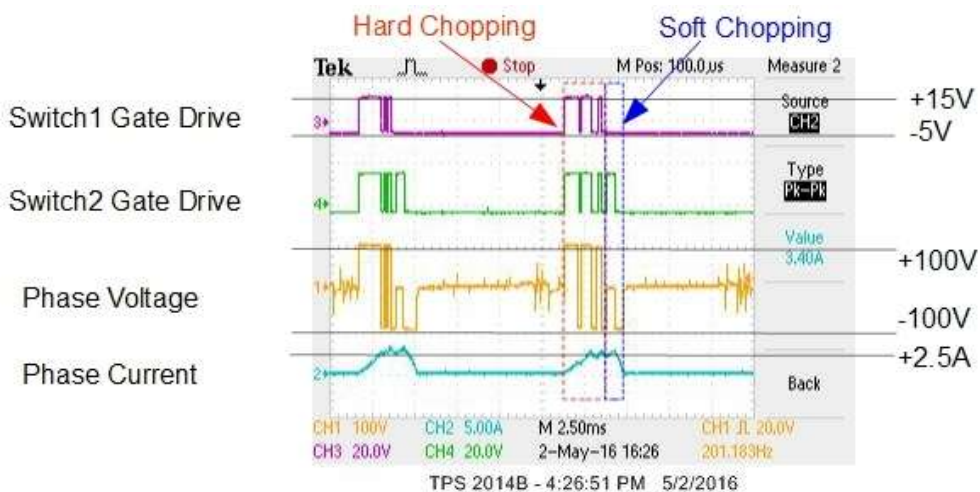


Fig 6.3 Generator Mode Waveforms – Gate Drive, Phase Voltage and Current

Fig 6.4 gives the excitation and generation bus components of phase current. Refer the "Asymmetric Half Bridge Converter" Card for a phase of the SR machine as shown in Fig 5.15. The Phase Voltage is measured across the SR Machine Phase "+" and "-" terminals. The Phase Current is measured at the SR Machine Phase "+" terminal. The Phase Excitation Current is measured at the "Excitation Bus" terminal. The Phase Generation Current is measured at the "Generation Bus" terminal. As shown in Fig 6.4, phase current is initially built up to the reference value using hard chopping. Here both the switches are turned on, the excitation bus voltage is applied across the winding and current is drawn from the excitation bus. When the current reaches the upper hysteresis limit both switches are turned off the diodes begin to conduct, the negative generation bus voltage is applied across the winding and generation current flows to the generation bus. Once current is detected at the reference value for three consecutive cycles it is maintained at reference value using soft chopping.

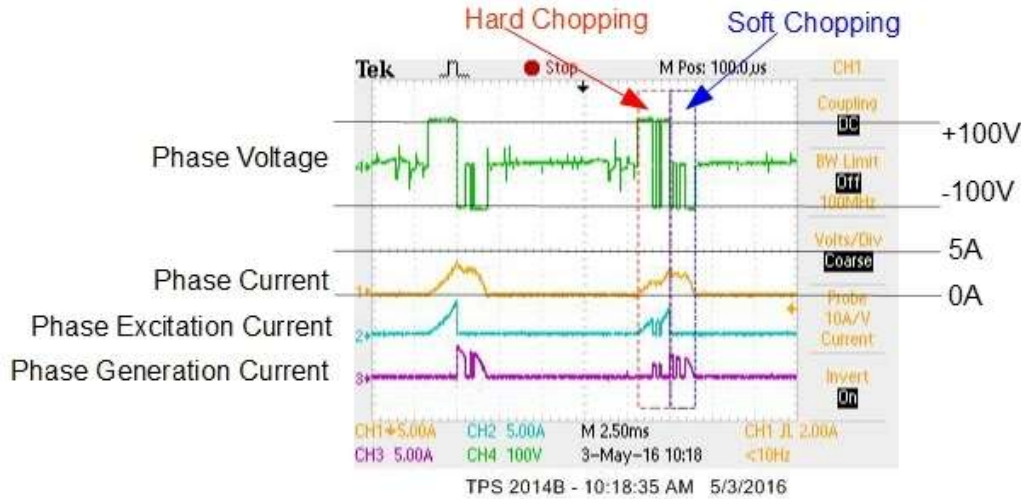


Fig 6.4 Generation Mode Waveforms – Excitation and Generation Phase Current

Load chopper is used to maintain the Generation Bus Voltage at reference value as seen in Fig 6.5. Gate Drive Signal is measured between the "Channel1" and "GND Digital" terminals of the IGBT Driver Card, shown in Fig 5.13, that drives the “Chopper For Dump Load” Card. Refer the “Chopper For Dump Load” Card shown in Fig 5.16. The Generation Bus Voltage is measured across the "Generation Bus" and "Common Return". The Load Current is measured at the Lamp Load "+" terminal. The Load Power is calculated on the DSO using the product of the Generation Bus Voltage and Load Current channels. The load power readings from the DSO and also the calculated values from CCS watch window are documented in Table 6.2 and Table 6.3.

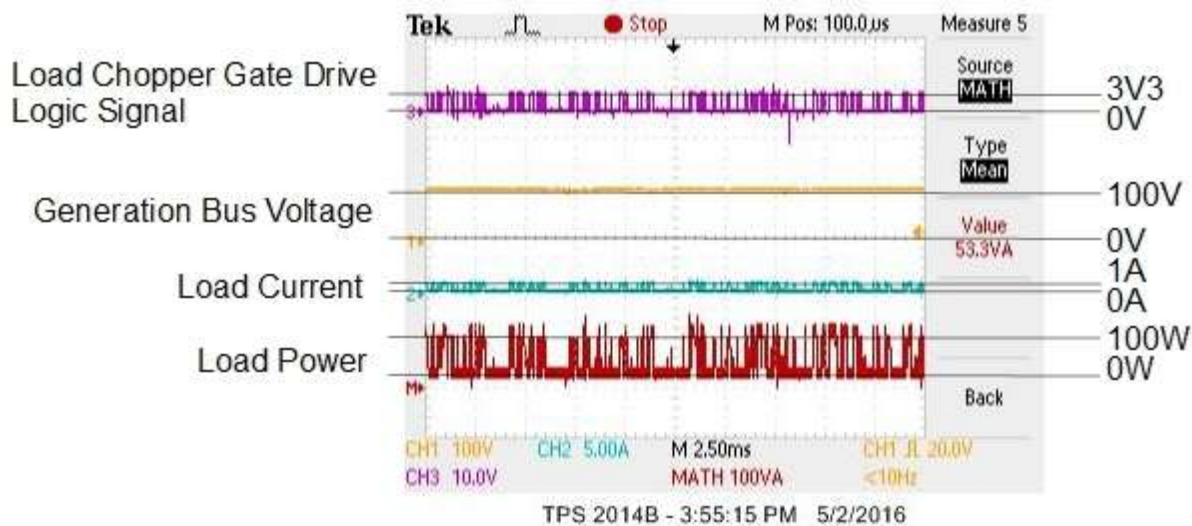


Fig 6.5 Dump Load Waveforms (Wind Speed = 9.99 m/s, SRG Shaft Speed = 905 rpm, Load Power=53.3 W)

### 6.3 Wind Energy System Results

With the vector controlled AC drive of the induction motor operating in torque mode as configured in Table 5.1 the SRG is operated in speed control mode and readings are taken at different speeds. Table 6.2 is for the lower power speed-torque characteristic corresponding to

lower wind speed and Table 6.3 is for the higher power speed-torque characteristic corresponding to higher wind speed. The shaft output power is read out from the Siemens drive parameter r0032. Load Power is calculated from the DSO and also in the DSP and displayed in the CCS watch window. Current set point and actual current readings are also taken from the CCS watch window. The efficiency is calculated using the equation:

$$\text{Efficiency}(\%) = \frac{\text{Load Power DSO}}{\text{Wind Turbine Output Power Actual r30032}} \times 100 \quad (6.1)$$

Table 6.2 SRG Readings for Lower Wind Speed

Wind Speed 1 ( $v_1$ ) = 7.88m/s										
	SRG Shaft Speed		AC Drive Output = Wind Turbine Output Power		Load Power		Current		Efficiency	
Sr No	Set-point (RPM)	Actual (RPM)	Program As per Table 5.1 (W)	Actual r0032 (W)	DSO $V_{load}$	I <sub>load</sub> (W)	DSP (W)	Set-point Min-Max (A)	Actual Min-Max (A)	Scope (W) / Actual (W) (%)
1	600	640	88	90	24	10	3.8 - 5	3.5 - 5	26.67	26.66
2	650	680	~91	90	25	15.5	3.4 - 5	3.5 - 5	27.78	11.25
3	700	730	95	100	26	21	3 - 5	3.3 - 5	26.00	9.23
4	750	785	100	100	30	19.4	2.8 - 5	1 - 4.4	30.00	7.69
5	800	826	95	90	24	13	1.2 - 3.1	1.4 - 3.4	22.22	
6	850	860	88	80-90	18	2.2	1.3 - 3.4	1 - 3.3	21.18	
7	900	906	80	80	9	0.6	1 - 3	1.1 - 1.8	18.75	
8	950	945	68	60-70	6	0.3	1 - 2.8	0.8 - 1.5	15.38	
9	1000	921	50	60-70	5	0.6	0.6 - 1.68	0 - 1.1	15.38	
10	1050	940	0	50-60	6	0.3	0.5 - 1.1	0 - 1	NA	
11	1100	921	0	50-60	7	0.3	0.5 - 1.1	0 - 1	NA	

Table 6.3 SRG Readings for Higher Wind Speed

Wind Speed 2 ( $v_2$ ) = 9.99m/s										
	SRG Shaft Speed		AC Drive Output = Wind Turbine Output Power		Load Power		Current		Efficiency	
Sr No	Set-point (RPM)	Actual (RPM)	Program As per Table 5.1 (W)	Actual r0032 (W)	DSO $V_{load}$	I <sub>load</sub> (W)	DSP (W)	Set-point Min-Max (A)	Actual Min-Max (A)	Scope (W) / Actual (W) (%)
1	600	645	88	90	23	10	3.8 - 5	3.5 - 5	30.00	25.55
2	650	690	~91	90-100	28	16	3.4 - 5	3.5 - 5	33.68	29.47
3	700	740	95	100-110	34	27	3 - 5	3.3 - 5	38.10	32.38
4	750	780	100	110	39	35	2.8 - 5	1 - 4.4	40.00	35.45
5	800	804	110	110-120	41	44	2.5 - 5	1.5 - 4.5	40.87	35.65
6	850	850	115	110-120	46	47	2 - 4	1 - 4.8	41.74	40
7	900	905	117	110-120	53	49	1.9 - 5	1 - 5	46.09	
8	950	955	120	110-120	55	50	1.7 - 5	1 - 5	47.83	
9	1000	1000	117	110-120	47	44	0 - 5	1 - 4.8	40.87	
10	1050	1050	95	90-100	25	17	0 - 3.9	1 - 4.5	26.32	
11	1100	1060	70	80	20	8	1.2 - 3.5	1 - 4	25.00	

Power calculation in DSP assumes fixed lamp resistance as shown in Eq 5.10. Hence as compared to the power calculated using the DSO, the DSP calculated power has the lower readings for lighter loads where actual lamp resistance will be lower due to lower duty cycles.

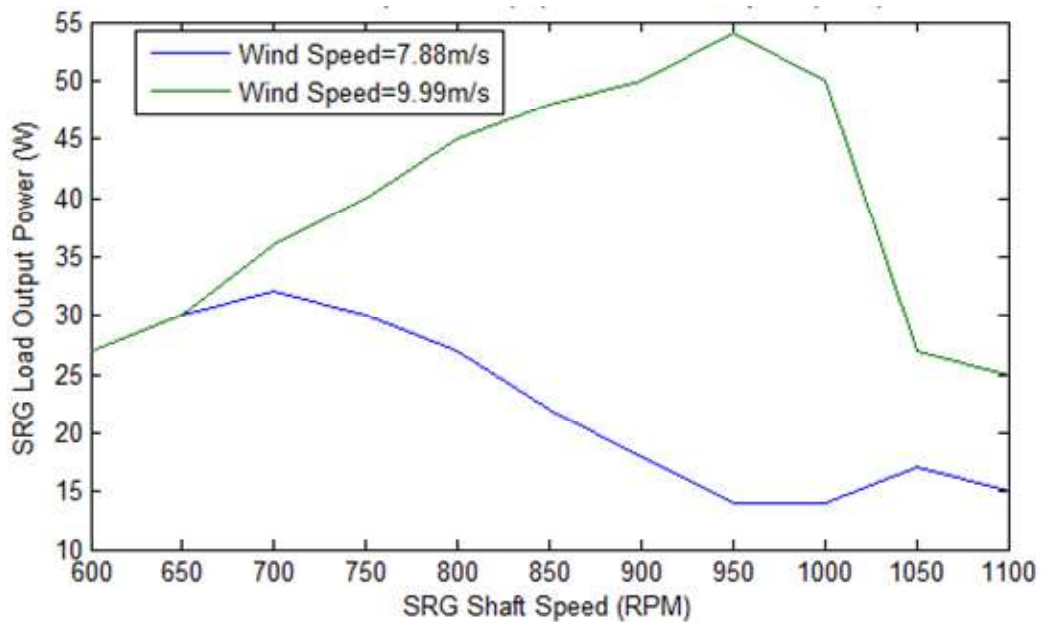


Fig 6.6 Dump Load Power (W) Vs SRG Shaft Speed Setpoint (RPM)

Fig 6.6, plotted in MATLAB, shows the variation in output power for various shaft speed set-points using the “SRG Shaft Speed Setpoint” and the “Load Power DSO” columns of Table 6.2 and Table 6.3. The variation in output power corresponds to the input power at the various speeds. The output power and system efficiency is found to increase with increase in input power as the fixed losses remain constant and constitute a smaller percentage of the handled power. Since the machine is not operated near its rated voltage and rated speed the power handling capacity is low and fixed losses make a significant percentage and hence the system efficiency is low throughout the operating range. Refer sections 6.3.2 and 6.3.3.

At lower shaft speeds in the 600-750 rpm range, the SRG is unable to apply sufficient braking torque as needed for the AC drive power output on the shaft hence the speed cannot be accurately maintained at setpoint and actual speed is higher than the setpoint speed. This could be corrected in the test setup by reducing the output power of the AC drive but it would result in very low power levels in the load. In an actual wind energy system, this requires proper selection of generator ratings and gear box so that the generator has sufficient torque to accurately control the speed over the entire operating range.

At higher shaft speeds, in the 1000-1100 rpm range for low wind speed ( $v_1$ ) and 1100 for higher wind speed ( $v_2$ ), the AC drive output power on the shaft is unable to maintain the required speed against friction, windage and minimum braking torque of the SRG, as a result speeds lower than the setpoint are observed.

### **6.3.1 MPPT Results**

#### ***6.3.1.1 Using Wind Sensor***

With AC drive and SRG wind speed input switch set for high wind speed  $v_2=9.99$  m/s, the SRG speed is controlled at 950 rpm and load power of 54W is observed. When the AC drive wind speed input switch is set for low wind speed  $v_1=7.88$ m/s with the SRG wind speed switch still set for high wind speed, the SRG speed stays at 950 rpm and lower output power of 6W is observed. When the SRG wind speed switch now set for low wind speed, the SRG speed is controlled at 750 rpm and output power of 30W is observed. Hence MPPT using speed sensor is verified.

#### ***6.3.1.2 Using Hill Climbing Technique***

MPPT by Hill Climbing is enabled by setting the “MPPTHillClimb” flag in the DSP to 1 using the CCS watch-window. With the AC Drive wind speed input switch set to low wind speed  $v_1 =7.88$ m/s the SRG shaft speed is controlled around the maximum power point of 750 rpm and observed to iterate back and forth between 700 – 750 – 800 rpm. If the AC Drive wind speed input switch is now set to high wind speed  $v_2 =9.99$ m/s the SRG shaft speed increases towards the maximum power point of 950 rpm and observed to iterate back and forth between 850 – 900 – 950-1000 rpm.

### **6.3.2 Reason for Low Efficiency**

In Fig 6.7(a)  $W_{f1}$  is the field energy stored in the SRG during excitation and  $W_{m1}$  is the converted energy by the SRG. The field energy,  $W_{f1}$  is supplied by the electrical system through the switches to set-up the magnetic field and is recovered by the electrical system over the diodes along with the converted energy. This field energy is analogous to reactive power in an AC system and is exchanged between the magnetic field and the dc bus capacitors. For a machine operating at low currents in the linear unsaturated region of the magnetic characteristics as in Fig 6.7(a), the field energy  $W_{f1}$  is almost equal to the converted energy,  $W_{m1}$ . This indicates that a larger percentage of energy is exchanged back and forth between the magnetic field and the dc bus capacitors resulting in proportionately more system losses for the converted mechanical power. For a machine operating at higher currents in the non-linear saturated region of the magnetic characteristics as in Fig 6.7(b), the converted energy loop  $W_{m2}$  is larger. The field energy supplied,  $W_{f2}$  is much less compared to the converted energy,  $W_{m2}$  resulting in proportionately less system losses for the converted mechanical power. As machine frame size increases with the air gap staying constant, the

machine is operated in the non-linear region of the magnetic characteristics resulting in higher efficiency [24].

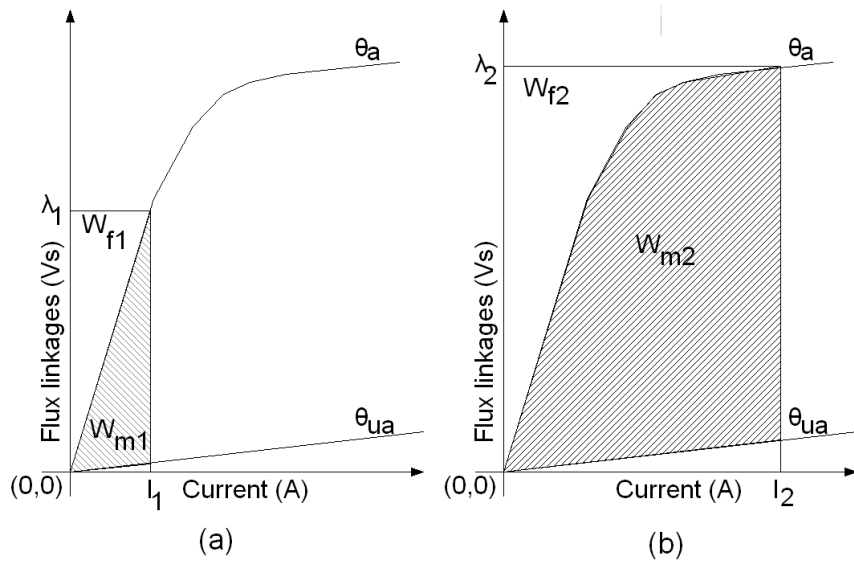


Fig 6.7 Effect of non-linear magnetic characteristics on energy conversion

### 6.3.3 Reason for Low Power Handling Capacity

For prime mover power output of more than 120W, the machine braking torque was not sufficient to maintain stable speed. The machine is operated at rated current so we assume that rated torque is developed by the machine as per the torque equation Eq 3.8. However the machine is operated at low speed of around 1000 rpm as against the rated speed of 2000 rpm and also at low voltage of 100V DC as against the rated voltage of 300V DC hence the power handling capacity of the machine is reduced from its rated value. As speed increases for the rated torque at rated current, the mechanical power handled by the machine increases.

In motor mode, as speed increases the back-emf also increases and higher bus voltage is needed to enable the phase current to rise quickly to rated value. In generator mode as speed increases, the induced-emf also increases and higher bus voltage is needed to limit the phase current to rated value. Hence with increase in speed, as voltage increases for rated current, the electrical power handled by the machine increases.

### 6.3.4 Comparison with simulation using the specific model

The MATLAB simulation using the SRG specific model described in section 4.8 was re-run with the hardware test set-up data for fixed speeds and fixed input torque to compare the

actual measurements on the motor and the experimental set-up with the theoretical values obtained from FEMM and Simulink simulations.

Simulation configured with  $V_{gen} = 100$  V DC, Dump Load =  $100 \Omega$

Table 6.4 Simulation Results using the specific model with system parameters similar to the hardware setup

Sr No	SRG Shaft Speed (RPM)	Shaft Torque (Nm)	Mechanical Input Power (W)	Output Power at Load (W)	System Efficiency (%)
1	750	1.2727	100	42	42
2	950	1.2057	120	62.72	52.26

Comparing the results in Table 6.4 with Table 6.2 and Table 6.3 we see good correlation between the specific model simulation and the hardware results. The hardware results show lower efficiency because all losses are not accurately modeled in the simulation. Fig 6.8 shows the simulation run for shaft speed of 950 rpm and shaft torque of 1.2057 Nm that corresponds to the wind turbine output at wind speed of  $v_2=9.99$ m/s.

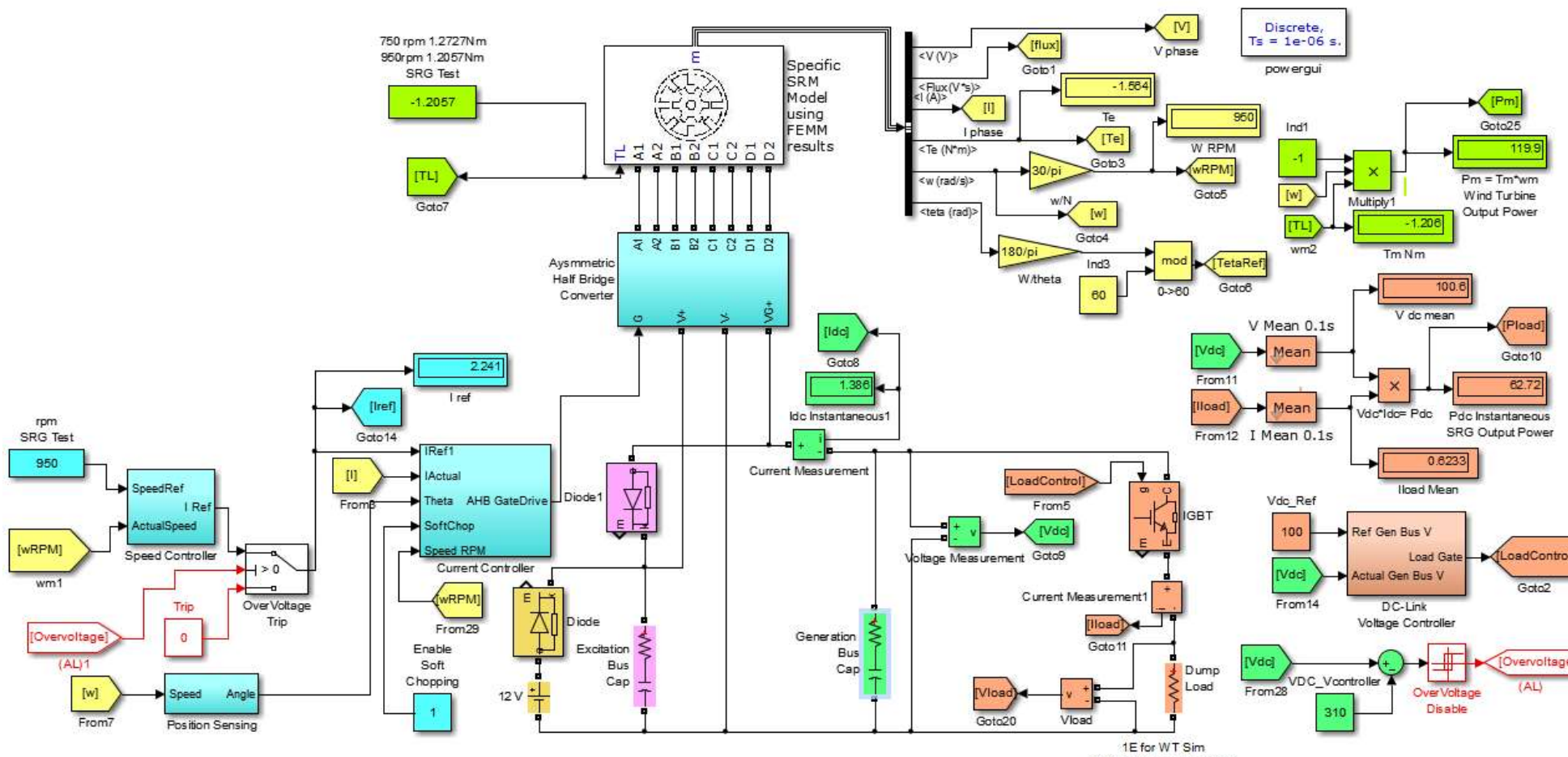


Fig 6.8 Simulation using FEMM results with Simulink SRM specific model for comparison with Hardware Test Results. Test for 950 rpm, 120W input power.

## **Chapter 7**

### **Summary and Conclusions**

Simulation is done in MATLAB for wind energy conversion system consisting of a wind turbine coupled with a switched reluctance generator. Initial excitation is applied from a 12 V battery and dc bus voltage is built up by self excitation to the rated value of 300 V dc. The MPPT controller adjusts the SRG speed for changes in wind speed, to generate maximum power. The simulation verified the feasibility of using a SRG with a wind turbine system to build up the dc bus voltage through self-excitation and to track maximum power from the wind by maintaining the optimum tip speed ratio.

Hardware implementation is done using power electronic devices, sensors and DSP controller. A vector controlled AC drive and induction motor are used for wind turbine emulation. For a given wind speed, the SRG speed is controlled at the optimal value for MPPT using “Hill Climbing” technique. DC link voltage is built up from 24 V to 100 V DC by self excitation and with 120 W of mechanical input power on the shaft a 50 W lamp load is sustained even after disconnecting the external excitation source.

The SRG was operated with a combination of hard and soft chopping and the noise levels from the SRG were found to be tolerable and comparable to the vector controlled induction motor. In motor mode with soft chopping, the noise levels were even lower. Motor phase current, speed and DC bus voltage could be controlled. Other than jerky operation in motor mode at low speeds, below 100 rpm, no major drawback was found in the operation of the SR machine.

## 7.1 Future Scope

The following areas need more investigation:

- Improvement of the current sensing circuit to eliminate high frequency noise. This would enable full soft-chopping operation in the generation mode and result in decrease in noise and some improvement in efficiency.
- In Motor mode: implementation of smooth starting and stable operation below 100 rpm
- In both Motor and Generator mode: Operation at rated speed and voltage
- In both Motor and Generator mode: simultaneous excitation of two phases for better current overlap and lesser torque ripple. Torque sensor would be required for implementing torque ripple reduction techniques.
- In both Motor and Generator mode: position sensor-less operation
- Reduction in cost and component count by the use of High and Low Side Driver ICs (example IR2113), current sensing ICs (example IR2175), lower cost Hall effect current sensors (example ACS712)
- Standalone system operation by booting from Flash memory and user interaction using alphanumeric display and keypad.
- In both Motor and Generator mode: fault tolerant operation
- In Generator mode: single pulse operation
- In Generator mode: coupling with actual wind turbine
- In Generator mode: addition of grid interface. The Generation Bus DC Link Voltage control loop is currently used to calculate the duty-cycle of the Dump Load Chopper. In grid interface using Voltage Oriented Control (VOC) the Generation Bus DC Link Voltage control loop would calculate the reference for the in-phase active component of current  $i_q$  to be supplied to the grid. In a grid interface using Direct Power Control (DPC) the Generation Bus DC Link Voltage control loop would calculate the reference for the active power P to be supplied to the grid.
- Investigation into other applications of switched reluctance machines found in literature like starter-generator systems for aircrafts and automobiles.

# **Appendix I**

## **I.1 Software used in the project**

- a. FEMM v4.2
- b. TinyCAD v2.80.03 Build #514
- c. Tina TI v9.3.50.40 SF-TI
- d. Kicad v4.0.0-rc2
- e. Dassault Systèmes DraftSight v1R4 x64
- f. Open Office v4.0.1
- g. Siemens Starter v4.4.1
- h. Tektronix Open Choice Desktop v2.4
- i. Texas Instruments Code Composer Studio v6.1.2.00015
- j. MATLAB v10

## **I.2 Test Equipment used in the project**

- a. Tektronix TPS2014B Four Channel Isolated Inputs Digital Storage Oscilloscope
  - i. Tektronix A622 AC/DC Current Probe 0-70A rms, 100A peak AC/DC  
Freq DC-100 kHz
  - ii. Tektronix P5122 High Voltage Probe X100
- b. Aplab Regulated Power Supply 100 V, 6A
- c. Kusam Meco KM-459 LCR-Q meter

## I.3 Datasheet excerpts for key components

### I.3.1 DC Bus Filter Capacitor Vishay 198PHR-SI



[www.vishay.com](http://www.vishay.com)

198 PHR-SI

Vishay BCcomponents

#### Aluminum Capacitors, Power High Ripple Current Snap-In

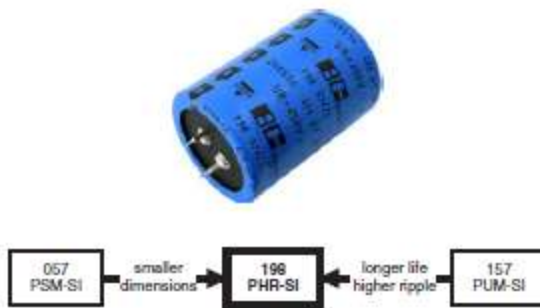


Fig. 1

#### FEATURES

- Useful life: 15 000 h at + 85 °C
- Very high ripple current capability
- High reliability
- Polarized aluminum electrolytic capacitors, non-solid electrolyte
- Large types, miniaturized dimensions, cylindrical aluminum case, insulated with a blue sleeve
- Keyed polarity version available
- Material categorization: For definitions of compliance please see [www.vishay.com/doc?99912](http://www.vishay.com/doc?99912)



RoHS  
COMPLIANT

#### APPLICATIONS

- Motor control and industrial systems
- Smoothing and filtering
- Standard and switched mode power supplies
- Energy storage in pulse systems

#### MARKING

The capacitors are marked (where possible) with the following information:

- Rated capacitance (in  $\mu$ F)
- Tolerance code on rated capacitance, code letter in accordance with IEC 60062 (M for  $\pm 20\%$ )
- Rated voltage (in V)
- Date code (YYMM)
- Name of manufacturer
- Code for factory of origin
- “-” sign to identify the negative terminal, visible from the top and side of the capacitor
- Code number
- Climatic category in accordance with IEC 60068

#### QUICK REFERENCE DATA

DESCRIPTION	VALUE
Nominal case size ( $\varnothing$ D x L in mm)	22 x 25 to 35 x 60
Rated capacitance range (E6/E12 series), $C_R$	56 $\mu$ F to 680 $\mu$ F
Tolerance on $C_R$	$\pm 20\%$
Rated voltage range, $U_R$	400 V and 450 V
Category temperature range	- 25 °C to + 85 °C
Endurance test at 85 °C	7000 h
Useful life at 85 °C	15 000 h
Shelf life at 0 V, 85 °C	1000 h
Based on sectional specification	IEC 60384-4/EN 130300
Climatic category IEC 60068	25/085/56

#### ELECTRICAL DATA AND ORDERING INFORMATION

$U_R$ (V)	$C_R$ 100 Hz ( $\mu$ F)	NOMINAL CASE SIZE $\varnothing$ D x L (mm)	$I_R$ 100 Hz 85 °C (A)	$I_{L1}$ 1 min ( $\mu$ A)	$I_{L5}$ 5 min ( $\mu$ A)	TYP. ESR 100 Hz (m $\Omega$ )	MAX. ESR 100 Hz (m $\Omega$ )	TYP. Z 10 kHz (m $\Omega$ )	MAX. Z 10 kHz (m $\Omega$ )	ORDERING CODE MAL2198.....	
										2-TERM.	3-TERM.
450	680	35 x 60	3.30	1840	616	88	140	70	140	57681E3	77681E3

## I.3.2 Isolation Amplifier TI ISO124



ISO124

SBOS074D - SEPTEMBER 1997 - REVISED JANUARY 2015

### ISO124 Precision Lowest-Cost Isolation Amplifier

#### 1 Features

- 100% Tested for High-Voltage Breakdown
- Rated 1500 Vrms
- High IMR: 140 dB at 60 Hz
- 0.010% Maximum Nonlinearity
- Bipolar Operation:  $V_O = \pm 10$  V
- DIP-16 and SO-28
- Ease of Use: Fixed Unity Gain Configuration
- $\pm 4.5$ -V to  $\pm 18$ -V Supply Range

#### 2 Applications

- Industrial Process Control:
  - Transducer Isolator, Isolator for Thermocouples, RTDs, Pressure Bridges, and Flow Meters, 4-mA to 20-mA Loop Isolation
- Ground Loop Elimination
- Motor and SCR Control
- Power Monitoring
- PC-Based Data Acquisition
- Test Equipment

#### 3 Description

The ISO124 is a precision isolation amplifier incorporating a novel duty cycle modulation-demodulation technique. The signal is transmitted digitally across a 2-pF differential capacitive barrier. With digital modulation, the barrier characteristics do not affect signal integrity, thus resulting in excellent reliability and good high-frequency transient immunity across the barrier. Both barrier capacitors are imbedded in the plastic body of the package.

The ISO124 is easy to use. No external components are required for operation. The key specifications are 0.010% maximum nonlinearity, 50-kHz signal bandwidth, and 200- $\mu$ V/ $^{\circ}$ C  $V_{OS}$  drift. A power supply range of  $\pm 4.5$  V to  $\pm 18$  V and quiescent currents of  $\pm 5$  mA on  $V_{S1}$  and  $\pm 5.5$  mA on  $V_{S2}$  make the ISO124 ideal for a wide range of applications.

The ISO124 is available in PDIP-16 and SOIC-28 plastic surface-mount packages.

#### Device Information<sup>(1)</sup>

PART NUMBER	PACKAGE	BODY SIZE (NOM)
ISO124	PDIP (16)	17.90 mm $\times$ 7.50 mm
	SOIC (28)	20.01 mm $\times$ 6.61 mm

(1) For all available packages, see the orderable addendum at the end of the data sheet.

## 7.5 Electrical Characteristics

At  $T_A = +25^\circ\text{C}$ ,  $V_{S1} = V_{S2} = \pm 15\text{ V}$ , and  $R_L = 2\text{ k}\Omega$ , unless otherwise noted.

PARAMETER	TEST CONDITIONS	ISO124P, U			UNIT
		MIN	TYP	MAX	
<b>ISOLATION</b>					
Rated Voltage, continuous ac 60 Hz		1500			Vac
100% Test <sup>(1)</sup>	1s, 5pc PD	2400			Vac
Isolation Mode Rejection	60 Hz	140			dB
Barrier Impedance		$10^{14} \parallel 2$			$\Omega \parallel \text{pF}$
Leakage Current at 60 Hz	$V_{ISO} = 240\text{ Vrms}$	0.18	0.5		$\mu\text{Arms}$
<b>GAIN</b>					
Nominal Gain	$V_O = \pm 10\text{ V}$	1			V/V
Gain Error		$\pm 0.05$	$\pm 0.50$		%FSR
Gain vs Temperature		$\pm 10$			ppm/ $^\circ\text{C}$
Nonlinearity <sup>(2)</sup>		$\pm 0.005$	$\pm 0.010$		%FSR
<b>INPUT OFFSET VOLTAGE</b>					
Initial Offset		$\pm 20$	$\pm 50$		mV
vs Temperature		$\pm 200$			$\mu\text{V}/^\circ\text{C}$
vs Supply		$\pm 2$			mV/V
Noise		4			$\mu\text{V}/\sqrt{\text{Hz}}$
<b>INPUT</b>					
Voltage Range		$\pm 10$	$\pm 12.5$		V
Resistance		200			k $\Omega$
<b>OUTPUT</b>					
Voltage Range		$\pm 10$	$\pm 12.5$		V
Current Drive		$\pm 5$	$\pm 15$		mA
Capacitive Load Drive		0.1			$\mu\text{F}$
Ripple Voltage <sup>(3)</sup>		20			mVp-p
<b>FREQUENCY RESPONSE</b>					
Small-Signal Bandwidth		50			kHz
Slew Rate		2			V/ $\mu\text{s}$
Settling Time 0.10%	$V_O = \pm 10\text{ V}$	50			$\mu\text{s}$
Settling Time 0.01%		350			$\mu\text{s}$
Overload Recovery Time		150			$\mu\text{s}$
<b>POWER SUPPLIES</b>					
Rated Voltage		$\pm 15$			V
Voltage Range		$\pm 4.5$	$\pm 18$		V
$V_{S1}$	Quiescent Current	$\pm 5.0$	$\pm 7.0$		mA
$V_{S2}$		$\pm 5.5$	$\pm 7.0$		
<b>TEMPERATURE RANGE</b>					
Specification		-25	85		$^\circ\text{C}$
Operating		-25	85		$^\circ\text{C}$
Storage		-40	125		$^\circ\text{C}$
$R_{JA1}$	Thermal Resistance	100			$^\circ\text{C/W}$
$R_{JA2}$		65			$^\circ\text{C/W}$

(1) Tested at 1.6 X rated, fail on 5 pC partial discharge.

(2) Nonlinearity is the peak deviation of the output voltage from the best-fit straight line. It is expressed as the ratio of deviation to FSR.

(3) Ripple frequency is at carrier frequency (500 kHz).

### I.3.3 Current Sensor LEM HX 05-P/SP2



$I_{PN} = 3 \dots 50 A$

#### Current Transducer HX 03..50-P/SP2

For the electronic measurement of currents: DC, AC, pulsed, mixed, with galvanic isolation between the primary circuit (high power) and the secondary circuit (electronic circuit).



All data are given with  $R_L = 2 k\Omega$

#### Electrical data

Primary nominal current rms $I_{PN}$ (A)	Primary current measuring range <sup>1)</sup> $I_{PM}$ (A)	Primary conductor diameter x turns (mm)	Type
3	$\pm 9$	0.6d x 20T	HX 03-P/SP2
5	$\pm 15$	0.8d x 12T	HX 05-P/SP2
10	$\pm 30$	1.1d x 6T	HX 10-P/SP2
15	$\pm 45$	1.4d x 4T	HX 15-P/SP2
20	$\pm 60$	1.6d x 3T	HX 20-P/SP2
25	$\pm 75$	1.6d x 2T	HX 25-P/SP2
50	$\pm 150$	1.2 x 6.3 x 1T	HX 50-P/SP2
$V_{out} = V_{oe} + (0.625/I_p) I_{PN}$			
$V_{out}$	Output voltage (Analog) @ $\pm I_{PN}$ , $R_L = 2 k\Omega$ , $T_A = 25^\circ C$	$V_{oe} \pm 0.625$	V
$R_{out}$	Output internal resistance	$< 50$	$\Omega$
$R_L$	Load resistance	$\geq 2$	$k\Omega$
$V_c$	Supply voltage ( $\pm 5\%$ )	$+ 12 \dots 15$	V
$V_c$	Current consumption	$< 15$	mA

#### Accuracy - Dynamic performance data

X	Accuracy @ $I_{PN}$ , $T_A = 25^\circ C$ (excluding offset)	$< \pm 1\% \text{ of } I_{PN}$
$\varepsilon_L$	Linearity error ( $0 \dots \pm I_{PN}$ )	$< \pm 1\% \text{ of } I_{PN}$
$V_{oe}$	Electrical offset voltage @ $I_p = 0$ , $T_A = 25^\circ C$	$+ 2.5V \pm 50 mV$
$V_{oh}$	Hysteresis offset voltage @ $I_p = 0$ after an excursion of $1 \times I_{PN}$	$< \pm 10 mV$
$TCV_{oe}$	Temperature coefficient of $V_{oe}$	$< \pm 1.5 mV/K$
$TCV_{oh}$	Temerature coefficient of $V_{out}$ (% of reading)	$\pm 0.1\% /K$
$t_r$	Response time to 90% of $I_{PN}$ step	$\leq 3 \mu s$
BW	Frequency bandwidth (-3 dB) <sup>2)</sup>	50 kHz

#### General data

$T_A$	Ambient operating temperature	-25 .. +85	$^\circ C$
$T_s$	Ambient storage temperature	-25 .. +85	$^\circ C$
$m$	Mass	8	g
	Standards	EN 50178: 1997	

Note: <sup>1)</sup> With  $R_L = 2 k\Omega$

<sup>2)</sup> Small signal only to avoid excessive heating of the magnetic cores.

#### Features

- Galvanic isolation between primary and secondary circuit
- Hall effect measuring principle
- Isolation voltage 3000V
- Low power consumption
- Extended measuring range ( $3 \times I_{PN}$ )
- Isolated plastic case recognized according to UL 94-V0.

#### Special features

- Single supply from +12V to +15V

#### Advantages

- Low insertion losses
- Easy to mount with automatic handling system
- Small size and space saving
- Only one design for wide current ratings range
- High immunity to external interference

#### Applications

- Switched Mode Power Supplies (SMPS)
- AC variable speed drives
- Uninterruptible Power Supplies (UPS)
- Electrical appliances
- Battery supplied applications
- DC motor drives

#### Application domain

- Industrial.

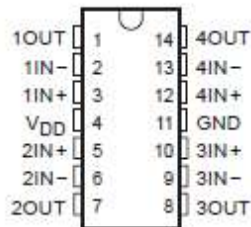
### I.3.4 Precision Op-amp TLC274

**TLC274, TLC274A, TLC274B, TLC274Y, TLC279  
LinCMOS™ PRECISION QUAD OPERATIONAL AMPLIFIERS**

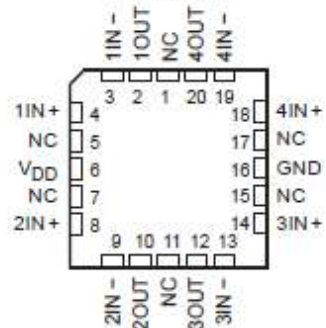
SLOG092D - SEPTEMBER 1987 - REVISED MARCH 2001

- Trimmed Offset Voltage:  
TLC279 . . . 900  $\mu$ V Max at 25°C,  
 $V_{DD} = 5$  V
  - Input Offset Voltage Drift . . . Typically  
0.1  $\mu$ V/Month, Including the First 30 Days
  - Wide Range of Supply Voltages Over  
Specified Temperature Range:  
0°C to 70°C . . . 3 V to 16 V  
-40°C to 85°C . . . 4 V to 16 V  
-55°C to 125°C . . . 4 V to 16 V
  - Single-Supply Operation
  - Common-Mode Input Voltage Range  
Extends Below the Negative Rail (C-Suffix  
and I-Suffix Versions)
  - Low Noise . . . Typically 25 nV/ $\sqrt{\text{Hz}}$   
at  $f = 1$  kHz
  - Output Voltage Range Includes Negative  
Rail
  - High Input Impedance . . .  $10^{12}$   $\Omega$  Typ
  - ESD-Protection Circuitry
  - Small-Outline Package Option Also  
Available in Tape and Reel
  - Designed-In Latch-Up Immunity

D, J, N, OR PW PACKAGE  
(TOP VIEW)



**FK PACKAGE  
(TOP VIEW)**



**TLC274, TLC274A, TLC274B, TLC274Y, TLC279**  
**LinCMOS™ PRECISION QUAD OPERATIONAL AMPLIFIERS**

SLOS092D – SEPTEMBER 1987 – REVISED MARCH 2001

electrical characteristics at specified free-air temperature,  $V_{DD} = 5\text{ V}$  (unless otherwise noted)

PARAMETER	TEST CONDITIONS	$T_A^\dagger$	TLC274C, TLC274AC, TLC274BC, TLC279C			UNIT
			MIN	TYP	MAX	
$V_{IO}$ Input offset voltage	TLC274C $V_O = 1.4\text{ V}, V_{IC} = 0, R_S = 50\text{ }\Omega, R_L = 10\text{ k}\Omega$	25°C	1.1	10	12	mV
		Full range				
	TLC274AC $V_O = 1.4\text{ V}, V_{IC} = 0, R_S = 50\text{ }\Omega, R_L = 10\text{ k}\Omega$	25°C	0.9	5	6.5	
		Full range				
	TLC274BC $V_O = 1.4\text{ V}, V_{IC} = 0, R_S = 50\text{ }\Omega, R_L = 10\text{ k}\Omega$	25°C	340	2000	3000	$\mu\text{V}$
		Full range				
	TLC279C $V_O = 1.4\text{ V}, V_{IC} = 0, R_S = 50\text{ }\Omega, R_L = 10\text{ k}\Omega$	25°C	320	900	1500	
		Full range				
$\alpha_{VIO}$	Average temperature coefficient of input offset voltage	25°C to 70°C		1.8		$\mu\text{V}/^\circ\text{C}$
$I_{IO}$ Input offset current (see Note 4)	$V_O = 2.5\text{ V}, V_{IC} = 2.5\text{ V}$	25°C	0.1	60	60	pA
		70°C	7	300	300	
		25°C	0.6	60	60	
		70°C	40	600	600	
$V_{ICR}$ Common-mode input voltage range (see Note 5)		25°C	-0.2 to 4	-0.3 to 4.2	4.2	V
		Full range				
$V_{OH}$ High-level output voltage	$V_{ID} = 100\text{ mV}, R_L = 10\text{ k}\Omega$	25°C	3.2	3.8	3.8	V
		0°C	3	3.8	3.8	
		70°C	3	3.8	3.8	
$V_{OL}$ Low-level output voltage	$V_{ID} = -100\text{ mV}, I_{OL} = 0$	25°C	0	50	50	mV
		0°C	0	50	50	
		70°C	0	50	50	
$A_{VD}$ Large-signal differential voltage amplification	$V_O = 0.25\text{ V to }2\text{ V}, R_L = 10\text{ k}\Omega$	25°C	5	23	23	$\text{V/mV}$
		0°C	4	27	27	
		70°C	4	20	20	
CMRR Common-mode rejection ratio	$V_{IC} = V_{ICR\min}$	25°C	65	80	80	dB
		0°C	60	84	84	
		70°C	60	85	85	
KSVR Supply-voltage rejection ratio ( $\Delta V_{DD}/\Delta V_{IO}$ )	$V_{DD} = 5\text{ V to }10\text{ V}, V_O = 1.4\text{ V}$	25°C	65	95	95	dB
		0°C	60	94	94	
		70°C	60	96	96	
$I_{DD}$ Supply current (four amplifiers)	$V_O = 2.5\text{ V}, V_{IC} = 2.5\text{ V}, \text{No load}$	25°C	2.7	6.4	6.4	mA
		0°C	3.1	7.2	7.2	
		70°C	2.3	5.2	5.2	

† Full range is 0°C to 70°C.

NOTES: 4. The typical values of input bias current and input offset current below 5 pA were determined mathematically.  
 5. This range also applies to each input individually.

operating characteristics at specified free-air temperature,  $V_{DD} = 5$  V

PARAMETER	TEST CONDITIONS	$T_A$	TLC274C, TLC274AC, TLC274AC, TLC274BC, TLC279C			UNIT
			MIN	TYP	MAX	
SR Slew rate at unity gain	$R_L = 10 \Omega$ , $C_L = 20 \text{ pF}$ , See Figure 1	$V_{IPP} = 1 \text{ V}$	25°C	3.6		$\text{V}/\mu\text{s}$
			0°C	4		
		$V_{IPP} = 2.5 \text{ V}$	70°C	3		
			25°C	2.9		
			0°C	3.1		
			70°C	2.5		
$V_n$ Equivalent input noise voltage	$f = 1 \text{ kHz}$ , See Figure 2	$R_S = 20 \Omega$ ,	25°C	25		$\text{nV}/\sqrt{\text{Hz}}$
$B_{OM}$ Maximum output-swing bandwidth	$V_O = V_{OH}$ , $R_L = 10 \text{ k}\Omega$ , See Figure 1	$C_L = 20 \text{ pF}$ , See Figure 1	25°C	320		$\text{kHz}$
			0°C	340		
			70°C	260		
$B_1$ Unity-gain bandwidth	$V_I = 10 \text{ mV}$ , See Figure 3	$C_L = 20 \text{ pF}$ ,	25°C	1.7		$\text{MHz}$
			0°C	2		
			70°C	1.3		
$\phi_m$ Phase margin	$V_I = 10 \text{ mV}$ , $C_L = 20 \text{ pF}$ ,	$f = B_1$ ,	25°C	46°		
			0°C	47°		
			70°C	44°		

### I.3.5 Precision Voltage Reference TL431

## TL431A, B Series, NCV431A, B Series, SCV431A

### Programmable Precision References

The TL431A, B integrated circuits are three-terminal programmable shunt regulator diodes. These monolithic IC voltage references operate as a low temperature coefficient zener which is programmable from  $V_{ref}$  to 36 V with two external resistors. These devices exhibit a wide operating current range of 1.0 mA to 100 mA with a typical dynamic impedance of  $0.22 \Omega$ . The characteristics of these references make them excellent replacements for zener diodes in many applications such as digital voltmeters, power supplies, and op amp circuitry. The 2.5 V reference makes it convenient to obtain a stable reference from 5.0 V logic supplies, and since the TL431A, B operates as a shunt regulator, it can be used as either a positive or negative voltage reference.

#### Features

- Programmable Output Voltage to 36 V
- Voltage Reference Tolerance:  $\pm 0.4\%$ , Typ @ 25°C (TL431B)
- Low Dynamic Output Impedance,  $0.22 \Omega$  Typical
- Sink Current Capability of 1.0 mA to 100 mA
- Equivalent Full-Range Temperature Coefficient of 50 ppm/ $^{\circ}\text{C}$  Typical
- Temperature Compensated for Operation over Full Rated Operating Temperature Range
- Low Output Noise Voltage



ON Semiconductor®

[www.onsemi.com](http://www.onsemi.com)



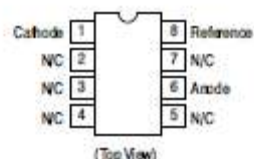
TO-92 (TO-226)  
LP SUFFIX  
CASE 29



PDIP-8  
P SUFFIX  
CASE 626



Micro8™  
DM SUFFIX  
CASE 846A



### I.3.6 Power Diode VS-APH3006-F3

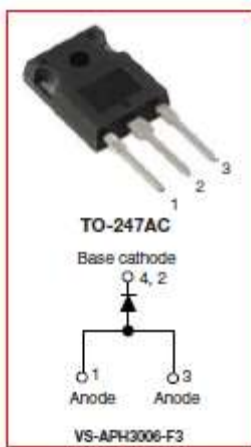


VS-APH3006-F3, VS-APH3006-N3, VS-EPH3006-F3, VS-EPH3006-N3

[www.vishay.com](http://www.vishay.com)

Vishay Semiconductors

#### Hyperfast Rectifier, 30 A FRED Pt®



TO-247AC  
Base cathode  
○ 4, 2  
○ 1  
Anode  
○ 3  
Anode  
VS-APH3006-F3  
VS-APH3006-N3



TO-247AC modified  
Base cathode  
○ 2  
Cathode  
○ 1  
Anode  
○ 3  
Anode  
VS-EPH3006-F3  
VS-EPH3006-N3

#### FEATURES

- Low forward voltage drop
- Hyperfast soft recovery time
- 175 °C operating junction temperature
- Designed and qualified according to JEDEC-JESD47
- Material categorization:  
For definitions of compliance please see [www.vishay.com/doc?99912](http://www.vishay.com/doc?99912)



RoHS  
COMPLIANT  
HALOGEN  
**FREE**  
Available

#### DESCRIPTION/APPLICATIONS

Hyperfast recovery rectifiers designed with optimized performance of forward voltage drop, hyperfast recovery time, and soft recovery.

The planar structure and the platinum doped life time control guarantee the best overall performance, ruggedness and reliability characteristics.

These devices are intended for use in PFC Boost stage in the AC/DC section of SMPS, inverters or as freewheeling diodes.

The extremely optimized stored charge and low recovery current minimize the switching losses and reduce over dissipation in the switching element and snubbers.

#### PRODUCT SUMMARY

Package	TO-247AC, TO-247AC modified (2 pins)
$I_F(AV)$	30 A
$V_R$	600 V
$V_F$ at $I_F$	2.65 V
$t_{rr}$ typ.	27 ns
$T_J$ max.	175 °C
Diode variation	Single die

### I.3.7 IGBT Switch IGW40H65H5



IGP40N65H5, IGW40N65H5

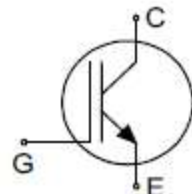
High speed switching series fifth generation

High speed 5 IGBT in TRENCHSTOP™ 5 technology

#### Features and Benefits:

High speed H5 technology offering

- Best-in-Class efficiency in hard switching and resonant topologies
- Plug and play replacement of previous generation IGBTs
- 650V breakdown voltage
- Low gate charge  $Q_g$
- Maximum junction temperature 175°C
- Qualified according to JEDEC for target applications
- Pb-free lead plating; RoHS compliant
- Complete product spectrum and PSpice Models:  
<http://www.infineon.com/igbt/>



#### Applications:

- Solar converters
- Uninterruptible power supplies
- Welding converters
- Mid to high range switching frequency converters

#### Package pin definition:

- Pin 1 - gate
- Pin 2 & backside - collector
- Pin 3 - emitter



#### Key Performance and Package Parameters

Type	$V_{CE}$	$I_c$	$V_{CE(on)}, T_{j}=25^{\circ}\text{C}$	$T_{vjmax}$	Marking	Package
IGP40N65H5	650V	40A	1.65V	175°C	G40EH5	PG-T0220-3
IGW40N65H5	650V	40A	1.65V	175°C	G40EH5	PG-T0247-3

# IGBT IGW40H65H5

## Maximum Ratings

For optimum lifetime and reliability, Infineon recommends operating conditions that do not exceed 80% of the maximum ratings stated in this datasheet.

Parameter	Symbol	Value	Unit
Collector-emitter voltage, $T_{VJ} \geq 25^\circ\text{C}$	$V_{CE}$	650	V
DC collector current, limited by $T_{VJ\max}$ $T_c = 25^\circ\text{C}$ $T_c = 100^\circ\text{C}$	$I_C$	74.0 46.0	A
Pulsed collector current, $t_p$ limited by $T_{VJ\max}$	$I_{CPuls}$	120.0	A
Turn off safe operating area $V_{CE} \leq 650\text{V}$ , $T_{VJ} \leq 175^\circ\text{C}$ , $t_p = 1\mu\text{s}$	-	120.0	A
Gate-emitter voltage Transient Gate-emitter voltage ( $t_p \leq 10\mu\text{s}$ , $D < 0.010$ )	$V_{GE}$	$\pm 20$ $\pm 30$	V
Power dissipation $T_c = 25^\circ\text{C}$ Power dissipation $T_c = 100^\circ\text{C}$	$P_{tot}$	250.0 125.0	W
Operating junction temperature	$T_{VJ}$	-40...+175	°C
Storage temperature	$T_{stg}$	-55...+150	°C
Soldering temperature, wave soldering 1.6mm (0.063in.) from case for 10s	PG-T0220-3 PG-T0247-3	260 260	°C
Mounting torque, M3 screw Maximum of mounting processes: 3	M	0.6	Nm

## Thermal Resistance

Parameter	Symbol	Conditions	Max. Value	Unit
<b>Characteristic</b>				
IGBT thermal resistance, junction - case	$R_{th(j-c)}$		0.60	K/W
Thermal resistance junction - ambient	$R_{th(j-a)}$	PG-T0220-3 PG-T0247-3	62 40	K/W

Electrical Characteristic, at  $T_{VJ} = 25^\circ\text{C}$ , unless otherwise specified

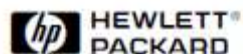
Parameter	Symbol	Conditions	Value			Unit
			min.	typ.	max.	
<b>Static Characteristic</b>						
Collector-emitter breakdown voltage	$V_{BR(CE)}$	$V_{GE} = 0\text{V}$ , $I_C = 0.20\text{mA}$	650	-	-	V
Collector-emitter saturation voltage	$V_{CESat}$	$V_{GE} = 15.0\text{V}$ , $I_C = 40.0\text{A}$ $T_{VJ} = 25^\circ\text{C}$ $T_{VJ} = 125^\circ\text{C}$ $T_{VJ} = 175^\circ\text{C}$	- - -	1.65 1.85 1.95	2.10 - -	V
Gate-emitter threshold voltage	$V_{GE(th)}$	$I_C = 0.40\text{mA}$ , $V_{CE} = V_{GE}$	3.2	4.0	4.8	V
Zero gate voltage collector current	$I_{CE0}$	$V_{CE} = 650\text{V}$ , $V_{GE} = 0\text{V}$ $T_{VJ} = 25^\circ\text{C}$ $T_{VJ} = 175^\circ\text{C}$	- -	-	40.0 2000.0	$\mu\text{A}$
Gate-emitter leakage current	$I_{GEO}$	$V_{CE} = 0\text{V}$ , $V_{GE} = 20\text{V}$	-	-	100	nA
Transconductance	$g_T$	$V_{CE} = 20\text{V}$ , $I_C = 40.0\text{A}$	-	50.0	-	S

# IGBT IGW40H65H5

Electrical Characteristic, at  $T_{VJ} = 25^\circ\text{C}$ , unless otherwise specified

Parameter	Symbol	Conditions	Value			Unit
			min.	typ.	max.	
<b>Dynamic Characteristic</b>						
Input capacitance	$C_{ies}$	$V_{CE} = 25\text{V}, V_{GE} = 0\text{V}, f = 1\text{MHz}$	-	2500	-	pF
Output capacitance	$C_{oes}$		-	40	-	
Reverse transfer capacitance	$C_{res}$		-	9	-	
Gate charge	$Q_g$	$V_{CC} = 520\text{V}, I_c = 40.0\text{A}, V_{GE} = 15\text{V}$	-	95.0	-	nC
Internal emitter inductance measured 5mm (0.197 in.) from case	$L_E$	PG-T0220-3 PG-T0247-3	-	7.0 13.0	-	nH
<b>Switching Characteristic, Inductive Load</b>						
Parameter	Symbol	Conditions	Value			Unit
			min.	typ.	max.	
<b>IGBT Characteristic, at <math>T_{VJ} = 25^\circ\text{C}</math></b>						
Turn-on delay time	$t_{d(on)}$	$T_{VJ} = 25^\circ\text{C}, V_{CC} = 400\text{V}, I_c = 20.0\text{A}, V_{GE} = 0.0/15.0\text{V}, R_{G(on)} = 15.0\Omega, R_{G(off)} = 15.0\Omega, L_{\sigma} = 30\text{nH}, C_{\sigma} = 30\text{pF}$ $L_{\sigma}, C_{\sigma}$ from Fig. E Energy losses include "tail" and diode reverse recovery.	-	22	-	ns
Rise time	$t_r$		-	12	-	ns
Turn-off delay time	$t_{d(off)}$		-	165	-	ns
Fall time	$t_f$		-	13	-	ns
Turn-on energy	$E_{on}$		-	0.39	-	mJ
Turn-off energy	$E_{off}$		-	0.12	-	mJ
Total switching energy	$E_{ts}$		-	0.51	-	mJ
Turn-on delay time	$t_{d(on)}$	$T_{VJ} = 25^\circ\text{C}, V_{CC} = 400\text{V}, I_c = 5.0\text{A}, V_{GE} = 0.0/15.0\text{V}, R_{G(on)} = 15.0\Omega, R_{G(off)} = 15.0\Omega, L_{\sigma} = 30\text{nH}, C_{\sigma} = 30\text{pF}$ $L_{\sigma}, C_{\sigma}$ from Fig. E Energy losses include "tail" and diode reverse recovery.	-	19	-	ns
Rise time	$t_r$		-	4	-	ns
Turn-off delay time	$t_{d(off)}$		-	190	-	ns
Fall time	$t_f$		-	24	-	ns
Turn-on energy	$E_{on}$		-	0.09	-	mJ
Turn-off energy	$E_{off}$		-	0.05	-	mJ
Total switching energy	$E_{ts}$		-	0.14	-	mJ

### I.3.8 IGBT Gate Drive Optocoupler HCPL-3120



## 2.0 Amp Output Current IGBT Gate Drive Optocoupler

### Technical Data

#### HCPL-3120

##### Features

- 2.0 A Minimum Peak Output Current
- 15 kV/us Minimum Common Mode Rejection (CMR) at  $V_{CM} = 1500$  V
- 0.5 V Maximum Low Level Output Voltage ( $V_{OL}$ ) Eliminates Need for Negative Gate Drive
- $I_{CC} = 5$  mA Maximum Supply Current
- Under Voltage Lock-Out Protection (UVLO) with Hysteresis

- Wide Operating  $V_{CC}$  Range: 15 to 30 Volts

- 500 ns Maximum Switching Speeds

- Industrial Temperature Range: -40°C to 100°C

- Safety Approval  
UL Recognized - 2500 V rms for 1 minute per UL1577  
CSA Approval

VDE 0884 Approved with  
 $V_{IORM} = 630$  V peak  
(Option 060 only)

##### Applications

- Isolated IGBT/MOSFET Gate Drive
- AC and Brushless DC Motor Drives

A 0.1  $\mu$ F bypass capacitor must be connected between pins 5 and 8.

##### Industrial Inverters

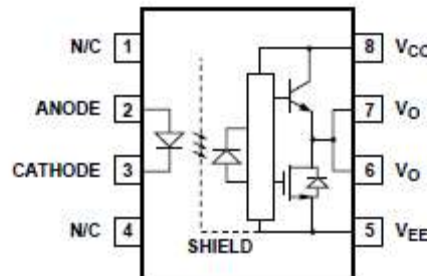
##### Switch Mode Power Supplies (SMPS)

##### Description

The HCPL-3120 consists of a GaAsP LED optically coupled to an integrated circuit with a power output stage. This optocoupler is ideally suited for driving power IGBTs and MOSFETs used in

motor control inverter applications. The high operating voltage range of the output stage provides the drive voltages required by gate controlled devices. The voltage and current supplied by this optocoupler makes it ideally suited for directly driving IGBTs with ratings up to 1200 V/100 A. For IGBTs with higher ratings, the HCPL-3120 can be used to drive a discrete power stage which drives the IGBT gate.

##### Functional Diagram



TRUTH TABLE

LED	$V_{CC} - V_{EE}$ "POSITIVE GOING" (i.e., TURN-ON)	$V_{CC} - V_{EE}$ "NEGATIVE GOING" (i.e., TURN-OFF)	$V_O$
OFF	0 - 30 V	0 - 30 V	LOW
ON	0 - 11 V	0 - 9.5 V	LOW
ON	11 - 13.5 V	9.5 - 12 V	TRANSITION
ON	13.5 - 30 V	12 - 30 V	HIGH

### I.3.9 Digital Input Buffer SN74AHC541

Used for 5V to 3.3V level translation

V<sub>CC</sub>=3.3V, V<sub>I</sub>=5V, V<sub>O</sub>=3.3V

V<sub>CC</sub>=3.3V, V<sub>I</sub>=0V, V<sub>O</sub>=0V



**SN74AHC541, SN54AHC541**

SCLS261O – OCTOBER 1995 – REVISED SEPTEMBER 2015

### SNx4AHC541 Octal Buffers/Drivers With 3-State Outputs

#### 6.1 Absolute Maximum Ratings

over operating free-air temperature range (unless otherwise noted)<sup>(1)</sup>      i/p voltage is 7V and not V<sub>CC</sub>+0.5 as normally mentioned

		MIN	MAX	UNIT
V <sub>CC</sub>	Supply voltage	-0.5	7	V
V <sub>I</sub>	Input voltage <sup>(2)</sup>	-0.5	7	V
V <sub>O</sub>	Output voltage <sup>(2)</sup>	-0.5	V <sub>CC</sub> + 0.5	V
I <sub>IK</sub>	Input clamp current V <sub>I</sub> < 0		-20	mA
I <sub>OK</sub>	Output clamp current V <sub>O</sub> < 0 or V <sub>O</sub> > V <sub>CC</sub>		±20	mA
I <sub>O</sub>	Continuous output current V <sub>O</sub> = 0 to V <sub>CC</sub>		±25	mA
	Continuous current through V <sub>CC</sub> or GND		±75	mA
T <sub>STG</sub>	Storage temperature	-65	150	°C

#### 6.3 Recommended Operating Conditions

over operating free-air temperature range (unless otherwise noted)<sup>(1)</sup>

		SN54AHC541		SN74AHC541		UNIT
		MIN	MAX	MIN	MAX	
V <sub>CC</sub>	Supply voltage	2	5.5	2	5.5	V
V <sub>IH</sub>	V <sub>CC</sub> = 2 V	1.5		1.5		
	V <sub>CC</sub> = 3 V	2.1		2.1		V
	V <sub>CC</sub> = 5.5 V	3.85		3.85		
V <sub>IL</sub>	V <sub>CC</sub> = 2 V		0.5		0.5	
	V <sub>CC</sub> = 3 V		0.9		0.9	V
	V <sub>CC</sub> = 5.5 V		1.65		1.65	
V <sub>I</sub>	Input voltage	0	5.5	0	5.5	V
V <sub>O</sub>	Output voltage	0	V <sub>CC</sub>	0	V <sub>CC</sub>	V
I <sub>OH</sub>	V <sub>CC</sub> = 2 V		-50		-50	µA
	V <sub>CC</sub> = 3.3 V ± 0.3 V		-4		-4	mA
	V <sub>CC</sub> = 5 V ± 0.5 V		-8		-8	
I <sub>OL</sub>	V <sub>CC</sub> = 2 V		50		50	µA
	V <sub>CC</sub> = 3.3 V ± 0.3 V		4		4	mA
	V <sub>CC</sub> = 5 V ± 0.5 V		8		8	
Δt/Δv	V <sub>CC</sub> = 3.3 V ± 0.3 V		100		100	ns/V
	V <sub>CC</sub> = 5 V ± 0.5 V		20		20	
T <sub>A</sub>	Operating free-air temperature	-55	125	-40	125	°C

### I.3.10 Digital Output Buffer 74HCT541

Used for 3.3V to 5V level translation

V<sub>CC</sub>=5V, V<sub>i</sub>=2.4V, V<sub>o</sub>=5V

V<sub>CC</sub>=5V, V<sub>i</sub>=0V, V<sub>o</sub>=0V

NXP Semiconductors

**74HC541; 74HCT541**

Octal buffer/line driver; 3-state

74HCT541											
V <sub>IH</sub>	HIGH-level input voltage	V <sub>CC</sub> = 4.5 V to 5.5 V	2.0	1.6	-	2.0	-	2.0	-	V	
V <sub>IL</sub>	LOW-level input voltage	V <sub>CC</sub> = 4.5 V to 5.5 V	-	1.2	0.8	-	0.8	-	0.8	V	
V <sub>OH</sub>	HIGH-level output voltage	V <sub>I</sub> = V <sub>IH</sub> or V <sub>IL</sub> ; V <sub>CC</sub> = 4.5 V									
		I <sub>O</sub> = -20 µA	4.4	4.5	-	4.4	-	4.4	-	V	
V <sub>OL</sub>	LOW-level output voltage	I <sub>O</sub> = -6.0 mA	3.98	4.32	-	3.84	-	3.7	-	V	
		V <sub>I</sub> = V <sub>IH</sub> or V <sub>IL</sub> ; V <sub>CC</sub> = 4.5 V									
		I <sub>O</sub> = 20 µA;	-	0	0.1	-	0.1	-	0.1	V	
		I <sub>O</sub> = 6.0 mA;	-	0.16	0.26	-	0.33	-	0.4	V	

## I.3.11 DSP TMS320F28069

TMS320F28069, TMS320F28068, TMS320F28067, TMS320F28066  
 TMS320F28065, TMS320F28064, TMS320F28063, TMS320F28062  
 SPRS698E –NOVEMBER 2010–REVISED JULY 2014



www.ti.com

### 5 Specifications

#### 5.1 Absolute Maximum Ratings<sup>(1) (2)</sup>

Supply voltage range, $V_{DDIO}$ (I/O and Flash)	with respect to $V_{SS}$	-0.3 V to 4.6 V
Supply voltage range, $V_{DD}$	with respect to $V_{SS}$	-0.3 V to 2.5 V
Analog voltage range, $V_{DDA}$	with respect to $V_{SSA}$	-0.3 V to 4.6 V
Input voltage range, $V_{IN}$ (3.3 V)		-0.3 V to 4.6 V
Output voltage range, $V_O$		-0.3 V to 4.6 V
Input clamp current, $I_{IK}$ ( $V_{IN} < 0$ or $V_{IN} > V_{DDIO}$ ) <sup>(3)</sup>		±20 mA
Output clamp current, $I_{OK}$ ( $V_O < 0$ or $V_O > V_{DDIO}$ )		±20 mA
Junction temperature range, $T_J$ <sup>(4)</sup>		-40°C to 150°C

#### 5.3 Recommended Operating Conditions

		MIN	NOM	MAX	UNIT
Device supply voltage, I/O, $V_{DDIO}$ <sup>(1)</sup>		2.97	3.3	3.63	V
Device supply voltage CPU, $V_{DD}$ (When internal VREG is disabled and 1.8 V is supplied externally)		1.71	1.8	1.995	V
Supply ground, $V_{SS}$			0		V
Analog supply voltage, $V_{DDA}$ <sup>(1)</sup>		2.97	3.3	3.63	V
Analog ground, $V_{SSA}$			0		V
Device clock frequency (system clock)		2	90		MHz
High-level input voltage, $V_{IH}$ (3.3 V)		2		$V_{DDIO} + 0.3$	V
Low-level input voltage, $V_{IL}$ (3.3 V)		$V_{SS} - 0.3$	0.8		V
High-level output source current, $V_{OH} = V_{OH(MIN)}, I_{OH}$	All GPIO/AIO pins			-4	mA
	Group 2 <sup>(2)</sup>			-8	mA
Low-level output sink current, $V_{OL} = V_{OL(MAX)}, I_{OL}$	All GPIO/AIO pins		4		mA
	Group 2 <sup>(2)</sup>		8		mA
Junction temperature, $T_J$	T version	-40	105		°C
	S version	-40	125		
Ambient temperature, $T_A$	Q version <sup>(3)</sup> (Q100 qualification)	-40	125		°C

(1)  $V_{DDIO}$  and  $V_{DDA}$  should be maintained within approximately 0.3 V of each other.

(2) Group 2 pins are as follows: GPIO16, GPIO17, GPIO18, GPIO19, GPIO28, GPIO29, GPIO36, GPIO37.

(3) The "Q" temperature option is *not* available on the 2806xU devices.

#### 5.4 Electrical Characteristics<sup>(1)</sup>

over recommended operating conditions (unless otherwise noted)

PARAMETER		TEST CONDITIONS		MIN	TYP	MAX	UNIT
$V_{OH}$	High-level output voltage	$I_{OH} = I_{OH\ MAX}$		2.4			V
		$I_{OH} = 50\ \mu A$			$V_{DDIO} - 0.2$		
$V_{OL}$	Low-level output voltage	$I_{OL} = I_{OL\ MAX}$			0.4		V
$I_{IL}$	Input current (low level)	Pin with pullup enabled	$V_{DDIO} = 3.3\ V, V_{IN} = 0\ V$	All GPIO	-80	-140	-205
				$\bar{X}_{RS}$ pin	-230	-300	-375
$I_{IH}$	Input current (high level)	Pin with pulldown enabled	$V_{DDIO} = 3.3\ V, V_{IN} = 0\ V$				±2
$I_{OZ}$	Output current, pullup or pulldown disabled	$V_O = V_{DDIO}$ or 0 V					±2
							μA
$C_I$	Input capacitance				2		pF

Table 6-27. ADC Electrical Characteristics

PARAMETER		MIN	TYP	MAX	UNIT
<b>DC SPECIFICATIONS</b>					
Resolution		12			Bits
ADC clock	90-MHz device	0.001		45	MHz
Sample Window		7		64	ADC Clocks
<b>ACCURACY</b>					
INL (Integral nonlinearity) <sup>(1)</sup>		-4		4	LSB
DNL (Differential nonlinearity), no missing codes		-1		1.5	LSB
Offset error <sup>(2)</sup>	Executing a single self-recalibration <sup>(3)</sup>	-20		20	LSB
	Executing periodic self-recalibration <sup>(4)</sup>	-4		4	
Overall gain error with internal reference		-60		60	LSB
Overall gain error with external reference		-40		40	LSB
Channel-to-channel offset variation		-4		4	LSB
Channel-to-channel gain variation		-4		4	LSB
ADC temperature coefficient with internal reference		-50			ppm/°C
ADC temperature coefficient with external reference		-20			ppm/°C
V <sub>REFLO</sub>		-100			µA
V <sub>REFHI</sub>		100			µA
<b>ANALOG INPUT</b>					
Analog input voltage with internal reference		0		3.3	V
Analog input voltage with external reference		V <sub>REFLO</sub>		V <sub>REFHI</sub>	V
V <sub>REFLO</sub> input voltage <sup>(5)</sup>		V <sub>SSA</sub>		0.66	V
V <sub>REFHI</sub> input voltage <sup>(6)</sup>		2.64		V <sub>DDA</sub>	V
	with V <sub>REFLO</sub> = V <sub>SSA</sub>	1.98		V <sub>DDA</sub>	
Input capacitance		5			pF
Input leakage current		±2			µA

Table 6-75. General-Purpose Output Switching Characteristics

over recommended operating conditions (unless otherwise noted)

PARAMETER		MIN	MAX	UNIT
t <sub>r(GPO)</sub>	Rise time, GPIO switching low to high	All GPIOs	13 <sup>(1)</sup>	ns
t <sub>f(GPO)</sub>	Fall time, GPIO switching high to low	All GPIOs	13 <sup>(1)</sup>	ns
f <sub>GPO</sub>	Toggling frequency		22.5	MHz

(1) Rise time and fall time vary with electrical loading on I/O pins. Values given in Table 6-75 are applicable for a 40-pF load on I/O pins.

Table 6-76. General-Purpose Input Timing Requirements

PARAMETER		MIN	MAX	UNIT
t <sub>w(SP)</sub>	Sampling period	QUALPRD = 0	1t <sub>c(SCO)</sub>	cycles
		QUALPRD ≠ 0	2t <sub>c(SCO)</sub> * QUALPRD	cycles
t <sub>w(IQSW)</sub>	Input qualifier sampling window		t <sub>w(SP)</sub> * (n <sup>(1)</sup> - 1)	cycles
t <sub>w(GPI)</sub> <sup>(2)</sup>	Pulse duration, GPIO low/high	Synchronous mode	2t <sub>c(SCO)</sub>	cycles
		With input qualifier	t <sub>w(IQSW)</sub> + t <sub>w(SP)</sub> + 1t <sub>c(SCO)</sub>	cycles

(1) "n" represents the number of qualification samples as defined by GPxQSELn register.

(2) For t<sub>w(GPI)</sub>, pulse width is measured from V<sub>IL</sub> to V<sub>IL</sub> for an active-low signal and V<sub>IH</sub> to V<sub>IH</sub> for an active-high signal.

## References

- [1] "Annual Report 2015-2016", Ministry of New and Renewable Energy, 2016, [http://mnre.gov.in/file-manager/annual-report/2015-2016/EN/Chapter%201/chapter\\_1.htm](http://mnre.gov.in/file-manager/annual-report/2015-2016/EN/Chapter%201/chapter_1.htm)
- [2] "Global Wind Report Annual Market Update 2015", Global Wind Energy Council, 2016, [www.gwec.net](http://www.gwec.net)
- [3] Javier Serrano-González and Roberto Lacal-Arántegui, "Technological evolution of onshore wind turbines—a market-based analysis", Wind Energ. (2016), The Authors Wind Energy, John Wiley & Sons Ltd., 2016, DOI: 10.1002/we
- [4] H. Li Z. Chen, "Overview of different wind generator systems and their comparisons", IET Renew. Power Gener., 2008, Vol. 2, No. 2, pp. 123–138, doi: 10.1049/iet-rpg:20070044
- [5] T. J. E. Miller, "Electronic Control of Switched Reluctance Machines", Newness Power Engineering Series, Oxford, 2001, ISBN 978-0750650731
- [6] Steve Cummins, "PowerTrain : Reluctant Heroes", iVT International Off-Highway 2012
- [7] "SIMOTICS Reluctance Motors with SINAMICS Converters", Catalog Add-On D 81.1 AO, Edition April 2015, Siemens AG [www.siemens.com/motors](http://www.siemens.com/motors) E.9115.29.LDT KG 0715 HOF 50 En
- [8] Freddy Gyllensten, Peter Isberg, Alessandro Castagnini, Giulio Secondo, Jouni Ikäheimo Ari Tammi, "Driving force", ABB review 1|16
- [9] Eila Nyman, Ari Tammi, Pietro Savio Termini and Tero Känsäkangas, "Magnet-free motor technology for fixed speed applications reaching "IE5" efficiency level", [www.abb.com/motors&generators](http://www.abb.com/motors&generators), 2015, 9AKK106684 EN 09-2015
- [10] "SynRM<sup>2</sup> Concept introduction", [www.abb.com/motors&generators](http://www.abb.com/motors&generators), 2014, 9AKK9AKK106176 EN 04-2014
- [11] Hoang Le-Huy and Patrice Brunelle, "A versatile nonlinear switched reluctance motor model in Simulink using realistic and analytical magnetization characteristics", Industrial Electronics Society, 2005. IECON 2005. 31st Annual Conference of IEEE, 6-10 Nov. 2005
- [12] R. Krishnan, "Switched Reluctance Motor Drives:Modelling, Simulation, Analysis, Design and Applications", CRC Press, 2001, ISBN 0-8493-0838-0
- [13] Roberto Cardenas, Ruben Pena, Marcelo Perez, Jon Clare, Greg Asher and Patrick Wheeler, "Control of a Switched Reluctance Generator for Variable-Speed Wind Energy Applications", IEEE Transactions On Energy Conversion, Vol. 20, No. 4, December 2005, pp 781-791
- [14] Yuan-Chih Chang and Chang-Ming Liaw, "On the Design of Power Circuit and Control Scheme for Switched Reluctance Generator", IEEE Transactions On Power Electronics,, VOL. 23, NO. 1, JANUARY 2008, pp 445-454
- [15] Kiwoo Park and Zhe Chen, "Self-Tuning Fuzzy Logic Control of a Switched Reluctance Generator for Wind Energy Applications", 3rd IEEE International Symposium on Power Electronics for Distributed Generation Systems (PEDG) 2012
- [16] Chandan Sikder, Iqbal Husain and Yilmaz Sozer, "Switched Reluctance Generator Controls for Optimal Power Generation with Current Regulation", 2012 IEEE Energy Conversion Congress and Exposition (ECCE), 15-20 Sept. 2012, Raleigh NC, pp 4322 - 4329
- [17] Yilmaz Sozer and David A. Torrey, "Closed Loop Control of Excitation Parameters for High Speed Switched-Reluctance Generators", IEEE Transactions On Power Electronics, Vol. 19, No. 2, March 2004, pp 355-362
- [18] Steven Lang and Eamon McKeogh, "LIDAR and SODAR Measurements of Wind Speed and Direction in Upland Terrain for Wind Energy Purposes" , Remote Sens. 2011, 3, 1871-1901; doi:10.3390/rs3091871 ISSN 2072-4292 [www.mdpi.com/journal/remotesensing](http://www.mdpi.com/journal/remotesensing)
- [19] Da-Woon Choi, Sang-In Byun, and Yun-Hyun Cho, "A Study on the Maximum Power Control Method of Switched Reluctance Generator for Wind Turbine", IEEE Transactions On Magnetics, Vol. 50, No. 1, January 2014
- [20] Lixin Xiong, Bingyin Xu, Houlei Gao and Lie Xu, "A Novel Algorithm of Switched Reluctance Generator for Maximum Power Point Tracking in Wind Turbine Application", International Conference on Sustainable Power Generation and Supply, 2009. SUPERGEN '09, 6-7 April 2009, pp 1-5
- [21] Siegfried Heier, "Grid Integration of Wind Energy", John Wiley & Sons Ltd, 2014, ISBN 978-1-119-96294-6
- [22] MATLAB v10 Online Help

- [23] Christos Mademlis and Iordanis Kioskeridis, "Optimizing Performance in Current-Controlled Switched Reluctance Generators", IEEE Transactions On Energy Conversion, Vol. 20, No. 3, September 2005 pp556-565
- [24] T. J. E. Miller, "Optimal Design of Switched Reluctance Motors", IEEE Transactions On Industrial Electronics, Vol. 49, No. 1, February 2002, pp 15-27
- [25] "SINAMICS G120 Control Units CU240B-2/CU240E-2 List Manual" A5E33839529 04/2015  
www.siemens.com

## Publication

Nereus Fernandes, Bindu R and Sincy George, "Control of Switched Reluctance Generator in Wind Energy System", IEEE Sponsored 3<sup>rd</sup> International Conference on Innovations in Information Embedded and Communication Systems (ICIIECS'16), 17-18 Mar 2016, Vol-1 pp 354-360, ISBN 978-1-4673-8207-6

Online Conference Proceedings is available at :  
<http://www.iciiecs.in/acc.html> Volume-1 SNo: 65 PaperID: 801

## **Acknowledgements**

I would like to thank my guide Mrs. Bindu R. for help, support and encouragement throughout this dissertation.

I am thankful to our HOD of Electrical Dept, Dr Sincy George, for inspiring and initiating this study in the fields of wind energy and switched reluctance machines, guidance during paper publication and also for providing the facilities and equipment for the project.

I am thankful to our Principal, Dr S. M. Khot, for providing the facilities for the hardware set-up.

I would like to thank Dr Sushil Thale for very helpful queries and suggestions during the review presentations and also at the time of hardware implementation.

I sincerely thank the University of Mumbai for grant of ₹ 40,000 towards the project.

I would also like to express my profound gratitude to all the Management, Staff and Students of FCRIT, Vashi for the encouragement and support I received throughout my student tenure here.

Signature of the student

Nereus Fernandes

Roll Number: 441406

Reg No: FR.C-162

Date: